National Library of Canada
Bibliothèque nationale du Canada

Canadian Theses Service
Service des thèses canadiennes

Ottawa, Canada
K1A 0N4

NOTICE

The quality of this microform is heavily dependent upon the quality of the original thesis submitted for microfilming. Every effort has been made to ensure the highest quality of reproduction possible.

If pages are missing, contact the university which granted the degree.

Some pages may have indistinct print especially if the original pages were typed with a poor typewriter ribbon or if the university sent us an inferior photocopy.

Reproduction in full or in part of this microform is governed by the Canadian Copyright Act, R.S.C. 1970, c. C-30, and subsequent amendments.

AVIS

La qualité de cette microforme dépend grandement de la qualité de la thèse soumise au microfilmage. Nous avons tout fait pour assurer une qualité supérieure de reproduction.

S'il manque des pages, veuillez communiquer avec l'université qui a conféré le grade.

La qualité d'impression de certaines pages peut laisser à désirer, surtout si les pages originales ont été dactylographiées à l'aide d'un ruban usé ou si l'université nous a fait parvenir une photocopie de qualité inférieure.

La reproduction, même partielle, de cette microforme est soumise à la Loi canadienne sur le droit d'auteur, SRC 1970, c. C-30, et ses amendements subséquents.

NL-339 (r. 88/04) c

Canada

University of Alberta

Numerical Model of Convective Eversion

by

Steven W. Park

C

A thesis
submitted to the Faculty of Graduate Studies and Research
in partial fulfilment of the requirements for the degree of

Master of Science

Department of Mechanical Engineering

Edmonton, Alberta

Spring, 1990

National Library of Canada
Bibliothèque nationale du Canada

Canadian Theses Service
Service des thèses canadiennes

Ottawa, Canada
K1A 0N4

NOTICE

The quality of this microform is heavily dependent upon the quality of the original thesis submitted for microfilming. Every effort has been made to ensure the highest quality of reproduction possible.

If pages are missing, contact the university which granted the degree.

Some pages may have indistinct print especially if the original pages were typed with a poor typewriter ribbon or if the university sent us an inferior photocopy.

Reproduction in full or in part of this microform is governed by the Canadian Copyright Act, R.S.C. 1970, c. C-30, and subsequent amendments.

AVIS

La qualité de cette microforme dépend grandement de la qualité de la thèse soumise au microfilmage. Nous avons tout fait pour assurer une qualité supérieure de reproduction.

S'il manque des pages, veuillez communiquer avec l'université qui a conféré le grade.

La qualité d'impression de certaines pages peut laisser à désirer, surtout si les pages originales ont été dactylographiées à l'aide d'un ruban usé ou si l'université nous a fait parvenir une photocopie de qualité inférieure.

La reproduction, même partielle, de cette microforme est soumise à la Loi canadienne sur le droit d'auteur, SRC 1970, c. C-30, et ses amendements subséquents.

ISBN 0-315-60303-8

NL-339 (r. 88/04) c

Canada

University of Alberta

Release Form

Name of Author:	**Steven W. Park**
Title of Thesis:	**Numerical Model of Convective Eversion**
Degree:	Master of Science
Year this degree granted:	1990

Permission is hereby granted to **The University of Alberta Library** to reproduce single copies of this thesis and to lend or sell such copies for private, scholarly, or scientific research purposes only.

The author reserves other publication rights, and neither the thesis nor extensive tracts from it may be printed or otherwise reproduced without the author's written consent.

Steven W. Park

(Student's signature)

Steven W. Park
#72, 11265-31 Avenue
Edmonton, Alberta
T6J 3V7

Date : April 12 / 90

University of Alberta

Faculty of Graduate Studies and Research

The undersigned certify that they have read, and recommend to the Faculty of Graduate Studies and Research for acceptance, a thesis entitled

Numerical Model of Convective Eversion

submitted by

Steven W. Park

in partial fulfilment of the requirements for the degree of

Master of Science.

G.S.H. Lock
(Supervisor)

M.D. Checkel

R.L. Varty

J.H. Masliyah

Date : 9th April 1990

To My Wife and To My Mother

Abstract

The requirement for more efficient heat transfer systems has stimulated interest in methods to augment heat transfer. Among many techniques, the use of tube inserts has been shown to be very effective. Typically, augmentation is achieved by increasing the effectiveness of transport process through increased mixing (e.g. static-mixer elements) or by creating rotating and/or secondary flow (e.g. twisted-tape inserts).

In the present study, the concept of convective eversion has been studied as an alternative means of augmenting tubeside convective heat transfer in laminar flow heat exchangers. It consists of interchanging the relatively hot (cool) fluid adjacent to the tube wall with the relatively cool (hot) fluid nearer to the tube axis. This process of turning the flow inside out creates higher temperature gradients at the wall and higher near-wall velocities, resulting in an increase in heat transfer and concomitant pressure drop.

No particular eversion device was analyzed. Instead, the eversion process was idealized by three separate models to cover the likely behaviour of practical evertors: ideal eversion, laminate eversion, and mixed eversion. The analysis, using the algorithm of Patankar, focused on the numerical solution of the governing equations for steady, axisymmetric flow and heat transfer in a circular duct into which a variety of hypothetical evertors were introduced. Initially, a tube containing a single evertor of each type was studied as a thermal entrance problem. Large increases in the local Nusselt number and friction factor were obtained in the first few diameters downstream of the evertors. This led to the study of repeated eversion, with a tube containing five regularly spaced evertors. The results showed that heat transfer augmentation was encouragingly high without the frictional penalty being excessive.

A systematic survey of the effect of principal variables was also undertaken. Some results were compared with data from a high performance augmentation device: the twisted-tape. These indicated that eversion can produce very similar thermal performance with a lower frictional penalty.

Acknowledgements

The author would like to express his sincere appreciation to Dr. G. S. H. Lock, who supervised the preparation of this thesis. His thoughtful guidance, encouragement, and advice were greatly appreciated.

The author is also thankful to the Department of Mechanical Engineering for the generous award of Teaching Assistantship and a large sum of computing fund.

Finally, the author is most thankful to his wife and family for their immeasurable emotional support and encouragement during his study at the University of Alberta.

Contents

Nomenclature xiii

Chapter 1

Introduction 1

1.1 General Background 1

1.2 The Concept of Eversion 4

1.3 Outline of Thesis 6

Chapter 2

Mathematical Formulation 8

2.1 Definition of the problem and assumptions 8

2.2 Eversion Models 10

2.2.1 Ideal Eversion Model 11

2.2.2 Laminate Eversion Model 14

2.2.3 Mixed Eversion Model 15

2.3 Governing Equations and Boundary Conditions 17

2.4 Non-dimensionalization 18

Chapter 3

Numerical Implementation 21

3.1 Introduction 21

3.2 Finite Difference Equations 23

3.2.1 Grid Definition and Control Volumes 23

3.2.2 Some Details of Discretization 23

3.3 The Algorithm 28

3.4 Convergence Criteria and Accuracy Considerations 31

3.5 Test of Computer Program 32

Chapter 4

Single Eversion 38

4.1 Introduction 38

4.2 Velocity and Friction Results 39

4.3 Temperature and Heat Transfer Results 49

Chapter 5

Repeated Eversion 54

5.1 Introduction 54

5.2 Results and Discussion 56

5.3 Effects of Reynolds Number Variation 60

5.4 Effects of Prandtl Number Variation 63

5.5 Effects of Spacing Variation 63

5.6 Effects of r_* Variation 65

5.7 Comparison with Twisted-Tape Data 68

Chapter 6

Conclusions and Recommendations 74

References 77

Appendix A

Listing of Computer Program 84

List of Figures

1.1 Sketch of evertor in a tube. 5

2.1 Sketch of the problem to be investigated. 9
2.2 Flow division in a circular tube. 12
2.3 Ring exchanges in ideal eversion model. 13
2.4 Ring exchanges in laminate eversion model. 14

3.1 Control volume and notation in the staggered grid. 24
3.2 Axial velocity profiles in developing region of a circular duct for $Re = 100$. 33
3.3 Comparison of the apparent Fanning friction factor for laminar flow in entrance region of a circular duct. 35
3.4 Comparison of local Nusselt number for simultaneously developing laminar flow in a circular duct with uniform wall temperature. 37

4.1 Sketch of single eversion problem. 39
4.2 Velocity profile development for $Re = 1000$, $H = 50$, and $r_* = 0.707$: ideal eversion. 41
4.3 Velocity profile development for $Re = 1000$, $H = 50$, and $r_* = 0.707$: laminate eversion. 42
4.4 Velocity profile development for $Re = 1000$, $H = 50$, and $r_* = 0.707$: mixed eversion. 43
4.5 Composite pressure profile after eversion. 45
4.6 Pressure profile for $Re = 1000$, $H = 50$, and $r_* = 0.707$: single eversion. 47

4.7 friction factor profile for $Re = 1000$, $H = 50$, and $r_* = 0.707$: single eversion. 48

4.8 Temperature profile development for $Re = 1000$, $Pr = 0.71$, $H = 50$, and $r_* = 0.707$: single eversion. 51

4.9 Local Nusselt number development for $Re = 1000$, $Pr = 0.71$, $H = 50$, and $r_* = 0.707$: single eversion. 52

5.1 Pressure profile for $Re = 1000$, $Pr = 10$, and $s = 5$: repeated eversion. 57

5.2 Friction factor profile for $Re = 1000$, $Pr = 10$, and $s = 5$: repeated eversion. 58

5.3 Local Nusselt number development for $Re = 1000$, $Pr = 10$, and $s = 5$: repeated eversion. 59

5.4 Effect of Re on friction factor for $Pr = 10$, $r_* = 0.707$, and $s = 8$. . . 61

5.5 Effect of Re on mean Nusselt number for $Pr = 10$, $r_* = 0.707$, and $s = 8$. 62

5.6 Effect of Pr on mean Nusselt number for $Re = 1000$, $r_* = 0.707$, and $s = 8$. 64

5.7 Effect of s on friction factor for $Re = 1000$, $Pr = 10$, and $r_* = 0.707$. 66

5.8 Effect of s on mean Nusselt number for $Re = 1000$, $Pr = 10$, and $r_* = 0.707$. 67

5.9 Effect of r_* on friction factor for $Re = 1000$, $Pr = 10$, and $s = 8$. . . . 69

5.10 Effect of r_* on mean Nusselt number for $Re = 1000$, $Pr = 10$, and $s = 8$. 70

5.11 Comparison of friction factor with twisted-tape data for $Pr = 10$, $s = 8$, and $r_* = 0.707$. 72

5.12 Comparison of mean Nusselt number with twisted-tape data for $Pr = 10$, $s = 8$, and $r_* = 0.707$. 73

Nomenclature

A	sensible heat; also used to denote the area of a control volume face
a	coefficient in the discretization equation
b	constant term in the discretization equation
C	coefficient
c_p	specific heat at constant pressure
D	tube diameter; also used to denote diffusion conductance
d	coefficient of the pressure-difference term
F	flow rate through a control volume face
f_{app}, f	apparent Fanning friction factor
H	length/diameter ratio
h	convective heat transfer coefficient
J	total (convective + diffusion) flux
k	fluid thermal conductivity

L	length of tube
L_{hy}	hydrodynamic entrance length
L_{th}	thermal entrance length
l	length of evertor
M	momentum
m	mass
Nu_x	peripheral average axially local Nusselt number
Nu_m	mean Nusselt number
n	number of radial nodal points
P, p	pressure; P is also used to denote cell Peclect number
p'	pressure correction
Pe	Peclect number
Pr	Prandtl number
R, r	radial coordinate
R_h	hydraulic radius
Re	Reynolds number based on diameter
Δr	r-direction width of a control volume
δr	r-direction distance between two adjacent grid points

S	pitch (distance between two evertors)
s	S/D
T	absolute temperature
U, u	axial velocity
U_m	average fluid velocity
u'	axial velocity correction
u^*	axial velocity based on guessed pressure p^*
V, v	radial velocity
X, x	axial coordinate
$\Delta x, \delta x$	similar to Δr, δr
x^+	axial coordinate for the hydrodynamic entrance region, $X/D\,Re$
x^*	axial coordinate for the thermal entrance region, $X/D\,Pe$

Greek

α	relaxation factor
ρ	mass density
μ	fluid dynamic viscosity
ϕ	fluid temperature

Subscripts

A	annulus
C	core
d	drag
e	evertive
E, W, S, N	neighbor grid point on the east, west, south, and north, respectively
e, w, s, n	control volume face on the east, west, south, and north, respectively
i	inlet
k	kth radial nodal point
m	mixed mean
nb	general neighbor grid point
o	bare tube
P	central grid point under consideration
w	wall
$*$	core/annulus interface

Superscripts

$\cdot$	per unit time
$'$	after eversion
$*$	previous-iteration value of a variable

Chapter 1

Introduction

1.1 General Background

A heat exchanger is a device which provides for transfer of thermal energy between two or more fluids at different temperatures. Over the years, problems associated with heat exchangers have been a challenge to many investigators. Thermo-hydraulic fundamentals in many different flow regimes and design of heat exchangers have been a classical subject of study. In recent years, interest in heat exchangers with more compact surfaces has been increasing at an accelerated pace. As a result, smaller, light-weight and lower-cost heat exchangers are being designed. Because of the smaller flow passage hydraulic diameter, especially with gas flows, the heat exchanger design range falls well within the laminar flow range ($Re < 2300$). In addition to compact heat exchangers, laminar flow heat transfer in tubes occurs in other engineering applications. The following examples can be cited: heating or cooling of viscous liquids in the petroleum, chemical, and food industries; heating of the circulating fluid in solar collectors; and other applications in the aerospace, nuclear, biomedical,

electronics and instrumentation fields.

Heat transfer coefficients for laminar flow in plain tubes are well described in the literature [1, 2, 3]. They are generally low and therefore frequently represent the dominant thermal resistance in tubular heat exchangers. This results in the relatively large size and cost of these heat exchangers. In recent years there has been considerable interest in improving the performance of such exchangers through the augmentation of tubeside convective heat transfer. The study of improved heat transfer performance is referred to as heat transfer augmentation, enhancement or intensification. In general, this means an increase in heat transfer rate with a penalty in the form of increased pressure loss or external energy consumption. Often the goal is to reduce the size of heat exchangers required for a specific heat duty, thereby reducing capital cost and energy expended in manufacturing the equipment. It may also be necessary to upgrade the heat transfer capability of an existing heat exchanger. More effective heat transfer may be required to prevent excessive temperature or system destruction in situations where heat generation is fixed.

Techniques to augment heat transfer inside tubes are generally classified as passive or active. Passive techniques, which require no external energy to produce the augmentation, include the use of extended surfaces, the use of artificially roughened surfaces, the use of swirl flow devices such as twisted tapes or inlet vortex generators, the use of displaced promoters such as disks or static mixers, and the use of additives such as gas bubbles or solid particles. Active techniques, which require external energy to produce the augmentation, include mechanical agitation, vibration of the surface or fluid, application of electrostatic fields, and injection or suction. Detailed surveys of the many augmentative methods presently employed are given in references [4, 5, 6, 7]. A recent survey focused on laminar flow heat transfer augmentation in tubes is given in reference [8].

The passive technique in the form of tube inserts has been of great interest for augmenting forced convection heat transfer. Inserts can be categorized into two groups according to Bergles [7]: those that indirectly improve energy transport through increased mixing such as metallic mesh, static mixer elements, rings, and disks (i.e. displaced promoters); and those that enhance heat transfer by creating rotating and/or secondary flow such as inlet vortex generators and twisted tapes (i.e. swirl flow devices). These inserts generally are known to produce significant heat transfer augmentation. But they are also known to introduce a large pressure drop. Sununu [9] and Genetti and Priebe [10] used Kenics static mixers for heating of viscous oil. The increase in heat transfer was about 150-200 percent but the increase in friction factor was almost 900 percent. Van Der Meer and Hoogendoorn [11] used Sulzer mixers for heating of silicon oil. About 400 percent increase in heat transfer was reported, but no friction factor data were reported. Based on the manufacturer's data, Bergles [8] reported that these mixers gave a pressure drop increase of about 1400 percent above smooth tube values.

A good heat transfer increase with a mild increase in pressure drop is reported with twisted-tape inserts. Marner and Bergles [12] reported a set of heat transfer and pressure drop data for laminar flow of a viscous liquid in circular tubes with twisted-tape inserts and a uniform wall temperature boundary condition. Using ethylene glycol as a working fluid, they observed up to a 70 percent increase in Nusselt number and about 300 percent increase in friction factor over smooth tube values. Subsequently, Marner and Bergles [13] published another set of heat transfer and isothermal pressure drop data. Using Polybutene 20, a highly viscous liquid (Prandtl number range: 1000-7000), they obtained heating and cooling data in the deep laminar region (Reynolds number range: 15-575). The observed enhancement in Nusselt numbers was about 50 to 125 percent, while the isothermal friction factor

increase was 238 percent. Numerous other studies on twisted-tape inserts, either experimental or numerical, can be found in the literature [14, 15, 16, 17, 18].

1.2 The Concept of Eversion

In the present study, a different concept is considered as a means of convective heat transfer augmentation. While heat transfer augmentation can be achieved indirectly through improved transport processes, it can also be achieved directly through artificially increased local temperature gradient created by deliberately interchanging regions of hot fluid with regions of cold fluids. Specifically, if the heated (or cooled) film adjacent to a duct wall is exchanged with the colder (or hotter) fluid further away, the local temperature gradient near the wall will be greatly increased, thus increasing the heat transfer rate. Such an exchange process, in which the flow system is turned inside out, may be described as *eversion*.

Convective eversion in a heated duct is any process whereby the annulus of hotter fluid near the wall is interchanged with the core of cooler fluid. An *evertor* is any device which will achieve this. Figure 1.1 illustrates one possibility in which the evertor divides the flow into two streams of a core and an annulus and then exchanges the fluid in these regions. With a proper choice of the relative size of the core and the annulus, eversion can also increase local near-wall velocities and further enhance heat transfer. In this study, transport enhancement due to increased mixing is viewed as a further improvement on that achieved through eversively-induced alterations in the local velocity and temperature field.

Perhaps the simplest way to evert a duct flow is through secondary motion. If this motion induces a single vortex as in twisted pipes [19, 20], the resulting secondary motion runs roughly parallel to the duct wall and therefore produces no

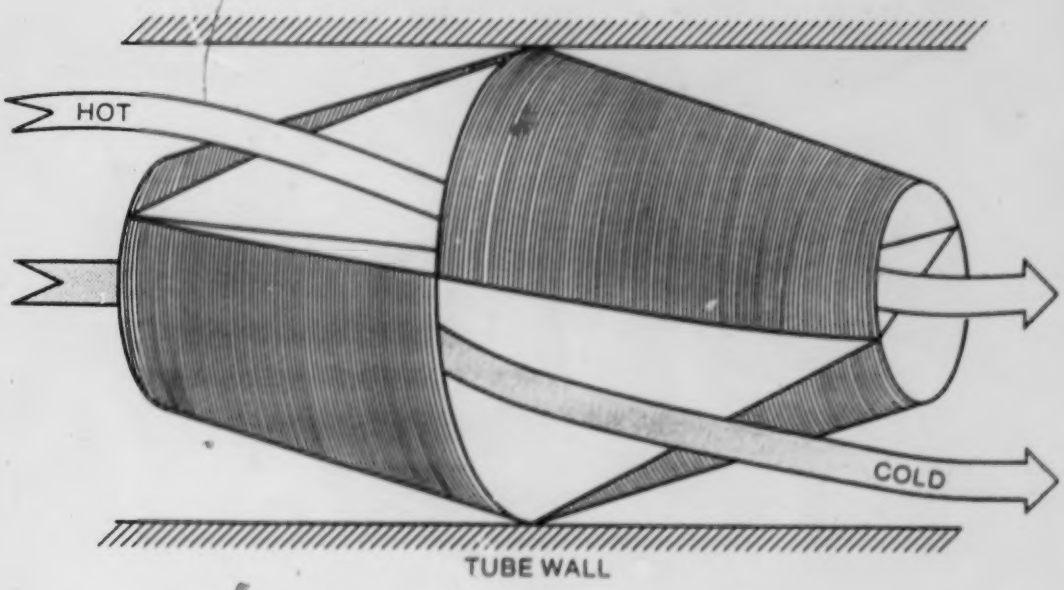

Figure 1.1: Sketch of evertor in a tube.

eversion. With two or more vortices, the required eversion effect takes place with a corresponding increase in heat transfer: the simplest situation is a vortex pair. The twisted-tape produces two vortices separated by the tape. Obviously, variations on this theme are possible [8].

A form of evertor, similar to the one shown in figure 1.1, was first used by Bayley and Lock [21] when they studied the flow conditions at the junction of a closed thermosyphon. Application of the device as a useful means of augmenting forced convective heat transfer inside ducts was investigated by Maezawa and Lock [22].

They studied heat transfer and friction characteristics of turbulent flow inside a circular duct containing a number of different turbulence promoters, among which were evertors of various geometry. For the heating of air with a constant wall temperature boundary condition, they reported that a duct fitted with regularly spaced evertors resulted in about 120- 200 percent increase in average heat transfer coefficients while the concomitant increase in friction coefficients was about 400- 3000 percent depending on the geometry of evertors and their spacing. Tests of this device were not conducted for laminar flow conditions.

In laminar flow augmentation, a distinguishing feature is that the increase in heat transfer coefficients for tube inserts are, in general, of the same order of magnitude as the increase in friction factors. By contrast, increases in turbulent flow heat transfer coefficients are accompanied by pressure drops which are several orders of magnitude greater than the plain tube values [23]. This fact implies that evertors may prove very promising devices for augmenting laminar flow heat transfer. This work attempts to provide some answers to the above proposition. The purpose of this study is not to present an analysis of any particular eversion device or process. Instead, an attempt will be made to model eversion in general terms and thereby explore its prospects and its limitations. To this end, the analysis will focus on the numerical solution of the governing equations for steady, axisymmetric flow and heat transfer in a circular duct into which a variety of hypothetical evertors are introduced.

1.3 Outline of Thesis

In chapter 2, the problem to be investigated and the solution strategy are described. To facilitate the numerical calculations, three eversion models along with necessary assumptions are introduced. Then, the governing differential equations and

the boundary conditions are described.

Chapter 3 deals with the numerical implementation of the problem. Finite difference equations and the SIMPLE-C algorithm are briefly explained. The accuracy of the developed computer program is tested by solving the combined hydrodynamic and thermal entry length problem and by comparing the solutions with other known solutions.

To explain how eversion produces heat transfer augmentation and the concomitant pressure drop increase, a tube enhanced by a single evertor is studied in chapter 4. The velocity and temperature profiles after eversion and their subsequent development further downstream are used to explain the characteristics of pressure drop and heat transfer of each eversion model.

Chapter 5 studies the use of repeated eversion by investigating a tube enhanced by a train of five equally spaced evertors. A systematic study of the effects of the principal variables on hydraulic and thermal performance is conducted. Some results are compared with those of twisted-tape inserts.

Finally, conclusions and recommendations for further study are included in chapter 6.

Chapter 2

Mathematical Formulation

2.1 Definition of the problem and assumptions

The study of enhanced heat transfer, theoretical or experimental, basically consists of comparing heat transfer and friction characteristics of an enhanced heat transfer tube to those of a reference (i.e. smooth) tube. The same scheme is followed in this study.

Figure 2.1 is a schematic sketch of an enhanced tube to be investigated. The problem concerns the prediction of steady, forced laminar flow and heat transfer in a circular duct of diameter D and length L containing one or more evertors of length l. The fluid is idealized as liquid or low-speed gas (incompressible) with the fluid properties ρ, μ, c_p and k constant (independent of temperature). Viscous dissipation and compression work are assumed to be negligible in the energy equation.

The fluid enters the duct with a uniform inlet velocity U_m or a fully developed velocity profile and with a uniform temperature T_i. It is heated by the duct wall which has a uniform temperature both axially and peripherally. When the fluid,

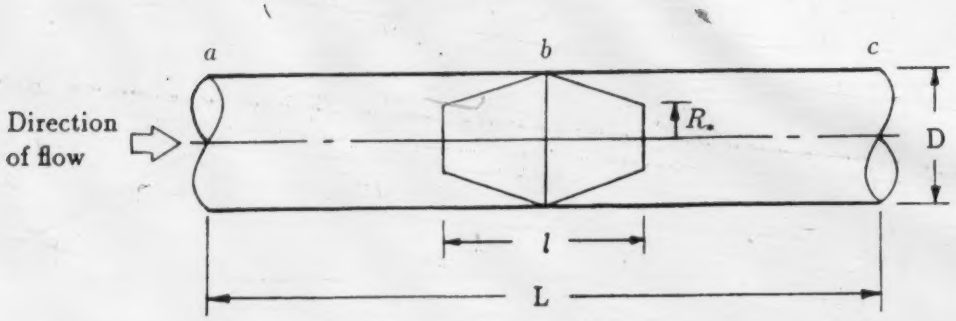

Figure 2.1: Sketch of the problem to be investigated.

having a certain velocity and a temperature profile, passes through an evertor, it is turned inside out and has a different velocity and a temperature profile. Accurate calculation of the velocity and temperature profile at any cross-section of the solution domain requires solution of the differential equations which describe the transport of momentum and heat in the region. But the existence of the evertors makes boundary conditions prohibitively difficult to describe. Therefore, a simplified approach will be used. First, solutions will be obtained in the domain a to b. Then, the velocity and temperature profiles obtained at b will be everted according to three different eversion models that will be described in the next section. The everted profiles then serve as the new inlet boundary conditions for the domain of b to c. This process is continued until the whole solution domain is covered. Thus, each section is considered as a developing entry length problem. An important assumption used here is that the eversion process occurs instantaneously at b, even though, in reality, it occurs over the length of the evertor l.

This approach of section-by-section solution is somewhat similar to a streamwise marching solution [24, 25, 26] of parabolized Navier-Stokes equations in that both

methods use the assumption that no influence from downstream can penetrate upstream. Thus, it is assumed that the fluid does not know the existence of the downstream evertor until it reaches the evertor. However, unlike the streamwise marching solution, the complete Navier-Stokes equations are used here when each section is solved. This is because more accurate calculations are desired in the immediate vicinity of each entrance where very high local heat transfer and friction coefficients are expected to occur. For each section, zero gradient of each dependent variable is used as the exit boundary conditions needed to solve the elliptic equations. This may not always be true, especially when the length of the tube section is short and thus the flow is still developing at the exit boundary. But this is the closest approximation at the exit boundary. Also the flow is assumed to be axisymmetric although real evertors may make the flow three dimensional.

2.2 Eversion Models

For present purposes, eversion may be defined as the turning of a flow inside out. This is the means by which, for any given micro or macro diffusion efficiency, the gradient of potential, temperature in particular, may be artificially increased. The precise mechanism of eversion is not important in this study, although it might be noted that there are many possibilities ranging from swirl flow devices to displacement promoters. Instead, eversion is modelled by three idealized processes. Since a flow carries with it a variety of extensive properties, it is perhaps worthwhile limiting the discussion to those quantities most appropriate to thermal convection: namely, mass flow rate and energy flow rate.

The rate of mass flow $\dot{m}$ down a circular duct is given from the velocity distribution

as

$$\dot{m} = 2\pi \int_0^{R_*} \rho U R dR + 2\pi \int_{R_*}^{R_w} \rho U R dR \tag{2.1}$$

where R_* is the radius at which the mass flow rate is divided into two generally unequal parts; this radius thus serves to distinguish between the core ($R < R_*$) and the annulus ($R > R_*$) which are to be interchanged. Similarly the thermal energy flow rate (the advective flow rate) $\dot{A}$ is obtained from the velocity and temperature distribution as

$$\dot{A} = 2\pi \int_0^{R_*} \rho c_p U T R dR + 2\pi \int_{R_*}^{R_w} \rho c_p U T R dR \tag{2.2}$$

Once again, the two contributions are not generally equal. If necessary, equation (2.2) may be written in more general terms by adding the conductive flux and the kinetic energy flux to give the complete energy flux, but these are ignored here for simplicity. The idea of eversion modelling is that the above two quantities of fluid immediately upstream of the evertor are conserved by the process of eversion and are thus maintained in the corresponding fluid discharged from the evertor.

2.2.1 Ideal Eversion Model

Under ideal circumstances, the hottest fluid would be exchanged with the coldest fluid. Suppose this is to be achieved by an array of $(n-1)$ rings which collect fluid in a series of thin annuli and, through the use of suitable plumbing, re-distribute it through the second set of $(n-1)$ rings. Figure 2.2 shows n radial nodal locations from $R = 0$ to $R = R_w$ and division of flow into $(n-1)$ rings. The ideal eversion model assumes the exchange of fluid between the first ring and the $(n-1)th$ ring, and between the second ring and the $(n-2)th$ ring, and so on, as is shown schematically in figure 2.3 using 6 rings. The fluid in each numbered ring before eversion is assumed

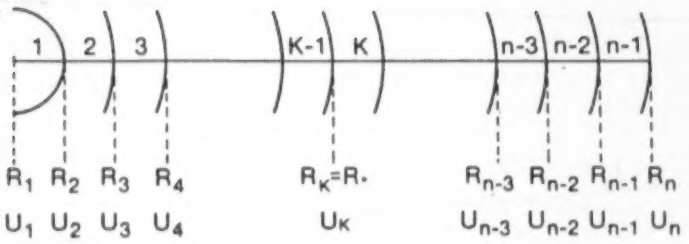

Figure 2.2: Flow division in a circular tube.

to be redirected to the corresponding ring after eversion. With the known velocity and temperature profile in the pre-eversion state, it is then possible to calculate the velocity and temperature profile in the post-eversion state. For example, consider the exchange between the first ring and the $(n-1)th$ ring. If the ring thicknesses are much less than the tube radius, and the velocities are linearly interpolated, the continuity requires that

$$\rho_1' \left(\frac{U_2' + U_1'}{2}\right) \pi(R_2^2 - R_1^2) = \rho_{n-1} \left(\frac{U_n + U_{n-1}}{2}\right) \pi(R_n^2 - R_{n-1}^2) \qquad (2.3)$$

where the prime denotes the post-eversion state quantities. This describes the everted mean velocity $(U_1' + U_2')/2$ in the first ring resulting from the mass collected from the $(n-1)th$ ring of a prescribed velocity profile. In general, the exchange takes place between the $(j)th$ ring and the $(n-j)th$ ring. Thus

$$\rho_j' \left(\frac{U_{j+1}' + U_j'}{2}\right) \pi(R_{j+1}^2 - R_j^2) = \rho_{n-j} \left(\frac{U_{n-j+1} + U_{n-j}}{2}\right) \pi(R_{n-j+1}^2 - R_{n-j}^2) \qquad (2.4)$$

in which j=1,2,3,$\cdots(n-1)$. Since density is assumed to be constant, equation (2.4) can be written as

$$\left(\frac{U_{j+1}' + U_j'}{2}\right) = \left(\frac{R_{n-j+1}^2 - R_{n-j}^2}{R_{j+1}^2 - R_j^2}\right) \left(\frac{U_{n-j+1} + U_{n-j}}{2}\right) \qquad (2.5)$$

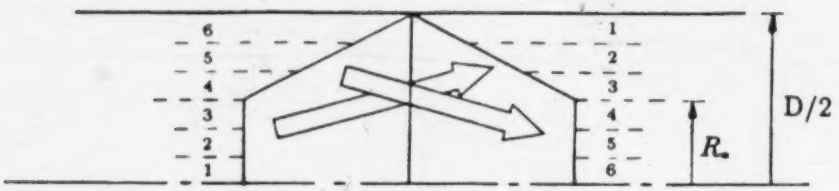

Figure 2.3: Ring exchanges in ideal eversion model.

When the everted mean velocities are obtained for all $(n-1)$ rings, they are converted back into nodal velocities by linear interpolation utilizing the no-slip condition at $R = R_n$.

The everted temperature profile is similarly obtained through the requirement of the energy conservation. Thus

$$\rho'_j c'_{p_j} \left(\frac{U'_{j+1} + U'_j}{2}\right) \left(\frac{T'_{j+1} + T'_j}{2}\right) \pi(R^2_{j+1} - R^2_j) =$$
$$\rho_{n-j} c_{p_{n-j}} \left(\frac{U_{n-j+1} + U_{n-j}}{2}\right) \left(\frac{T_{n-j+1} + T_{n-j}}{2}\right) \pi(R^2_{n-j+1} - R^2_{n-j}) \qquad (2.6)$$

where j=1,2,3,$\cdots(n-1)$. However, when equation (2.5) is substituted, it reduces to

$$\left(\frac{T'_{j+1} + T'_j}{2}\right) = \left(\frac{T_{n-j+1} + T_{n-j}}{2}\right) \qquad (2.7)$$

Equation (2.7) shows that temperature plays a passive role in eversion. That is, the mean fluid temperature in a ring immediately upstream of the evertor is unchanged by the process of eversion and thus is preserved in the corresponding ring of fluid discharged from the evertor.

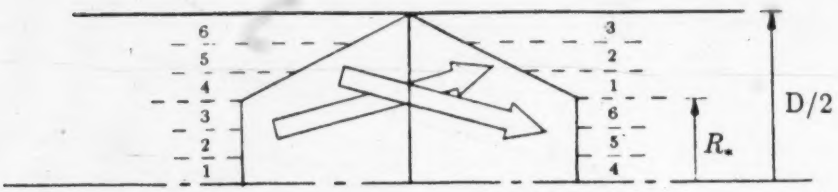

Figure 2.4: Ring exchanges in laminate eversion model.

2.2.2 Laminate Eversion Model

The ideal eversion model described above may be more of a conceptual model rather than a practical one, and therefore it might be difficult to achieve in practice. A more realistic model would be the exchange of fluid on both sides of R_* in bulk. The laminate eversion model assumes that the fluid is exchanged in bulk and that the laminate structure of the fluid is preserved during eversion, considering the flow field is laminate (though not necessarily laminar) before eversion. That is, the exchange takes place, referring to figure 2.2, between the first ring and the $(k)th$ ring, and between the second ring and $(k+1)th$, and so on: k is the half-way point (i.e. $k = n/2 + 1$) in an even number of rings. The schematic diagram of this eversion model is shown in figure 2.4 again using 6 rings. The conservation of mass in this model gives

$$\left(\frac{U'_{k-j+1} + U'_{k-j}}{2}\right) = \left(\frac{R^2_{n-j+1} - R^2_{n-j}}{R^2_{k-j+1} - R^2_{k-j}}\right)\left(\frac{U_{n-j+1} + U_{n-j}}{2}\right) \qquad (2.8)$$

in which j=1,2,3 $\cdots (k-1)$. And the conservation of energy gives

$$\left(\frac{T'_{k-j+1} + T'_{k-j}}{2}\right) = \left(\frac{T_{n-j+1} + T_{n-j}}{2}\right) \tag{2.9}$$

showing that temperature, again, plays a passive role in eversion. The equations (2.8) and (2.9) explicitly give the velocity and temperature field, respectively, from $R = R_1$ to $R = R_k$ after laminate eversion in terms of the pre-eversion field. The expressions are inverted when k is replaced by n and n by k to give the velocity and temperature field from $R = R_k$ to $R = R_n$.

2.2.3 Mixed Eversion Model

This model is similar to laminate eversion model in that it also assumes the bulk exchange of fluid. But unlike the laminate eversion model, it does not assume that the laminate structure is preserved during the process of eversion. Instead, it assumes that each of the two streams discharged from the evertor is completely mixed and emerges with a constant mean velocity. Then, the everted core velocity formed from the annulus is given by

$$\overline{U'_c} = \frac{2}{R_*^2} \int_{R_*}^{R_n} U\, R\, dR \tag{2.10}$$

and the everted annulus velocity formed from the core is given by

$$\overline{U'_a} = \frac{2}{R_n^2 - R_*^2} \int_0^{R_*} U\, R\, dR \tag{2.11}$$

Similarly, the everted core temperature formed from the annulus is given by

$$\overline{T'_c} = \frac{2}{\overline{U'_c} R_*^2} \int_{R_*}^{R_n} U\, T\, R\, dR = \int_{R_*}^{R_n} T\, dR \tag{2.12}$$

and the everted annulus temperature formed from the core is given by

$$\overline{T'_a} = \int_0^{R_*} T\, dR \tag{2.13}$$

Once again temperature is shown to play a passive role in eversion.

Several comments can be made concerning eversion modelling:

- Both ideal eversion model and laminate eversion model use the ring interchange about R_*. The choice of R_* is a variable. With a given R_*, the same number of rings in both core and annulus must be used. The choice of ring thickness, however, is arbitrary. The chosen thicknesses follow the hypothetical plumbing arrangements. Two obvious choices are: rings of equal area and rings of equal thickness. The latter will be used here, but with the core and annulus ring thicknesses being different.

- In practice, secondary conduction between adjacent streams of fluid may occur as they cross through the evertor. As mentioned before, any transport enhancement caused by the molecular intermixing is viewed as a further improvement.

- Momentum has not been considered in the above equations even though the area changes in the ring exchange undoubtedly create changes in the fluid velocity profile. It is thus expected that the momentum flux of the annulus prior to eversion would not be the same as that of the core following eversion; a similar statement applies to the upstream core and downstream annulus. There is, in general, a change in total momentum flux resulting from eversion. Such a change implies a force which is manifest here as a change in pressure across the evertor. Different types of eversion therefore carry with them different pressure characteristics. The pressure changes thus incurred have been incorporated in the calculation of the friction factors, as will be discussed in chapter 4.

2.3 Governing Equations and Boundary Conditions

The problem described in section 2.1 can now be expressed as that of solving the governing partial differential equations. The conservation equations for mass, momentum and energy in a circular tube are well known. For steady, laminar, axisymmetric, constant property conditions in cylindrical coordinate systems they are:

Mass conservation:

$$\frac{\partial U}{\partial X} + \frac{1}{R}\frac{\partial}{\partial R}(RV) = 0 \tag{2.14}$$

Axial momentum:

$$\rho\left(U\frac{\partial U}{\partial X} + V\frac{\partial U}{\partial R}\right) = -\frac{\partial P}{\partial X} + \mu\frac{1}{R}\frac{\partial}{\partial R}\left(R\frac{\partial U}{\partial R}\right) + \mu\frac{\partial^2 U}{\partial X^2} \tag{2.15}$$

Radial momentum:

$$\rho\left(U\frac{\partial V}{\partial X} + V\frac{\partial V}{\partial R}\right) = -\frac{\partial P}{\partial R} + \mu\frac{1}{R}\frac{\partial}{\partial R}\left(R\frac{\partial V}{\partial R}\right) - \mu\frac{V}{R^2} + \mu\frac{\partial^2 V}{\partial X^2} \tag{2.16}$$

Energy conservation:

$$\rho c_p\left(U\frac{\partial T}{\partial X} + V\frac{\partial T}{\partial R}\right) = k\frac{1}{R}\frac{\partial}{\partial R}\left(R\frac{\partial T}{\partial R}\right) + k\frac{\partial^2 T}{\partial X^2} \tag{2.17}$$

The above equations are subject to the following initial and boundary conditions:

Inlet($X = 0$):

$$U = 2U_m[1 - (\frac{R}{R_w})^2], \quad V = 0, \quad T = T_0 \qquad \text{for all R} \tag{2.18}$$

Outlet($X = L$):

$$\frac{\partial U}{\partial X} = 0, \quad V = 0, \quad \frac{\partial T}{\partial X} = 0 \qquad \text{for all R} \tag{2.19}$$

Wall boundaries($R = R_w$):

$$U = 0, \quad V = 0, \quad T = T_w = \text{constant} \qquad \text{for all X} \qquad (2.20)$$

Axis of symmetry($R = 0$):

$$\frac{\partial U}{\partial R} = 0, \quad V = 0, \quad \frac{\partial T}{\partial R} = 0 \qquad \text{for all X} \qquad (2.21)$$

The initial conditions at the inlet given in equation (2.18) represent hydrodynamically developed flow entry. For a developing flow the uniform flow entry ($U = U_m$ and $V = 0$) or the irrotational flow entry ($U = U_m$ and $\partial V/\partial X = 0$) can be used. These boundary conditions indicate that it is only necessary to consider half of the tube due to the symmetry about the center of the tube.

2.4 Non-dimensionalization

It is common practice to non-dimensionalize the governing equations before performing a numerical analysis. The advantages of non- dimensionalization are various: parameters are combined into familiar dimensionless groups; solutions obtained are more easily applied to different situations; debugging of computer program is easier since relative orders of magnitude become predictable. The following dimensionless parameters were introduced.

$$x = \frac{X}{L} \qquad (2.22)$$

$$r = \frac{R}{R_w} \qquad (2.23)$$

$$u = \frac{U}{U_m} \qquad (2.24)$$

$$v = \frac{V}{\left(\frac{R_w U_m}{L}\right)} \qquad (2.25)$$

$$\phi = \frac{T - T_0}{T_w - T_0} \tag{2.26}$$

$$p = \frac{P - P_L}{\rho U_m^2} \tag{2.27}$$

Substitution of the above parameters into equations (2.14) to (2.17) yields the following non-dimensionalized equations.

$$\frac{\partial u}{\partial x} + \frac{1}{r}\frac{\partial}{\partial r}(rv) = 0 \tag{2.28}$$

$$u\frac{\partial u}{\partial x} + v\frac{\partial u}{\partial r} = -\frac{\partial p}{\partial x} + \frac{4H}{Re}\frac{1}{r}\frac{\partial}{\partial r}\left(r\frac{\partial u}{\partial r}\right) + \frac{1}{Re\,H}\frac{\partial}{\partial x}\left(\frac{\partial u}{\partial x}\right) \tag{2.29}$$

$$u\frac{\partial v}{\partial x} + v\frac{\partial v}{\partial r} = -4H^2\frac{\partial p}{\partial r} + \frac{4H}{Re}\frac{1}{r}\frac{\partial}{\partial r}\left(r\frac{\partial v}{\partial r}\right) - \frac{4H}{Re}\frac{v}{r^2} + \frac{1}{Re\,H}\frac{\partial}{\partial x}\left(\frac{\partial v}{\partial x}\right) \tag{2.30}$$

$$u\frac{\partial \phi}{\partial x} + v\frac{\partial \phi}{\partial r} = \frac{4H}{Pe}\frac{1}{r}\frac{\partial}{\partial r}\left(r\frac{\partial \phi}{\partial r}\right) + \frac{1}{Pe\,H}\frac{\partial}{\partial x}\left(\frac{\partial \phi}{\partial x}\right) \tag{2.31}$$

where

$Re = \frac{\rho U_m D}{\mu}$ is the Reynolds number based on diameter;

$Pr = \frac{c_p \mu}{k}$ is the Prandtl number;

$Pe = Re\,Pr$ is the Peclet number;

$H = \frac{L}{D}$ is the length/diameter ratio.

The initial and boundary conditions are also expressed in non- dimensionalized form as

Inlet($x = 0$): $u = 2(1 - r^2)$, $v = 0$, and $\phi = 0$.

Outlet($x = 1$): $\frac{\partial u}{\partial x} = 0$, $v = 0$, and $\frac{\partial \phi}{\partial x} = 0$.

Wall boundaries($r = 1$): $u = 0$, $v = 0$, and $\phi = 1$.

Axis of symmetry($r = 0$): $\frac{\partial u}{\partial r} = 0$, $v = 0$, and $\frac{\partial \phi}{\partial r} = 0$.

Chapter 3

Numerical Implementation

3.1 Introduction

The governing equations (2.28) to (2.31) form a set of non-linear partial differential equations. They cannot be solved analytically in a closed form and hence must be solved numerically. In this problem, where the properties are assumed to be independent of temperature, the major calculation step is the solution of the Navier-Stokes equations which govern the fluid velocity field. Once the velocity field is obtained, the solution of the energy equation is relatively simple.

The difficulty in the solution of the Navier-Stokes equations lies in the unknown pressure field. Each equation contains a pressure gradient term. Yet, there is no explicit equation for obtaining pressure. The pressure field is rather indirectly specified via the continuity equation. This is realized from the fact that when the correct pressure field is substituted into the momentum equation, the resulting velocity field satisfies the continuity equation. Thus, a method of utilizing the continuity equation to obtain the pressure field is required.

In early simulation methods, this was often done by cross- differentiating the momentum equations to eliminate the pressure terms at the cost of increasing the order of the equations and the number of variables. This approach may lead to the stream function/vorticity method with the dependent variables becoming stream function and vorticity. The method enjoys the major advantages of avoiding the explicit appearance of the pressure and not having to solve the continuity equation directly. The method, however, suffers some major shortcomings. The values of vorticity at the boundaries, especially at the solid walls, are not known *a priori*. Instead, approximate vorticity boundary values are arrived at during the course of the solution by extrapolating to the boundary using the latest available field variables. These extrapolation techniques are generally not consistent with the overall numerical scheme and often cause trouble in obtaining a converged solution [27]. Another major disadvantage of the method is that it cannot easily be extended to three- dimensional situations, for which a stream function does not exist.

A more recent approach for treating the velocity-pressure coupling is to transform the continuity equation into an equation for obtaining the pressure, with the understanding that the pressure is only an agent to enforce the continuity requirement. This approach has led to the development of the SIMPLE (Semi-Implicit Method for the Pressure Linked Equations) algorithm. The method uses the so-called primitive variables, namely the velocity components and pressure. Developed in 1972 by Patankar and Spalding [24], the SIMPLE algorithm has been extensively used over the last two decades in resolving the pressure-velocity coupling in incompressible flow problems. Over the years, a number of modifications to the SIMPLE algorithm have been proposed and shown to have better convergence properties. The SIMPLE-R (SIMPLE Revised) algorithm of Patankar [27, 28] and SIMPLE-C (SIMPLE Consistent) algorithm of Van Doormaal and Raithby [11] are examples of such

modifications. The SIMPLE-C algorithm, in particular, has been shown to possess the property of good convergence and improved economy, and thus is used in this study.

3.2 Finite Difference Equations

3.2.1 Grid Definition and Control Volumes

The finite difference grid consists of orthogonal, intersecting grid lines, dispersed over the computational domain along directions parallel to the x- and r- coordinate directions. The spacing between grid lines is, in principle, arbitrary but is normally chosen to minimize the total number of nodes while representing the steep gradients with a greater density of nodes.

In this study, a $M \times N$ unequally spaced grid is employed, where the numbers M and N are to be decided later. The grid is staggered so that the velocities are located at the cell faces, where they are required for mass flow rate calculations, and the scalar variables are located at the nodal points. The advantages of using the staggered grid are described by many researchers [27, 30, 31] and will not be repeated here. The typical control volume of each variable on the staggered grid and the conventional notation of Patankar surrounding a control volume are shown in figure 3.1.

3.2.2 Some Details of Discretization

The finite difference equations are derived by volume integration of the governing equations (2.28) to (2.31) over the cells defined in figure 3.1. Although the full details of derivation are described in references [27, 28], illustration of some major steps as

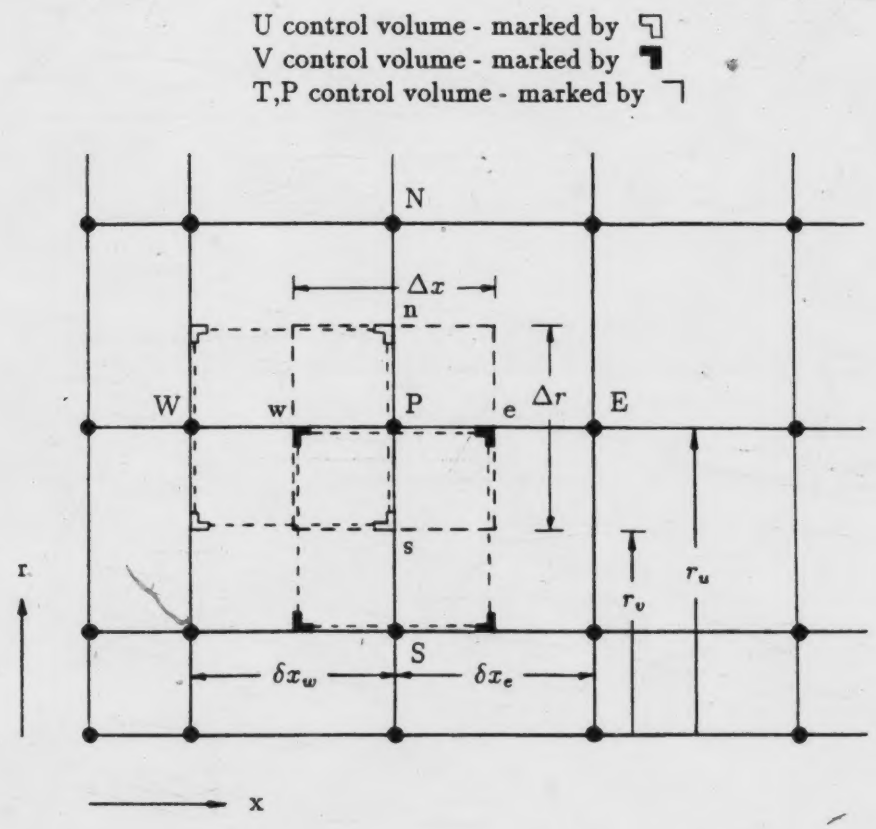

Figure 3.1: Control volume and notation in the staggered grid.

well as comments on the choice of discretization scheme seem appropriate. For these purposes, consider the axial momentum equation. The equation (2.29) can be written as

$$\frac{1}{r}\frac{\partial J_x}{\partial x} + \frac{1}{r}\frac{\partial J_r}{\partial r} = -\frac{\partial p}{\partial x} \tag{3.1}$$

where J_x and J_r are the total (convective plus diffusion) fluxes given by

$$J_x = ruu - \left(\frac{1}{Re\,H}\right) r\frac{\partial u}{\partial x} \tag{3.2}$$

and

$$J_r = rvu - \left(\frac{4H}{Re}\right) r\frac{\partial u}{\partial r} \tag{3.3}$$

The integration of the equation (3.1) over a control volume and using the notation shown in figure 3.1 gives

$$J_e\Delta r - J_w\Delta r + J_n\Delta x - J_s\Delta x = (p_w - p_e)r\Delta r \tag{3.4}$$

The evaluation of flux terms at the control volume faces require an interpolation scheme. The usual second order accurate central difference approximation, using a piecewise-linear profile, presents no particular problem in approximating the diffusion terms. However, convection (e.g. ruu and rvu), which is by its nature a non-symmetrical process, may lead to oscillatory solutions or non-convergent solutions for most practical cell Peclet numbers ($P > 2$), when the central difference scheme is used. A well known treatment for the above difficulty is the first order accurate upwind difference scheme [32, 33]. This scheme guarantees a converged solution; however, at a sacrifice in the solution accuracy by inducing a false diffusion, especially for small cell Peclet numbers. Thus, a compromise must be made between the accuracy and the numerical stability for a successful scheme. Such schemes include: the hybrid difference scheme [33, 34], the quadratic upstream difference scheme [35, 36], the locally exact difference scheme [37] and the power difference scheme [27]. In this

study, the power difference scheme recommended by Patankar is used, because it is unconditionally stable and solutions are accurate if they are grid independent [35]. The scheme switches from one expression to another depending on the cell Peclet number. That is, for a cell Peclet number greater than 10 in magnitude, the power difference scheme reverts to the upwind scheme; otherwise an approximation of the locally exact profile is obtained using a fifth power curve.

The application of this scheme to equation (3.4) leads to the final discretized equation in the following form:

$$a_P u_P = a_E u_E + a_W u_W + a_N u_N + a_S u_S + b \tag{3.5}$$

or more simply.

$$a_P u_P = \sum a_{nb} u_{nb} + b \tag{3.6}$$

where the summation is over the appropriate neighbour points. The coefficients are given as

$$a_E = D_e A(|P_e|) + MAX(-F_e, 0) \tag{3.7}$$

$$a_W = D_w A(|P_w|) + MAX(F_w, 0) \tag{3.8}$$

$$a_N = D_n A(|P_n|) + MAX(-F_n, 0) \tag{3.9}$$

$$a_S = D_s A(|P_s|) + MAX(F_s, 0) \tag{3.10}$$

$$a_P = a_E + a_W + a_N + a_S \tag{3.11}$$

$$b = (p_w - p_e) r \Delta r \tag{3.12}$$

The cell flow rates are given as

$$F_e = u_e r_e \Delta r \tag{3.13}$$

$$F_w = u_w r_w \Delta r \tag{3.14}$$

$$F_n = v_n r_n \Delta x \tag{3.15}$$

$$F_s = v_s r_s \Delta x \tag{3.16}$$

The cell conductances are given as

$$D_e = \frac{r_e \Delta r}{Re\, H(\delta x)_e} \tag{3.17}$$

$$D_w = \frac{r_w \Delta r}{Re\, H(\delta x)_w} \tag{3.18}$$

$$D_n = \frac{4H\, r_n \Delta x}{Re(\delta r)_n} \tag{3.19}$$

$$D_s = \frac{4H\, r_s \Delta x}{Re(\delta r)_s} \tag{3.20}$$

The cell Peclet number P is taken as the ratio of F and D; thus, $P_e = F_e/D_e$ and so on. The function $A(|P|)$ is given as

$$A(|P|) = MAX[0,\ (1 - 0.1|P|)^5] \tag{3.21}$$

The function MAX chooses the larger of the two arguments in the bracket.

The radial momentum equation and the energy equation are similarly discretized, resulting in the same form as equation (3.5) except with minor differences in the coefficients: for the radial momentum equation,

$$a_P = a_E + a_W + a_N + a_S + \frac{4H}{Re}\left(\frac{1}{r}\Delta r \Delta x\right) \tag{3.22}$$

$$b = 4H^2(p_s - p_n) r \Delta x \tag{3.23}$$

and for the energy equation, the Reynolds number Re is replaced by the Peclet number Pe in equations (3.17) to (3.20), and $b = 0$. The indices, of course, should be appropriately interpreted for each equation since each equation uses a different control volume on the staggered grid.

The coefficients in equations such as equation (3.5) depend on the solution for other dependent variables (e.g. v). To handle the resulting inter-equation linkages and nonlinearities, an iterative solution procedure is required. At the beginning of each iteration cycle, the coefficients are evaluated using u, v values obtained in the

previous cycle. With cycle-by-cycle change in coefficients, the resulting change in the u, v values can be quite large, and this may cause slow convergence or even divergence. To moderate the changes in consecutive solutions, under-relaxation is introduced to momentum equations through α as

$$\begin{aligned} \frac{a_P}{\alpha} u_P &= \sum a_{nb} u_{nb} + r\Delta r(p_w - p_e) + \frac{1-\alpha}{\alpha} a_P u_P^* \\ &= \sum a_{nb} u_{nb} + A_P(p_w - p_e) + b_P \end{aligned} \tag{3.24}$$

where u_P^* is the value of u_P from the previous cycle, A_P $(= r\Delta r)$ is the area of the face of the control volume at P, and b_P is the $\frac{1-\alpha}{\alpha} a_P u_P^*$

3.3 The Algorithm

As mentioned before, the continuity equation is converted into a pressure correction equation. Using the staggered grid shown in figure 3, the finite-volume equations for u and v, respectively, have the form of equation (3.24). Rewriting the u- momentum equation for the control volume centered at e, one gets

$$a_e u_e = \sum a_{nb} u_{nb} + A_e(p_P - p_E) + b_e \tag{3.25}$$

where a_e is now $\sum a_{nb}/\alpha$. For a guessed pressure field p^*, the velocity u^* satisfies

$$a_e u_e^* = \sum a_{nb} u_{nb}^* + A_e(p_P^* - p_E^*) + b_e \tag{3.26}$$

If equation (3.26) is subtracted from equation (3.25), the fully implicit velocity correction equation for u is obtained as

$$a_e u_e' = \underbrace{\sum a_{nb} u_{nb}'} + A_e(p_P' - p_E') \tag{3.27}$$

where

$$u = u' + u^* \tag{3.28}$$

$$p = p' + p^* \tag{3.29}$$

In the SIMPLE algorithm, the marked term in equation (3.27) is neglected for economic calculation. In the SIMPLE-C algorithm, however, the velocity correction equations are obtained by subtracting the marked term from both sides of the equation. This yields

$$(a_e - \sum a_{nb})u'_e = \underbrace{\sum a_{nb}u'_{nb} - u'_e} + A_e(p'_P - p'_E) \tag{3.30}$$

The marked term is now neglected, resulting in

$$u_e = u^*_e + d_e(p'P' - p'_E) \tag{3.31}$$

where

$$d_e = \frac{A_e}{a_e - \sum a_{nb}} \tag{3.32}$$

To obtain the pressure correction equation, equations like equation (3.31) for u and v are substituted into the discretized continuity equation for the control volume around the main grid point. i.e.,

$$u_e r_e \Delta r - u_w r_w \Delta r + v_n r_n \Delta x - v_s r_s \Delta x = 0 \tag{3.33}$$

The resulting pressure correction equation has the following form.

$$a_P p'_P = a_E p'_E + a_W p'_W + a_N p'_N + a_S p'_S + b \tag{3.34}$$

where

$$a_E = A_e d_e \tag{3.35}$$

$$a_W = A_w d_w \tag{3.36}$$

$$a_N = 4H^2 A_n d_n \tag{3.37}$$

$$a_S = 4H^2 A_s d_s \tag{3.38}$$

$$a_P = a_E + a_W + a_N + a_S \tag{3.39}$$

$$b = A_w u_w^* - A_e u_e^* + A_s v_s^* - A_n v_n^* \tag{3.40}$$

The SIMPLE-C algorithm uses the TDMA (Tri-Diagonal Matrix Algorithm) procedure to solve for the dependent variables. Each algebraic equation along a constant line (e.g. in the r-direction) can be written as

$$a_P \phi_P = a_N \phi_N + a_S \phi_S + S \tag{3.41}$$

where the other neighbouring (e.g. east and west) terms are incorporated in S and are assumed temporarily as known. It is this formulation (3.41) which allows a line-by-line iteration method. A brief description of the solution procedure is presented below. Details that are omitted here may be found in the original references [11, 27, 28].

1. Guess the pressure field p^*.

2. Solve the momentum equations such as equation (3.26) for u and v using the line-by-line iterations based on TDMA procedure. The obtained velocities u^* and v^* do not, in general, satisfy continuity.

3. Solve the pressure correction equation (3.34) for p'.

4. Apply the pressure corrections to correct pressure using equation (3.26) and velocities using equation (3.31). This eliminates the continuity errors in the current iteration cycle.

5. Using the p found in step 4 as the new p^*, return to step 2. Repeat this iteration cycle until the convergence has been reached to a specified tolerance.

6. Solve the energy equation.

3.4 Convergence Criteria and Accuracy Considerations

This algorithm has been embodied in a computer program using FORTRAN-77 language. Application of the velocity and temperature boundary conditions is straightforward since functions or their gradients are specified at the boundaries. The boundary conditions for the pressure correction equation are not so obvious. The procedure recommended in reference [11] is used to implicitly assure the appropriate boundary treatment of p' depending on the velocity boundary conditions: when the velocity normal to the boundary is specified, $\partial p'/\partial n$ becomes the boundary condition; when the pressure is specified, one should set $p = p^*$ and $p' = 0$ at the boundary. Because of the relative nature of pressure, $p = 0$ can be set as a reference value at any suitable grid point. For the outflow boundary conditions of $\partial u/\partial x = 0$ and $v = 0$, as in the present problem, $p = 0$ is set along the boundary at $x = 1$.

When solving each algebraic equation for a dependent variable, the TDMA solver is applied in alternating directions of x and r. The double sweep is terminated when the residual is smaller than a certain small number or when the number of double sweeps exceeds 10. Usually one double sweep is enough except for the first few cycles of iteration. The overall iteration is terminated when the grid average change in u for two successive iterations is smaller than 0.5×10^{-4} percent, together with the requirement that the grid average continuity error be less than 0.5×10^{-5} percent. In general, the former requirement is satisfied before the latter. The complete code is listed in Appendix A.

3.5 Test of Computer Program

The validity of the computer program was tested by solving a problem of laminar forced convection heat transfer in a smooth circular duct. This problem has been thoroughly studied and well documented. Among many different cases, the combined hydrodynamic and thermal entry length (or simultaneously developing flow) problem is considered here.

The irrotational inlet initial condition (i.e. $u = 1$, $\partial v/\partial x = 0$) and the constant wall temperature thermal boundary condition were used for the purpose of comparison with existing results. The solutions were obtained on the Åmdahl 5870 mainframe computer using a 22×15 unequally spaced grid system, with the fine grid size near the entrance region and near the wall, and a coarser grid as the fully developed region is approached. With the optimum under-relaxation factor of 0.75, a convergence was obtained after 45 iterations requiring about 32 seconds of CPU time. For an indication of the accuracy of the numerical solutions, some calculations were carried out using a 44×30 grid. The largst disagreement of the local friction factors and local Nusselt numbers was smaller than one percent.

Figure 3.2 shows the development of the axial velocity profile for $Re = 100$. The small Reynolds number was deliberately chosen to show the so- called velocity overshoots or axial velocity inflections [1, 25]: the velocity profiles have a local minimum at the tube centerline and symmetrically located maxima on either side of the centerline near the tube wall. The velocity overshoots have also been observed by other investigators [25, 38, 39]. These peculiar velocity profiles occur near the entrance region ($x^+ \leq 0.005$) for $Re \leq 400$, when the effects of axial diffusion of momentum and radial pressure gradient are included in the analysis (i.e. when the full Navier-Stokes equations are solved). The detailed explanation of this phenomenon

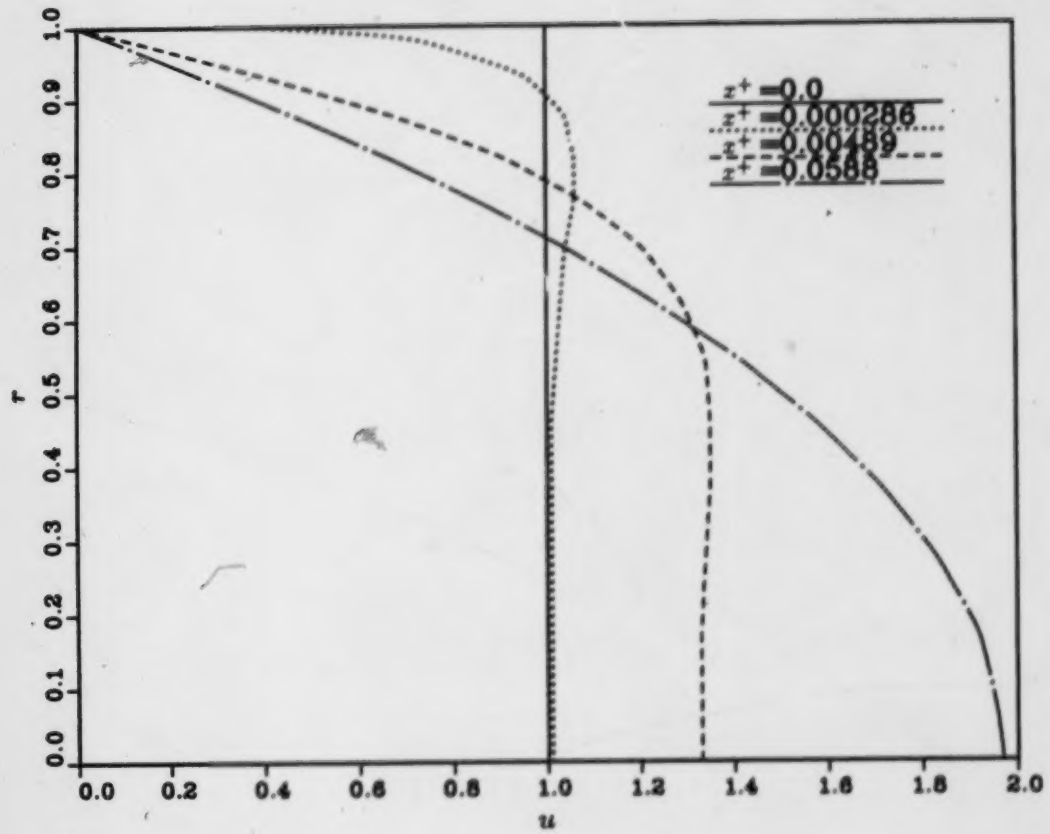

Figure 3.2: Axial velocity profiles in developing region of a circular duct for $Re = 100$.

is given in reference [1].

The hydrodynamic entrance length L_{hy} is defined, following Shah and London [1], as the duct length required to achieve a maximum velocity of 99 percent of the corresponding fully developed magnitude when the entering flow is uniform. For the circular tube, its commonly accepted value is given as

$$\frac{L_{hy}}{D} = 0.59 + 0.056Re \tag{3.42}$$

The present study produces L_{hy} values within 2 percent of the equation (3.42).

Figure 3.3 compares the calculated friction coefficient data, expressed as $f_{app}Re$ as a function of x^+, with those of other researchers. In the literature, f_{app} is called an apparent Fanning friction factor, defined as

$$f_{app} = \frac{\left(\frac{\Delta P}{\frac{1}{2}\rho U_m^2}\right)}{\left(\frac{X}{R_h}\right)} = \frac{\Delta p}{2H\,x} \tag{3.43}$$

Thus, f_{app} is based on the total pressure drop from $x = 0$ to x. It takes into account both the skin friction and the change in momentum rate due to change in the shape of the velocity profile in the hydrodynamic entrance region. For convenience, the subscript will be dropped and f will have the same meaning as f_{app} from now on. Due to the presence of the transverse pressure gradient in the entrance region, Δp is calculated by $p_0 - \overline{p_x}$, where $\overline{p_x}$ is the area integral average pressure at a specified axial location (this is calculated using the numerical spline integration method), and p_0 is the centerline pressure at the tube entrance. As shown in the figure, $f_{app}Re$ values of the present study are very close to those of Schmidt [40] at $Re = 500$ except for low values of x^+. For $x^+ < 0.002$, Schmidt's results are said to be questionable according to Shah and London [1]. Liu's solutions involve the boundary layer approximations (they are independent of Re or the inlet block profiles) and therefore they are considered to be less accurate, especially near the inlet region.

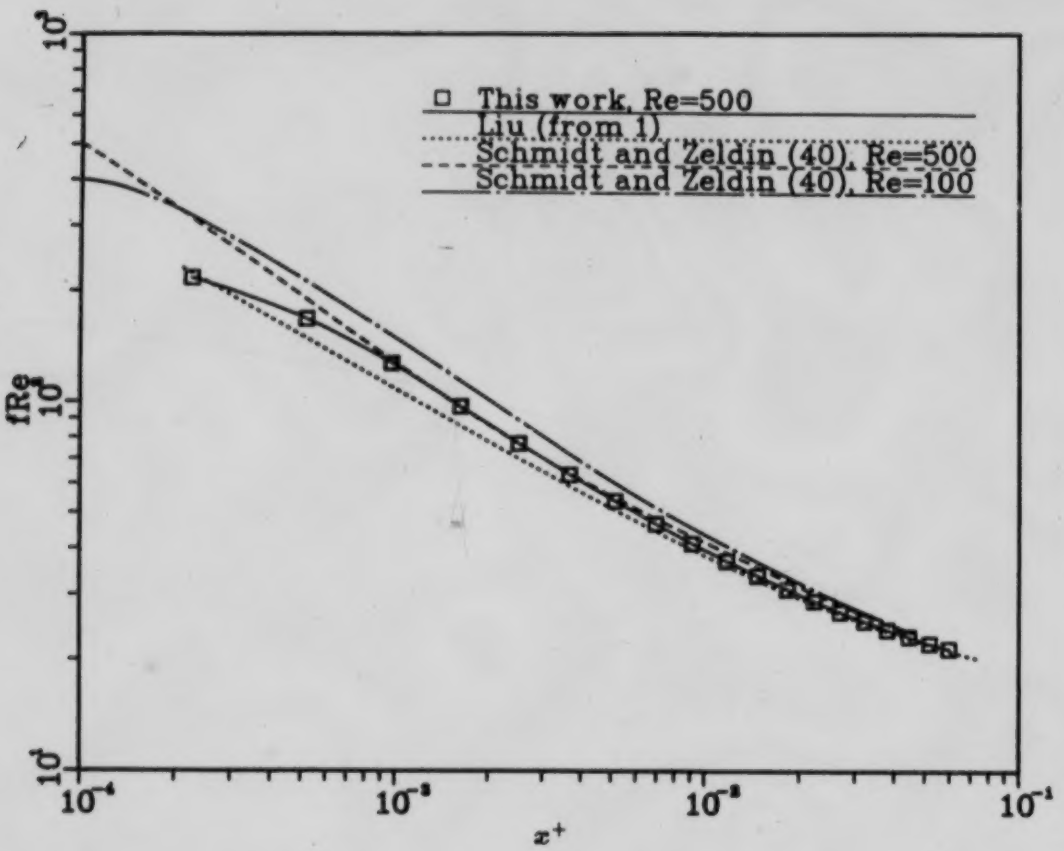

Figure 3.3: Comparison of the apparent Fanning friction factor for laminar flow in entrance region of a circular duct.

Figure 3.4 shows the comparison of the local Nusselt number obtained from this work with results of other studies. The local Nusselt number is given by

$$Nu_x = \frac{hD}{k} = \frac{D\frac{\partial T}{\partial R}|_w}{T_w - T_m} = \frac{2\frac{\partial \phi}{\partial r}|_{r=1}}{1 - \phi_m} \tag{3.44}$$

where ϕ_m is the fluid bulk mean temperature at an arbitrary cross section x defined as

$$\phi_m = 2\int_0^1 u\,\phi\,r\,dr \tag{3.45}$$

and is again evaluated using the spline integration method. The figure shows that the calculated Nusselt numbers closely follow those of Schmidt. Away from the immediate inlet, the boundary layer type solutions of Manohar [42] and Hwang and Shew [43] also agree quite well. The Nu_x asymptotically approaches the exact value of 3.66. The thermal entrance length L_{th} is defined as the length required to achieve a value of local Nu_x equal to 1.05 Nu_x for fully developed flow. For simultaneously developing flow and $Pr = 0.7$, its value, according to references [40] and [41], is given as

$$\frac{L_{th}}{D\,Pe} = 0.037 \tag{3.46}$$

The value produced by the present study is 0.038, about 3 percent higher than the above value.

The results discussed so far indicate that the computer program is running with sufficient accuracy, and therefore the next step of eversion modelling study can be taken.

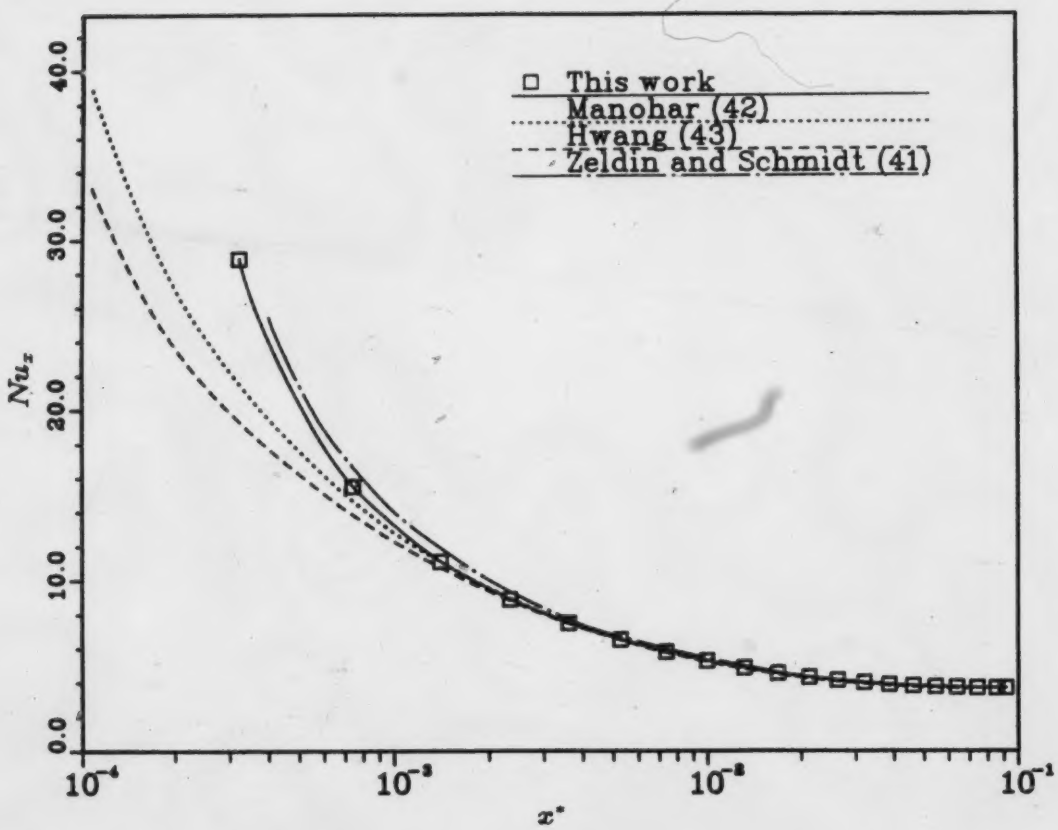

Figure 3.4: Comparison of local Nusselt number for simultaneously developing laminar flow in a circular duct with uniform wall temperature.

Chapter 4

Single Eversion

4.1 Introduction

In this chapter, enhancement by a single evertor is studied. The problem considered here is sketched in figure 4.1. The flow is everted at the inlet of the tube according to the three eversion models and the effect of each eversion on the pressure drop and heat transfer is investigated. A single evertor inserted in a long tube may not produce significant changes in the pressure drop or heat transfer. However, the study of single eversion can be useful to explain how eversion brings about such changes by examining the fluid velocity and temperature profiles after the process of eversion.

The fluid enters the tube with a fully-developed velocity profile and a block temperature profile ($\phi = 0$). The fluid is being heated by the wall which maintains a constant temperature ($\phi = 1$). The parameters involved are Re, Pr, r_* and H. As an initial study, the parameters are conveniently chosen to be as follows: Re=1000, Pr=0.71, r_*=0.707 and H=50. The effects of varying these parameters on

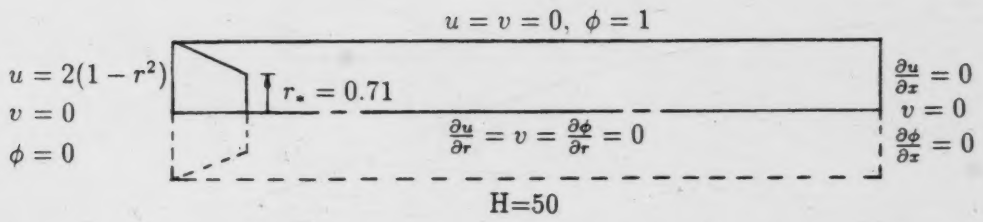
$u = v = 0,\ \phi = 1$
$u = 2(1 - r^2)$
$v = 0$
$\phi = 0$
$r_* = 0.71$
$\frac{\partial u}{\partial x} = 0$
$v = 0$
$\frac{\partial \phi}{\partial x} = 0$
$\frac{\partial u}{\partial r} = v = \frac{\partial \phi}{\partial r} = 0$
H=50

Figure 4.1: Sketch of single eversion problem.

the pressure drop and heat transfer will be studied in the next chapter.

4.2 Velocity and Friction Results

Solutions to the differential equations have been obtained with a 24×19 non-uniform mesh, first for the smooth tube and then for the tube containing a hypothetical evertor of three different kinds. Axially, the grid is designed to emphasize the region immediately downstream of the evertor where the effect of eversion is expected to be most significant, and progressively less as the outlet is approached. Radially, 10 equally spaced nodal points are placed from $r = 0$ to $r = r_*$ and another 10 from $r = r_*$ to $r = r_w$. This radial grid is chosen to accommodate the ring exchange in the eversion models, specifically the ideal eversion model and the laminate eversion model.

Figure 4.2 shows the effect of ideal eversion on a fully developed (parabolic) input velocity profile. The everted profile, calculated from the equation 2.5, is shown as a dotted line. It has rather a strange shape: the velocity near the wall is seen

to increase significantly while compensation takes place in the central region. The independence of the everted profile shape on the number of radial nodal points was tested by doubling the number of radial nodal points: maximum change in the local velocity was less than one percent. The conservation of mass flow was also tested by comparing mass flow calculated from the velocity profile before and after eversion: agreement was within one percent. The small discrepancy may be attributed to the averaging process involved in the model and the round-off error in numerical spline integration. The subsequent development of the everted profile is also shown in the figure. Re-establishment of fully-developed profile occurs after about 50 tube diameters.

Figure 4.3 shows laminate eversion under the same condition. The everted profile is enormously different from the fully developed form, creating a very high wall shear stress immediately downstream of the evertor and a surge in core velocity. Not surprisingly, the length required to restore the parabolic velocity profile is much greater. Figure 4.4 shows the corresponding profiles for mixed eversion. The everted profile is shown by the two block profiles separated at r_*. To avoid computational singularity at r_*, an average value was taken at that nodal point. The subsequent development of the two block profiles to a fully- developed profile is seen to occur relatively quickly. All of the above three figures show that eversion creates a velocity profile that is radically different from the parabolic profile and that its effect is maintained over a considerable distance from the entrance. This effect, specifically the increase in velocity near the wall, will contribute to the increase of heat transfer coefficients, as will be discussed in the next section.

Pressure changes during eversion are the result of two superimposed effects: the skin friction and the change in momentum flux (due to change in the shape of the

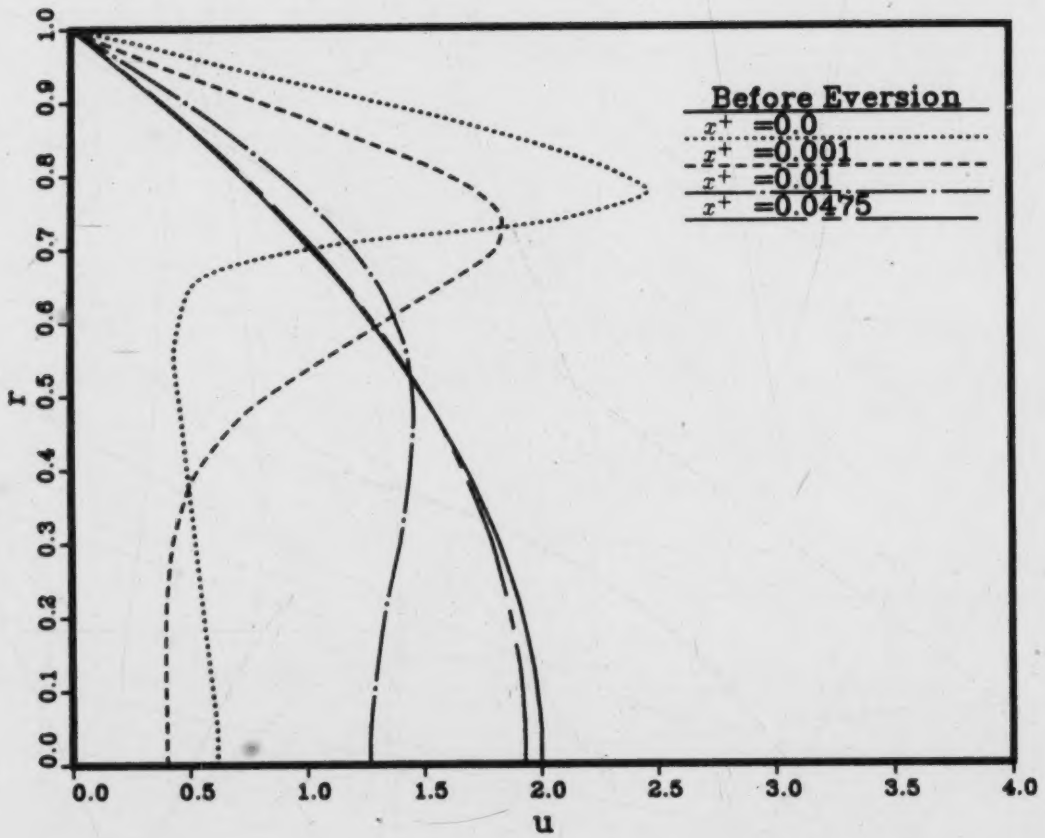

Figure 4.2: Velocity profile development for $Re = 1000$, $H = 50$, and $r_* = 0.707$: ideal eversion.

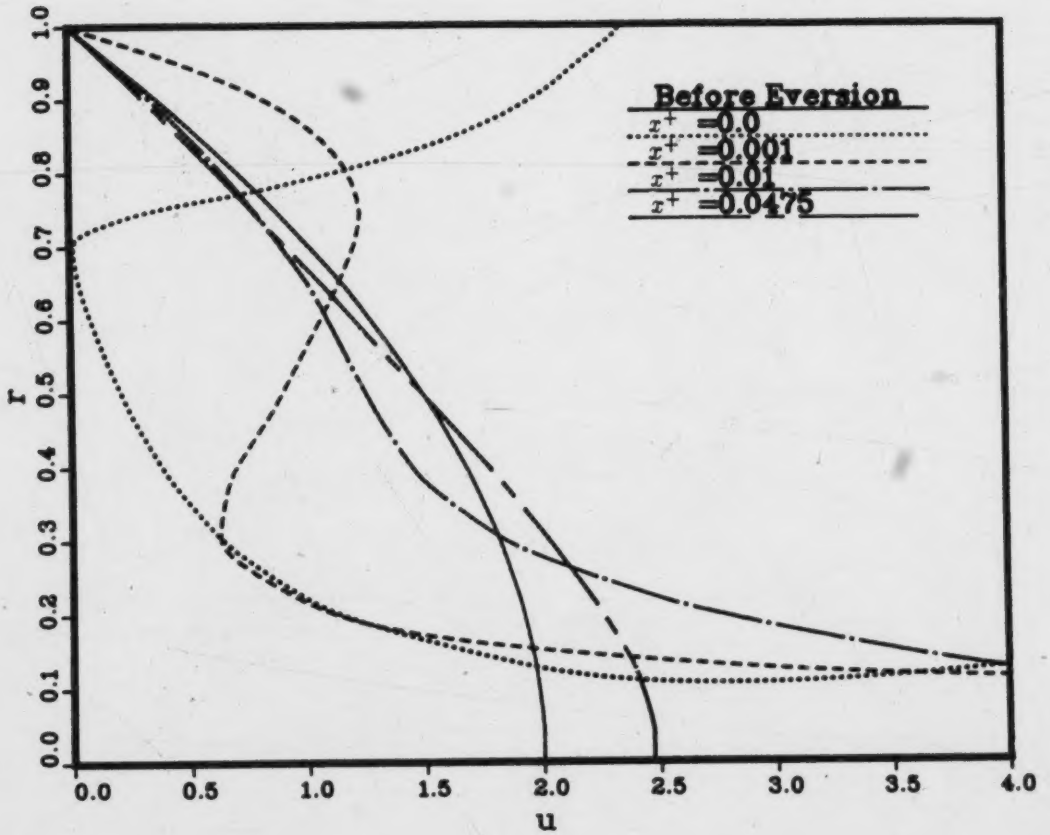

Figure 4.3: Velocity profile development for $Re = 1000$, $H = 50$, and $r_* = 0.707$: laminate eversion.

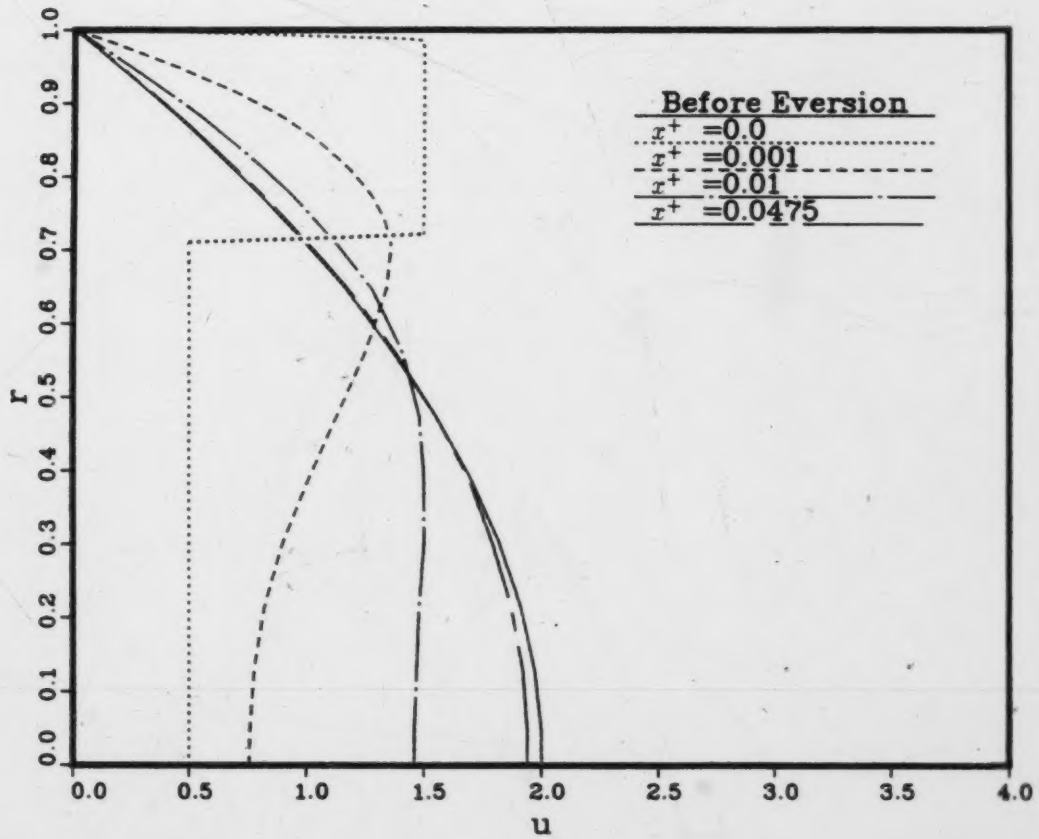

Figure 4.4: Velocity profile development for $Re = 1000$, $H = 50$, and $r_* = 0.707$: mixed eversion.

velocity profile). The skin (or drag) friction effect may be represented by

$$\Delta P_d = C\, l \left(\frac{dP}{dX}\right)_0 \tag{4.1}$$

where $\left(\frac{dP}{dX}\right)_0$ is the pressure gradient in the bare tube and C is a coefficient chosen to reflect the geometry of the evertor: notably the surface and cross-sectional areas to which the fluid is exposed. Values of $C = 2$ and $C = 3$ were tried and the difference was found to be minor, as will be shown later. However, in order to be conservative, a value of $C = 3$ has been used throughout. The length of evertor, l, was assumed to be $2D$. The change in momentum flux during the process of eversion may be translated into a pressure change by the expression

$$\Delta P_e = \frac{4(M' - M)}{\pi D^2} \tag{4.2}$$

where M is the momentum flux immediately upstream of the evertor and is calculated as

$$M = 2\pi\rho \int_0^{R_w} U^2\, R\, dR \tag{4.3}$$

M' is the momentum flux immediately downstream of the evertor and is similarly calculated.

In figure 4.5, the bare tube pressure profile is described by the curve ABE which would be altered to ABE' if velocity profile development alone were considered with eversion taking place at B. If the drag and momentum pressure changes are assumed to be localized at the plane of eversion, the pressure would follow the full line $ABCD$: the segment CD is simply BE' lowered by the amount BC. This composite pressure profile has been used to determine the friction factors discussed below. In reality, the pressure profile through the evertor may look more like the chain dotted curve, but this fact would not change the conclusions given later.

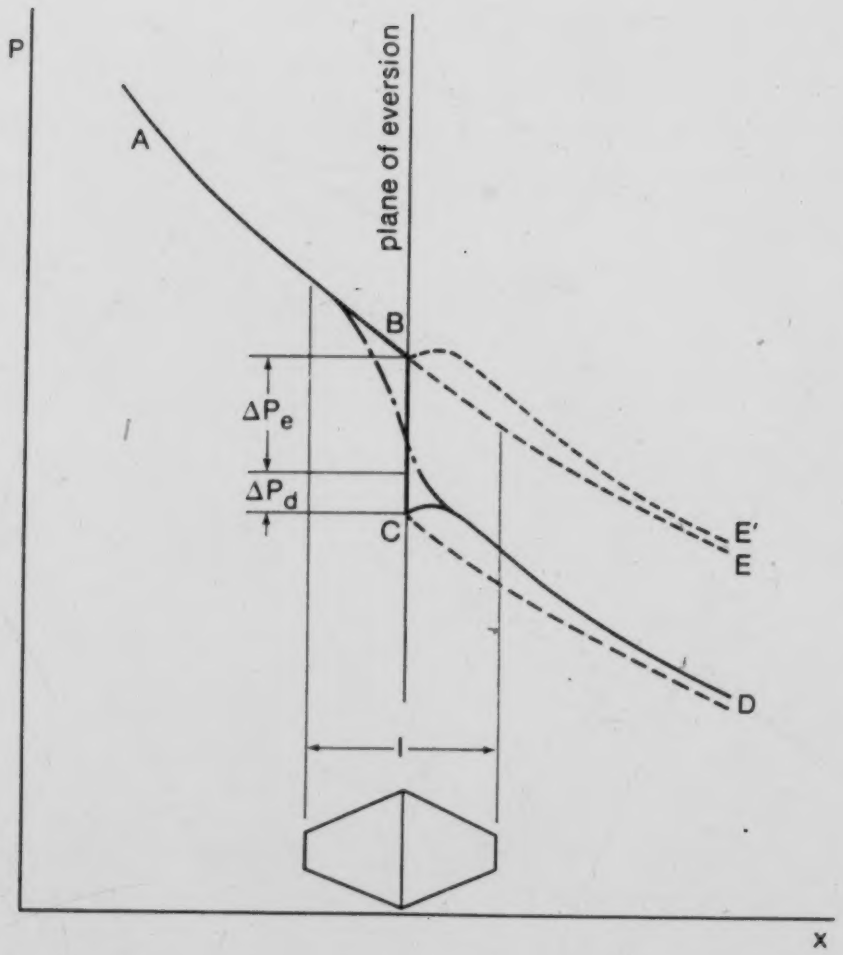

Figure 4.5: Composite pressure profile after eversion.

Figure 4.6 shows the pressure profile for each type of eversion. For each of the three eversion curves, the discontinuity at $X/D = 0$ (the initial pressure difference from the value of the smooth tube) represents the localized sudden pressure drop during the process of eversion. For the given conditions, Δp_e is calculated to 0.184, 0.877 and -0.113, for ideal, laminate and mixed eversion, respectively. Δp_d is found to be 0.091 in each case. The pressure drop downstream of the evertor depends on the everted velocity as it tends towards establishment of the fully-developed form further downstream. As figure 4.3 shows, the flow field after laminate eversion is slowest to recover and hence the pressure drop due to momentum change is the smallest, resulting in the smallest total pressure drop. The opposite is true for mixed eversion.

The corresponding apparent Fanning friction factors are shown in figure 4.7. Results from using both $C = 2$ and $C = 3$ are shown for each eversion to show that the resulting difference in friction factor is minor. The smooth tube data are in excellent agreement with the well-known analytical solution of $f = 16/Re$. Compared to this data, all of these curves show a significant increase in friction factor, as would be expected from the alterations in the velocity profile produced by eversion. For laminate eversion, the initial large Δp_e during the eversion process results in the highest friction factors over the first 20 tube diameters, but further downstream the friction factors become lowest due to the slow development of the velocity profile, as figure 4.6 suggests. On the other hand, the lowest initial disadvantage in mixed eversion is not maintained. Instead, mixed eversion ends up with the highest friction factors after 20 tube diameters.

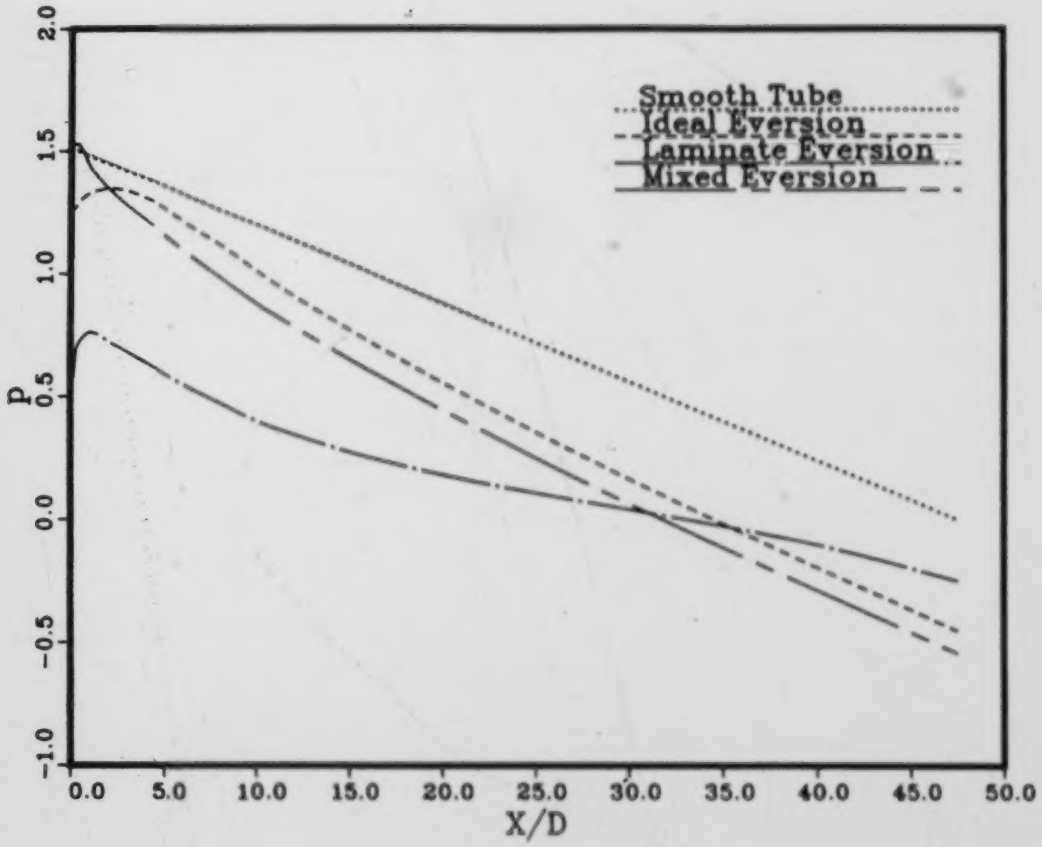

Figure 4.6: Pressure profile for $Re = 1000$, $H = 50$, and $r_* = 0.707$: single eversion.

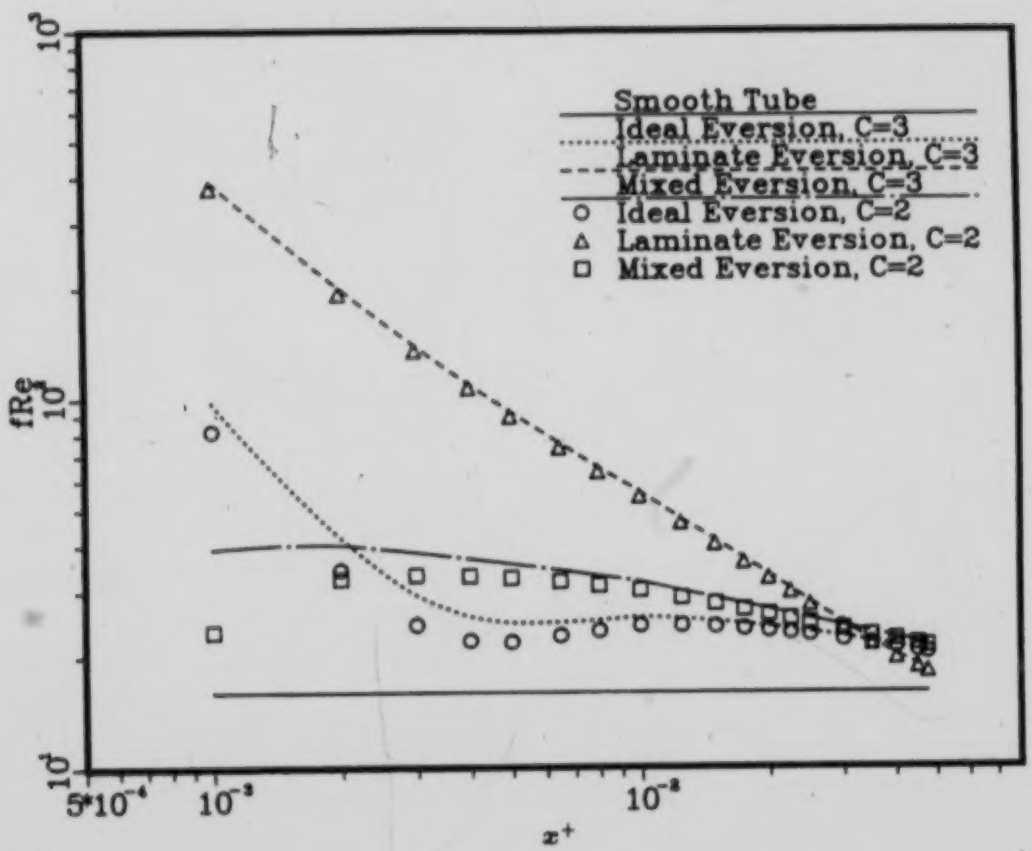

Figure 4.7: friction factor profile for $Re = 1000$, $H = 50$, and $r_* = 0.707$: single eversion.

4.3 Temperature and Heat Transfer Results

It was noted in chapter 2 that temperature plays a passive role during eversion and that the advective flux, unlike the momentum flux, is preserved across the evertor. Viscous dissipation has been neglected throughout, and the possibility that heat may be transferred between streams crossing each other has been ignored. In other words, it has been assumed that the rate of heat conduction between the tube wall and the fluid immediately adjacent to it changes discontinuously across the plane of eversion solely as the result of plumbing arrangements which exchange hotter and colder fluid.

If eversion is not considered, the thermal entrance problem with a parabolic inlet velocity profile is an extended Graetz problem with axial heat conduction when the tube is maintained at a constant and uniform temperature different from the uniform temperature of the fluid at the entrance. It has long been known that, except for the immediate neighbourhood of $x^* = 0$, axial heat conduction within the fluid is negligible for $Pe > 50$ [1]. Therefore, the solution to the classical Graetz problem essentially forms the basis for comparison with the results of eversion. The Graetz problem is one of the fundamental problems for internal flow convection heat transfer. In addition to its great practical importance, it has induced many applied mathematicians to apply and test different mathematical methods and approaches, since a closed-form solution exists for this problem. In figure 4.9, the comparison of the Graetz problem solution with the present solution for the case of $Pe = 710$ is shown. Agreement is seen to be excellent for a smooth tube.

With an evertor at the inlet, however, the problem becomes another kind of extended Graetz problem with non-uniform inlet temperature and/or non-parabolic velocity profiles. The Graetz problem with non-uniform inlet temperature was investigated by Hicken [from 1]. He considered five different one-period sinusoidal

fluid temperature profiles at $x^* = 0$. For the case of heat transfer from the fluid to the wall, he found the following results. For the case of sinusoidal variations in the inlet fluid temperature with the minimum temperature at the center of the pipe, the Nusselt numbers were higher than those for the uniform inlet temperature case. Decreasing this temperature at the pipe center increased the magnitude of the Nusselt number in the thermal entrance region. For the fluid temperature having a maximum value at the pipe center, the reverse effect on Nusselt number was found.

To investigate the effect of the non-parabolic inlet velocity profile, Barrow and Humphreys [from 1] analyzed the Graetz problem with slug, inverted conical, and inverted parabolic velocity profile for the thermal entrance region. They presented Nu_x as a function of x^* for different velocity profiles. Their results showed that for a given flow rate, the increase in velocities near the wall resulted in a shortening of the thermal entry length and an increase in the heat transfer coefficients, as expected.

It is thus expected that eversion, in general, would bring the combined results of the two effects discussed above, since eversion artificially forces the higher temperature gradients near the wall as well as increasing the velocities there.

The development of the everted temperature profile is shown in figure 4.8 for each type of eversion. In the present case, where the block temperature profile is used as an initial inlet condition, it is to be expected from the equations (2.7), (2.9), (2.12) and (2.13), that eversion would produce no immediate change in the everted temperature profile. As the figure indicates, the pre-eversion and post-eversion profiles are identical. The subsequent development of the temperature profile differs from the smooth tube development solely because the velocity field has been everted. As expected, all curves of eversion show an initial increase in temperature gradients at the wall over the smooth tube curves. The figure shows that ideal eversion creates the greatest initial steepening in the temperature profile adjacent to the wall, the

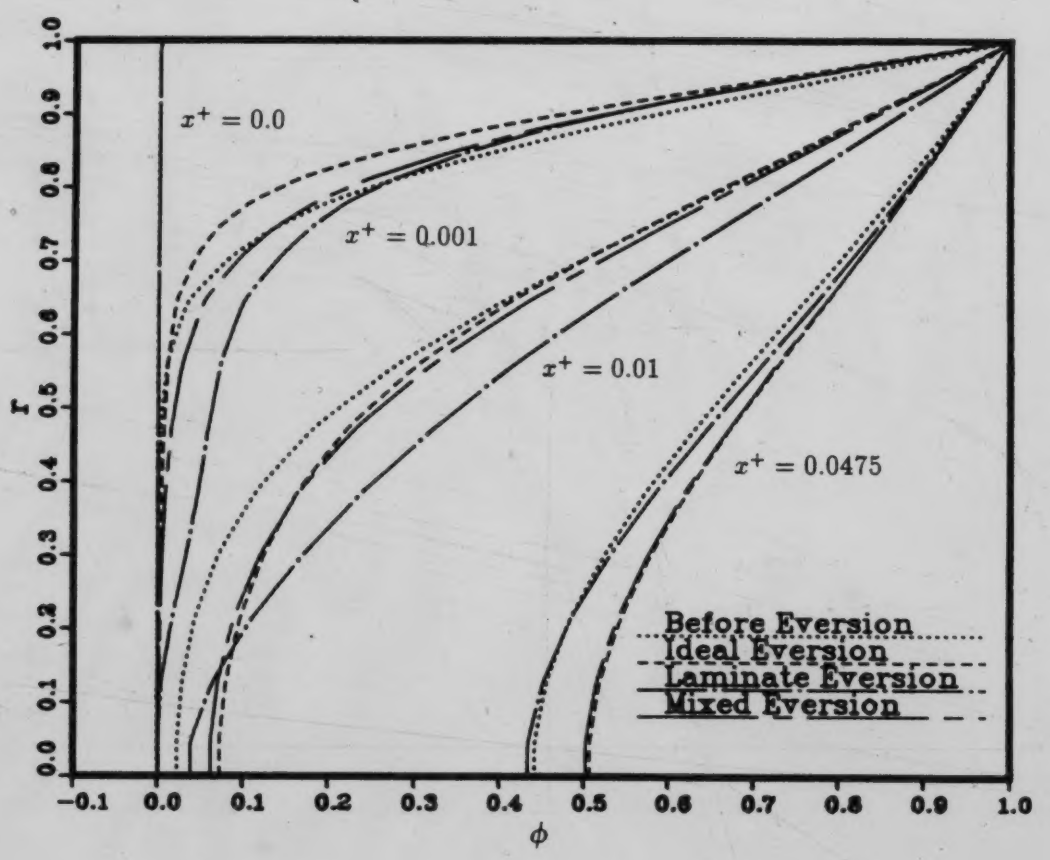

Figure 4.8: Temperature profile development for $Re = 1000$, $Pr = 0.71$, $H = 50$, and $r_* = 0.707$: single eversion.

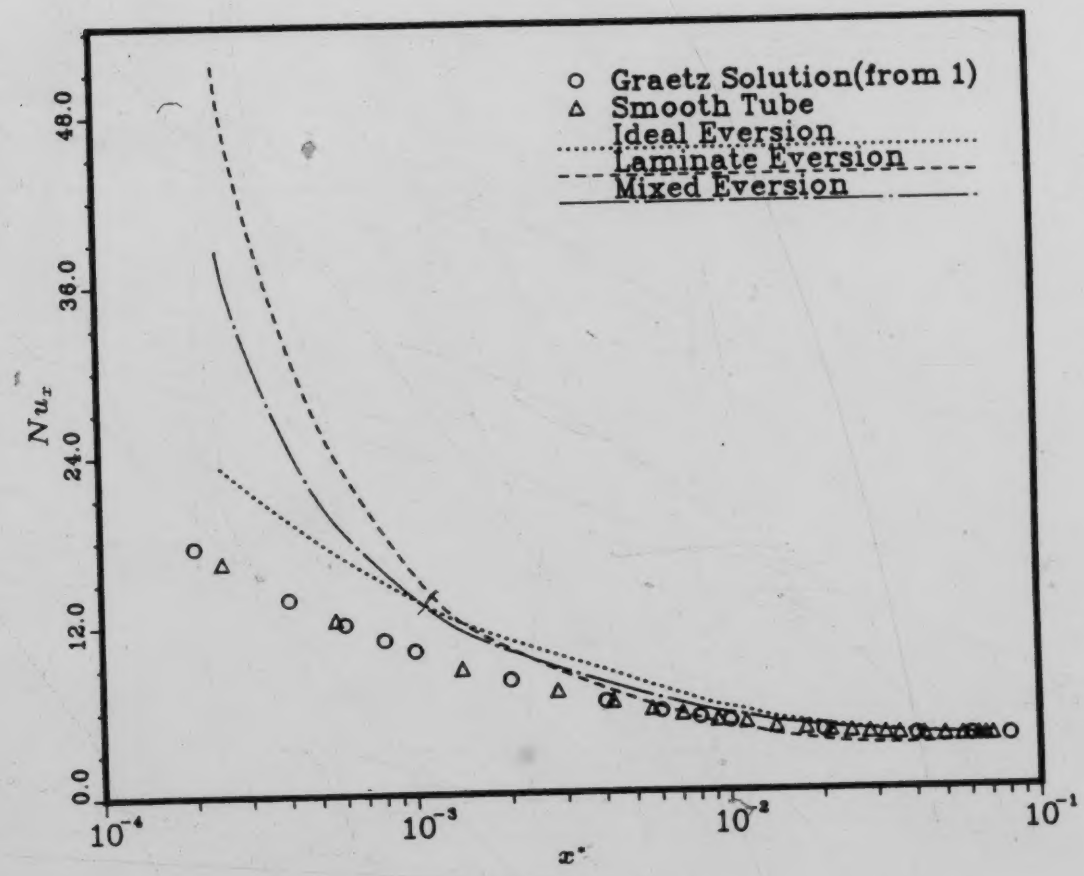

Figure 4.9: Local Nusselt number development for $Re = 1000$, $Pr = 0.71$, $H = 50$, and $r_* = 0.707$: single eversion.

effect being smaller for mixed eversion and smaller again for laminate eversion.

The effect of advection may be seen more clearly in figure 4.9 which shows the local Nusselt number for each type of eversion. It shows a significant increase in local Nusselt number in the first two diameters downstream of the evertor. Much further downstream, e.g., beyond 7 diameters, only a small increase in heat transfer coefficients is produced by ideal and mixed eversion. Laminate eversion even produces Nusselt numbers smaller than those for a bare tube for distances greater than about 6 diameters, under these conditions. The effect of eversion on advection, thus, generally extends over many tube diameters and is not necessarily uniform. The precise details follow from the solution of the energy equation.

The fact that the effectiveness of eversion on heat transfer is particularly high during the first few diameters downstream of an evertor suggests the use of repeated eversion in order to get maximum heat transfer augmentation. This problem will be dealt in the next chapter.

Chapter 5

Repeated Eversion

5.1 Introduction

In chapter 4, the idea of eversion to enhance heat transfer rates was studied in a very simple manner by examining a tube with a single evertor. Each of the involved parameters was given a fixed value. The results showed that an evertor produced very high local heat transfer augmentation for the first few diameters downstream, and its effectiveness was quickly reduced further downstream. From this result one can expect that a series of evertors placed a few diameters apart would produce the repeated effect of single eversion, resulting in a very high average heat transfer rate. This repeated eversion, along with the study of the effects of varying parameters, will be investigated in the present chapter.

The study of repeated eversion is carried out in a tube with five equally spaced evertors, the first evertor being at the tube inlet. The boundary conditions are unchanged. In numerical computations, the whole domain was divided into five sections, the first section being from the inlet to the next evertor, and so on. A

12×19 non-uniform mesh was laid out in the first section. Solutions were obtained in that section treating it as a separate single eversion problem. The solutions were stored. The same grid was then laid out in the next section which was considered as another single eversion problem. The velocity and temperature profiles at the exit from first section were treated as inlet conditions to the second. After the whole domain was covered, the section-by-section solutions were combined to form an overall solution.

The following range of the independent variables was used in the repeated eversion.

$$\text{Reynolds number: } 100 < Re < 2000$$
$$\text{Prandtl number: } 0.71 < Pr < 1000$$
$$\text{Spacing: } 3 < s < 12$$
$$r_*\text{: } 0.38 < r_* < 0.88$$

Reynolds number was limited to 2000 since we are only concerned with the laminar flow range. Prandtl number smaller than 0.71 was not included here. Different spacing can be set either by varying the number of evertors with a fixed tube length or by varying the length of tube with a fixed number of evertors. The former requires an excessive computational effort and cost, and therefore the latter was adopted using five evertors. A tube with a length of $H = 25$ would, thus, give $s = 5$. Since the length of each evertor is assumed to be $2D$, s must be greater than 2. The "standard" values of each parameter $Re = 1000$, $Pr = 10$, $s = 8$, and $r_* = 0.707$ were arbitrarily chosen for the purpose of presenting results: they are considered to be representative.

5.2 Results and Discussion

The pressure drop data and corresponding friction factor data for the "standard" parameter values are shown in figure 5.1 and 5.2, respectively. In generating these results it has been assumed that each evertor does not affect its neighbour upstream, but the pressure drop incurred inside the evertor influences the pressure level downstream. Instead of presenting the friction factor data on logarithmic axes, which is usually done, the abscissa is given in linear form for ease of interpretation. The sudden pressure change followed by a small pressure recovery is shown at, and immediately downstream of, the location of each evertor. Unlike the single eversion results, laminate eversion is seen to produce the highest friction factors here. In single eversion, the long tube after the process of eversion allowed the flow to develop almost fully, and the slow development of velocity profiles for laminate eversion resulted in the smallest friction factor despite the large initial ΔP_e. In repeated eversion, however, the fluid does not have much chance to develop due to the short tube length between evertors, and the large ΔP_e at the locations of evertors dominates the total pressure drop. For ideal eversion, a small initial ΔP_e and the fast development of velocity profiles result in the smallest friction factor. Mixed eversion has a negative ΔP_e at the locations of evertors (for evertors having r_* less than about 0.7), but the development of velocity profiles is fastest resulting in the second highest friction factor.

Turning to the heat transfer results, the local Nusselt number plotted against distance from the tube inlet is shown in figure 5.3. The improvement over the smooth tube values for the first eight diameters is seen to be rather small. This is because the region is well within the thermal entry length having already high heat transfer rates. The most striking improvement is that resulting from each subsequent eversion. A

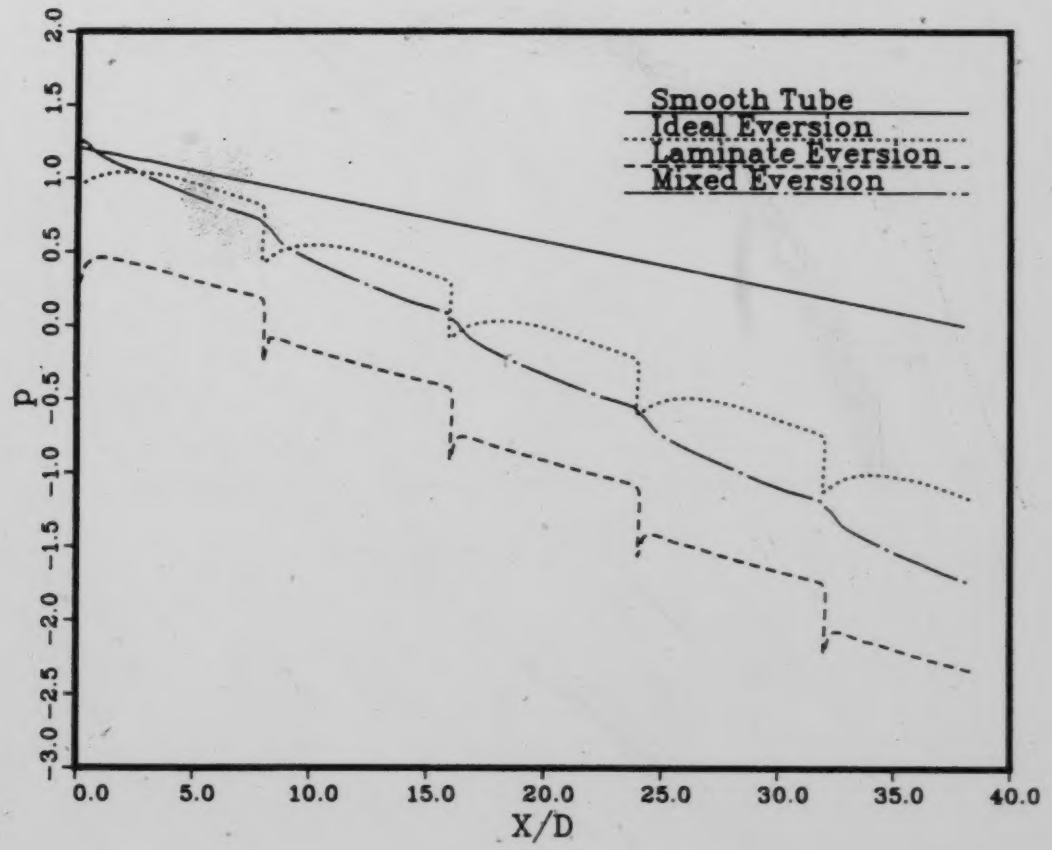

Figure 5.1: Pressure profile for $Re = 1000$, $Pr = 10$, and $s = 5$: repeated eversion.

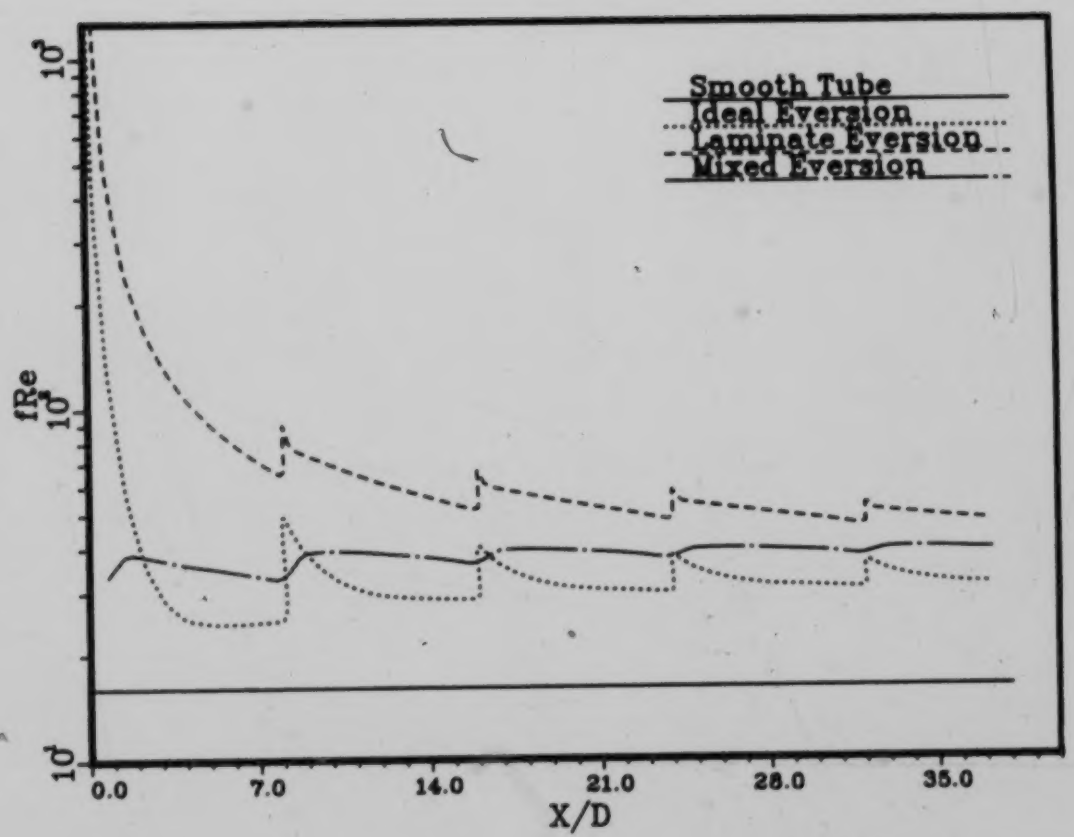

Figure 5.2: Friction factor profile for $Re = 1000$, $Pr = 10$, and $s = 5$: repeated eversion.

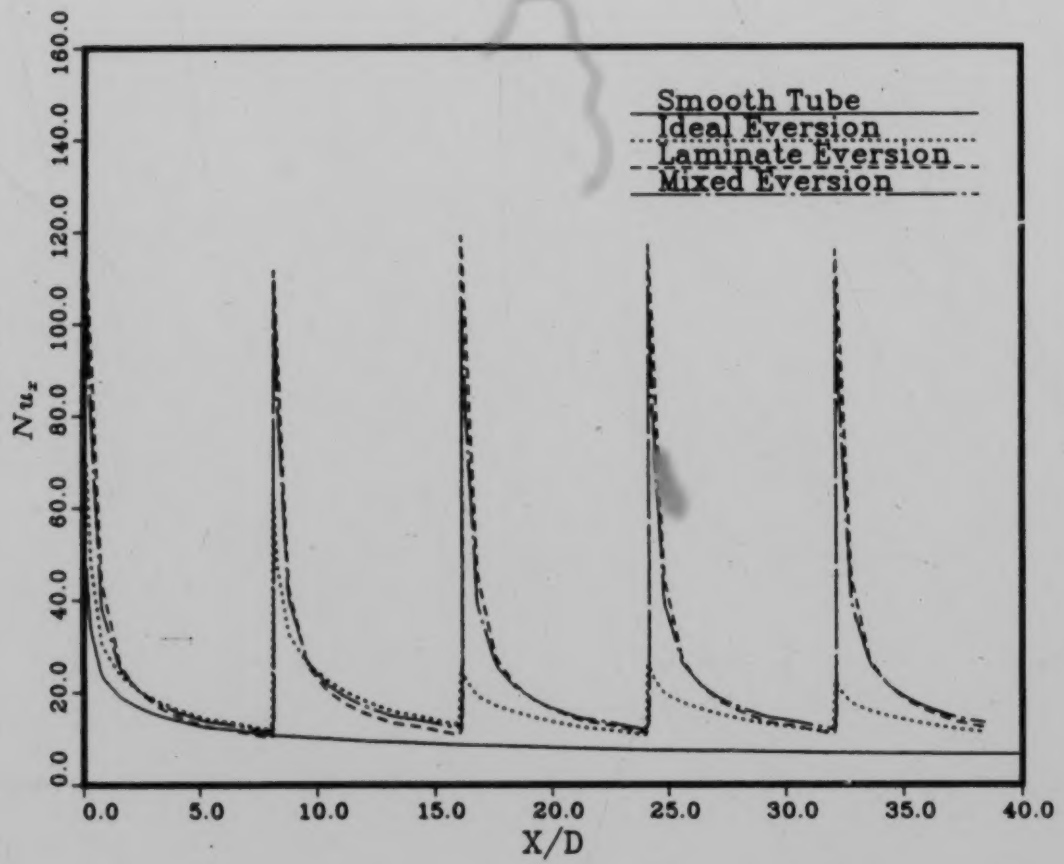

Figure 5.3: Local Nusselt number development for $Re = 1000$, $Pr = 10$, and $s = 5$: repeated eversion.

substantial increase in the local Nusselt numbers occurs for the entire region of eight diameters downstream of each evertor. Even at this high Peclet number of 10^4, where the thermal entry length is very long according to the equation (3.4), the local Nusselt numbers for the smooth tube after about 15 tube diameters are not significantly different from the asymptotic value of 3.66. Therefore, each subsequent evertive improvement is a significant gain.

5.3 Effects of Reynolds Number Variation

The variations of friction factor and mean Nusselt number with Reynolds number are shown in figure 5.4 and figure 5.5, respectively, for $Pr = 10$, $r_* = 0.707$, and $s = 8$. These figures clearly show the effectiveness of evertors in augmenting heat transfer rates. All three eversion models show a significant increase in mean Nusselt number with a comparable increase in friction factor at each Reynolds number. They also show that the increase depends on Reynolds number: in general, the higher the Reynolds number the higher increase in both heat transfer and pressure drop due to the inertial effect. At $Re = 100$, the friction factor is about 1.6 times that of the smooth tube, while the Nusselt number is about 1.8 times that of the smooth tube for all three eversion models. At $Re = 2000$, the friction factor is 4.3 times that of the smooth tube for laminate eversion, while the mean Nusselt number is 2.75 times that of the plain tube. Both laminate eversion and mixed eversion are seen to possess very similar heat transfer characteristics, but laminate eversion produces a greater pressure drop, especially at higher Reynolds numbers. The effectiveness of ideal eversion in augmenting heat transfer drops off significantly for Reynolds numbers greater than 200, producing the smallest increase in Nusselt number. Thus, mixed eversion seems to have the best combined characteristics of heat transfer and pressure

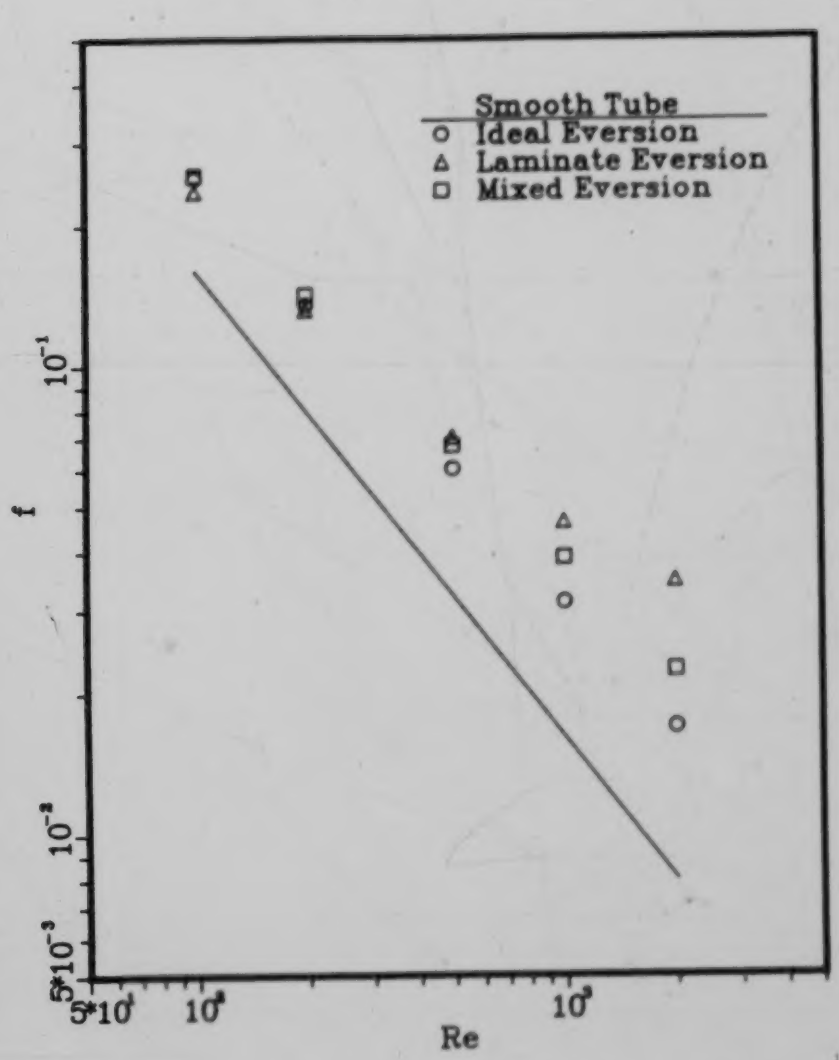

Figure 5.4: Effect of Re on friction factor for $Pr = 10$, $r_* = 0.707$, and $s = 8$.

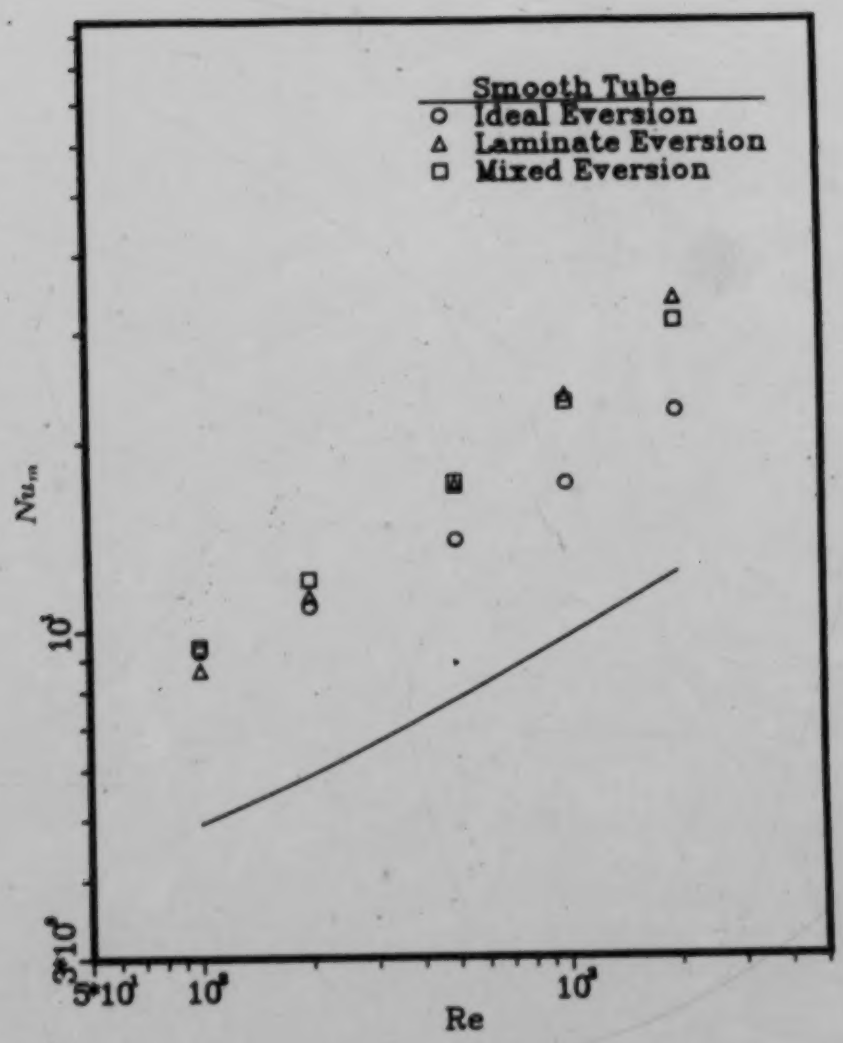

Figure 5.5: Effect of Re on mean Nusselt number for $Pr = 10$, $r_* = 0.707$, and $s = 8$.

drop. This is an encouraging result because, in practice, exact ring exchanges in ideal eversion or laminate eversion may be difficult to achieve and with evertors of simple geometry, such as the one shown in figure 1.1, mixed eversion is most likely to occur. At $Re = 200$, the mean Nusselt number is 2.52 times and the friction factor is 2.79 times the value of smooth tube for mixed eversion.

5.4 Effects of Prandtl Number Variation

Figure 5.6 shows the variation of mean Nusselt number with Prandtl number for $Re = 1000$, $s = 8$, and $r_* = 0.707$. It shows a very similar trend to figure 5.5. The increase of mean Nusselt number over the smooth tube value is seen to be almost constant at all Prandtl numbers (about 2.2 times for laminate eversion and mixed eversion, and about 1.7 times for ideal eversion). Thus, a power law relationship seems to exist just as in the case of twisted-tape inserts [15, 16]. It may be noted that the variation of fluid properties with temperature was not considered in the numerical calculations and hence the natural convection contribution, which might be significant in some cases, was not considered. Therefore, the actual numbers could be higher than the ones shown in the figure. Ideal eversion, again, is seen to produce the smallest heat transfer augmentation for all Prandtl numbers greater than about 1. The friction factor, of course, does not change with the variation of Prandtl number.

5.5 Effects of Spacing Variation

From figure 5.3, it is easy to see that greater heat transfer augmentation would result with smaller spacing between the evertors. This suggests a tight packing arrangement provided that the corresponding increase in pressure drop is acceptable.

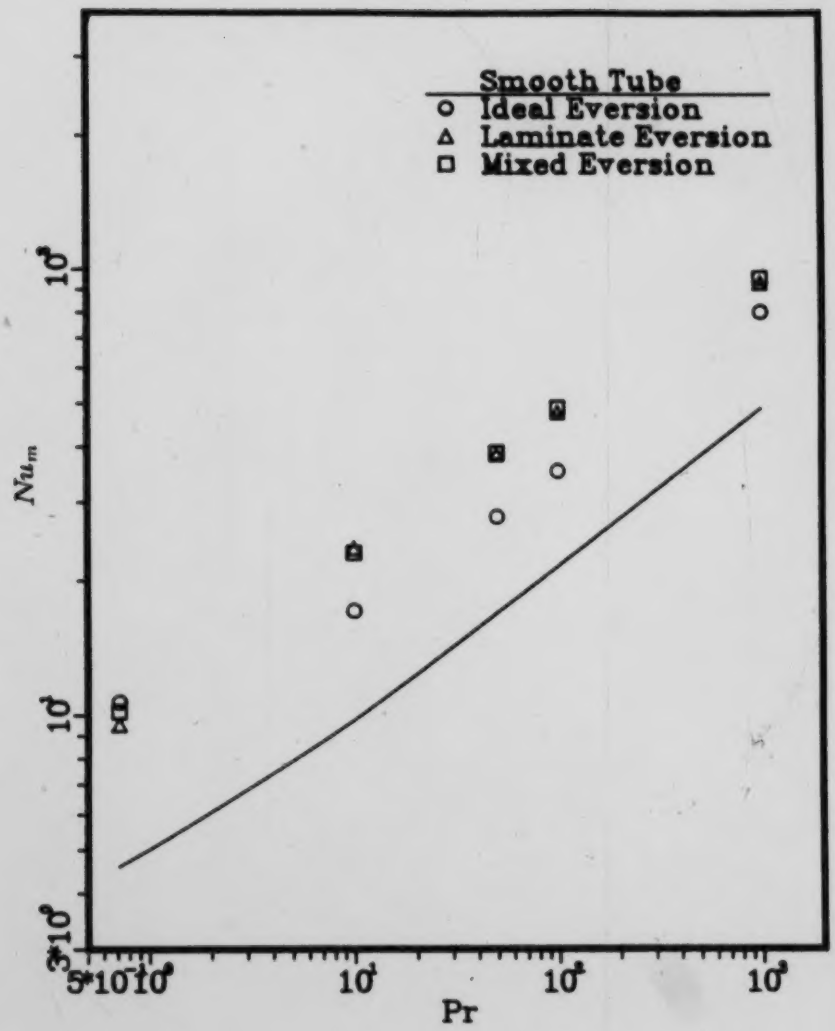

Figure 5.6: Effect of Pr on mean Nusselt number for $Re = 1000$, $r_* = 0.707$, and $s = 8$.

The spacing, of course, must be greater than about 2 for practical applications. Figure 5.7 and figure 5.8 show the effect of varying evertor spacing on friction factor and mean Nusselt number, respectively. Both figures exhibits a similar trend: both heat transfer rate and frictional loss increase as the spacing decreases. But the magnitude of the increase is different. For example, in the case of laminate eversion, with a large spacing of $s = 12$ the increases in Nusselt number and friction factor over the smooth tube are mild at 2.29 and 2.33, respectively. With a very tight spacing of $s = 3$, however, the increase in Nusselt number is 2.96 while the increase in friction factor is 6.01. Therefore, a very tight packing arrangement may be disadvantageous for some applications. The same argument applies to other eversion models to a less degree. At a spacing value around $s = 6$, a good heat transfer enhancement with a relatively mild pressure drop increase seems to occur.

5.6 Effects of r_* Variation

All of the results discussed up to now have been based on evertors of one geometry, namely $r_* = 0.707$ and $l = 2D$. If r_* changes, and thus the relative size of core and annulus changes, the velocity and temperature profiles after the process of eversion will change. Accordingly, changes will occur in the magnitude of pressure drop and heat transfer. When r_* is increased, an increased portion of fluid mass goes through the core region of an evertor. The resulting velocity and temperature profiles after the process of eversion will have sharper gradients at the wall. Thus, one would intuitively expect that the higher the value of r_* the higher the increase in pressure drop and heat transfer. Figure 5.9 and figure 5.10 show the effects of varying r_* values on friction factor and mean Nusselt number, respectively, for $Re = 1000$, $Pr = 10$, and $s = 8$. Two r_* values are worth noting: $r_* = 0.54$ divides the fluid *mass flow*

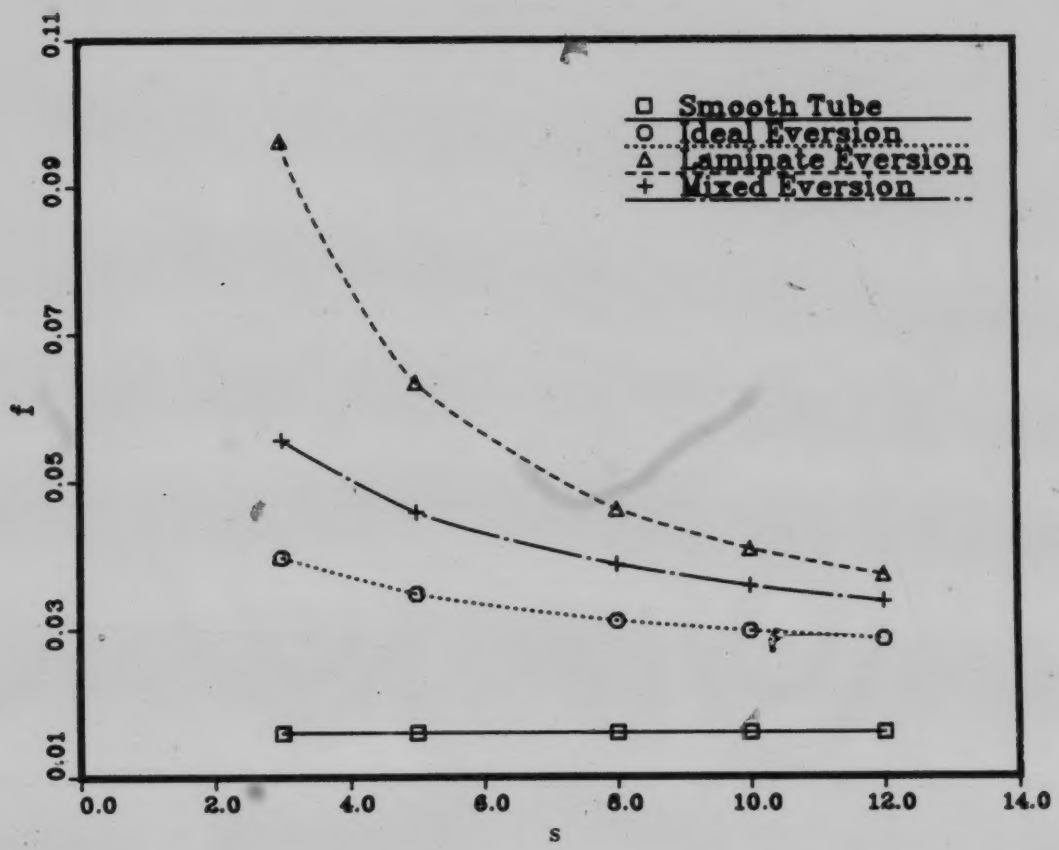

Figure 5.7: Effect of s on friction factor for $Re = 1000$, $Pr = 10$, and $r_* = 0.707$.

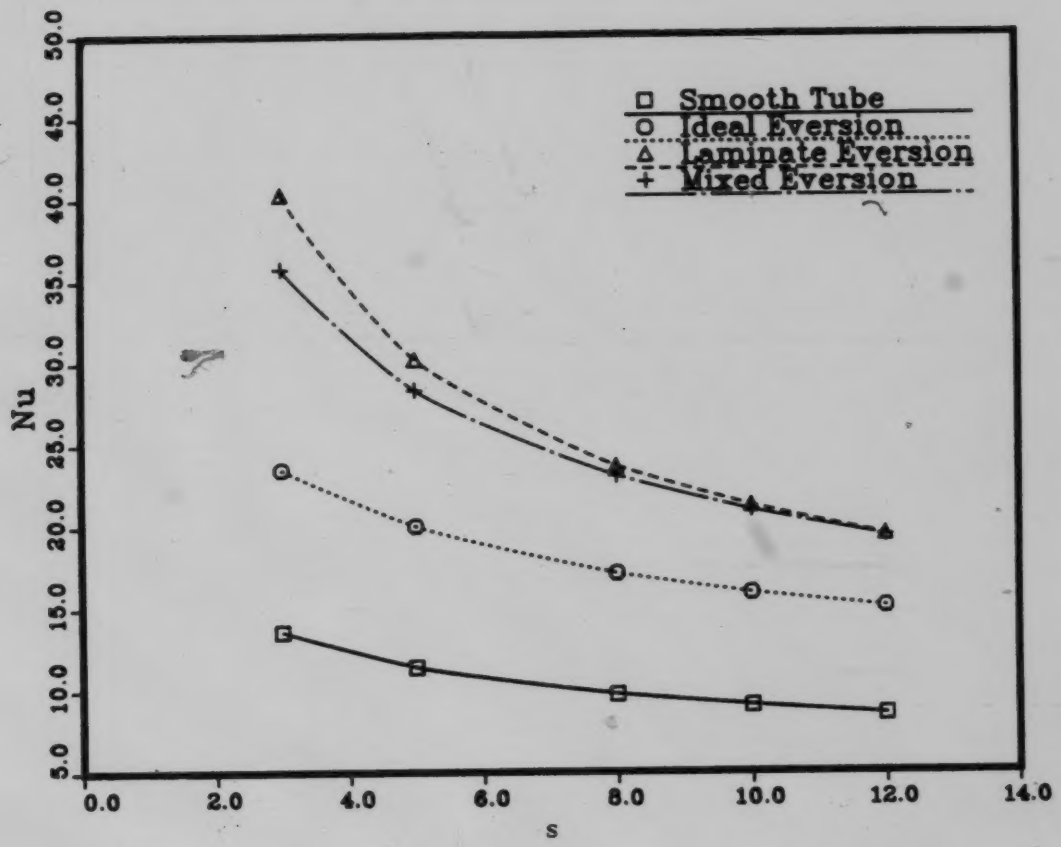

Figure 5.8: Effect of s on mean Nusselt number for $Re = 1000$, $Pr = 10$, and $r_* = 0.707$.

into two equal parts when the fluid entering the evertor has a fully developed velocity profile; $r_* = 0.707$ divides the *flow area* into two equal parts. The figures show that both pressure drop and heat transfer greatly depend on r_* and the designer must carefully choose an r_* value appropriate to the application.

In figure 5.9, the friction factor is seen to have a minimum, contrary to the above expectation, at r_* ranging from about 0.45 to 0.7 depending on the eversion model. Let's denote this value of r_* as $r_{*,min}$. Above $r_{*,min}$, friction factor increases sharply as r_* increases for each eversion model. However, below $r_{*,min}$, friction factor increases again as r_* decreases. It has been found that the above happens because as r_* decreases below $r_{*,min}$, total pressure drop increases due to a greater increase in ΔP_e at the locations of evertors than the decrease in pressure drop in the tube.

It is interesting to see that, from figure 5.10, the variation of mean Nusselt number does not have a minimum value. The mean Nusselt number increases monotonically as r_* increases. For small r_* values, the increase in Nusselt number is minor, and even a decrease is seen at $r_* = 0.38$ for ideal eversion.

Considering both figures 5.9 and 5.10 at the same time, it is clear that r_* values smaller than about 0.5 are not desirable. For r_* values greater than about 0.75, the increase in friction factor is much greater than the increase in mean Nusselt number, which is again not very desirable. Therefore, an r_* value near 0.7 appears to offer a reasonable compromise between gains in heat transfer and pumping power.

5.7 Comparison with Twisted-Tape Data

The pressure drop and heat transfer data presented so far already indicate that eversion is a good technique in augmenting laminar flow heat transfer rates inside

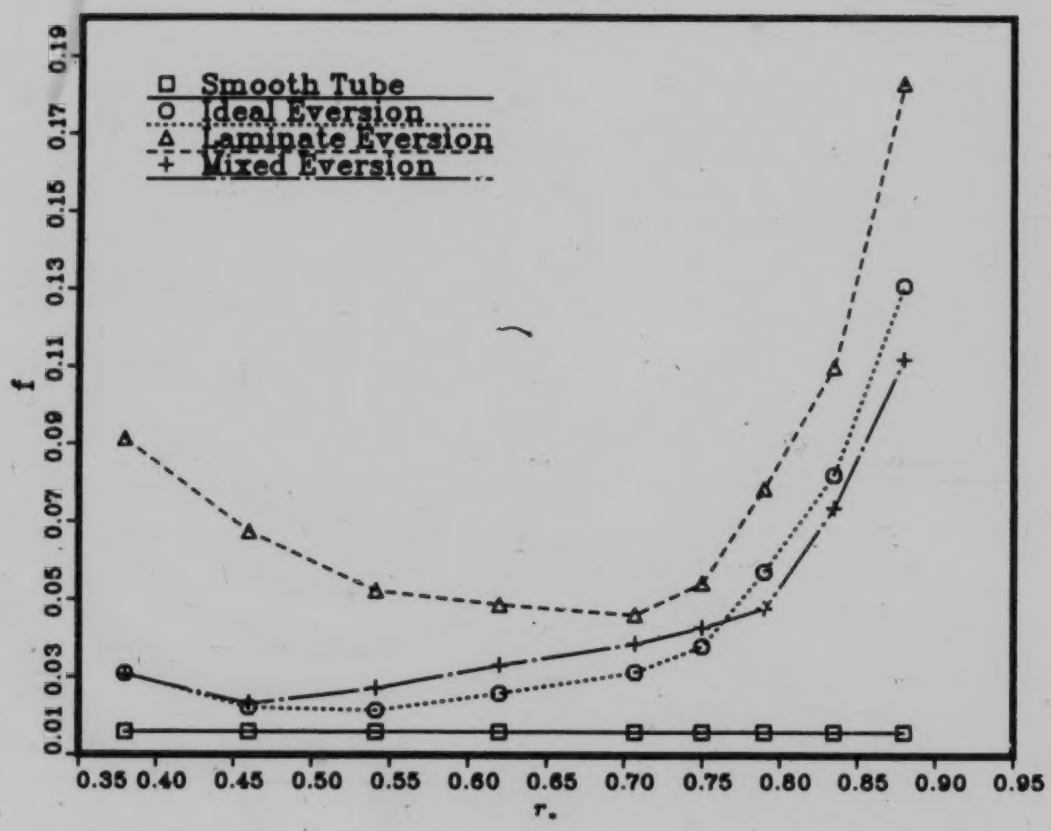

Figure 5.9: Effect of r_* on friction factor for $Re = 1000$, $Pr = 10$, and $s = 8$.

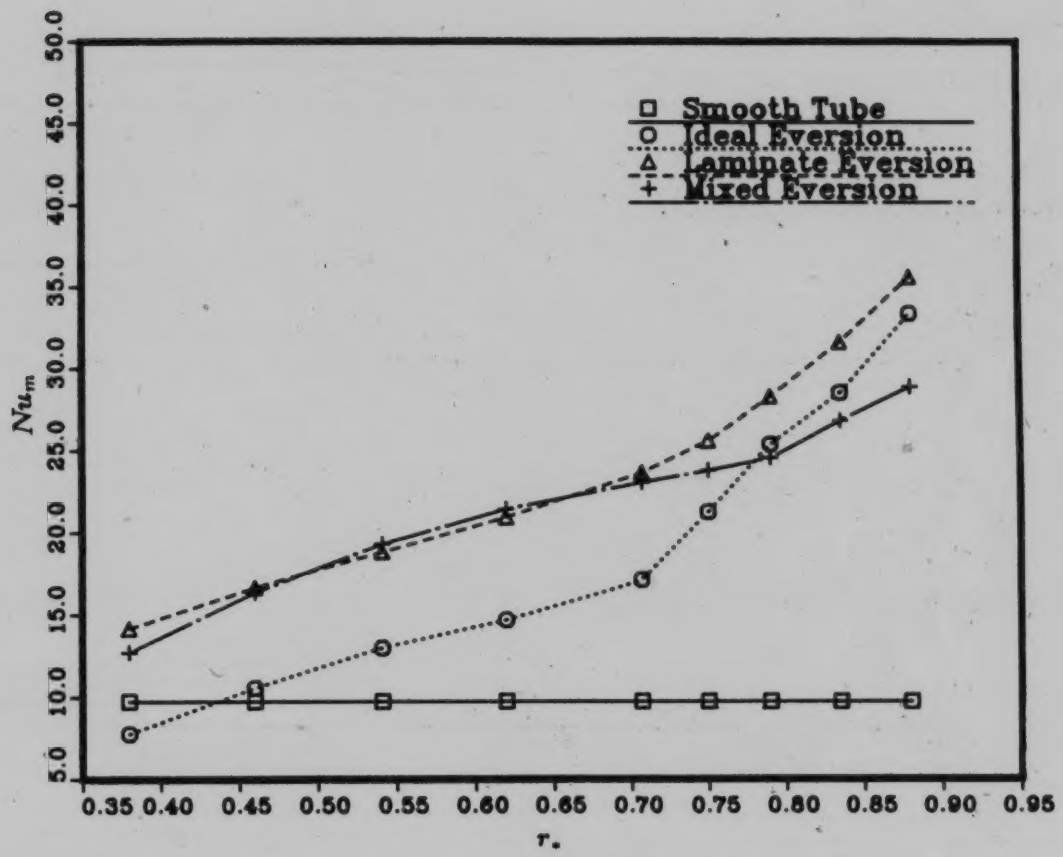

Figure 5.10: Effect of r_* on mean Nusselt number for $Re = 1000$, $Pr = 10$, and $s = 8$.

circular tubes. In order to determine the net improvement of a tube enhanced by eversion over the smooth tube, one of the performance evaluation criteria suggested by Webb [45] and Bergles [46] can be used: increase of heat transfer at fixed geometry and fixed pumping power, or reduction of pumping power at fixed geometry and fixed heat duty. These require correlations for friction factor and Nusselt number in terms of independent variables. The Nusselt number for eversion has been shown to depend on Re, Pr, s, and r_*, and the friction factor on Re, s, and r_*. Because the present study is not to evaluate any specific evertor of fixed geometry, correlations seem to have little meaning. Therefore, the effectiveness of eversion has been assessed by comparing the friction factor and Nusselt number data with those of another technique, e.g. twisted-tape inserts, on common axes. Twisted-tapes, either full or partial length, are probably the most comprehensively studied devices, and they are widely considered to have a high performance level.

Figures 5.11 and 5.12 show the comparison of f and Nu_m data with those of twisted-tape inserts at various Reynolds numbers. The twisted-tape data are from the references [16, 18] for full length twisted-tapes at a Prandtl number of 5. The eversion data were obtained using $Pr = 5$, $s = 6$, and $r_* = 0.707$. Thus, favourable values for both s and r_* were used. Figure 5.11 shows that all eversion models produce a friction factor much less than twisted-tapes for the laminar flow region. Only laminate eversion produces f values close to twisted-tape data at high Reynolds numbers. Figure 5.12 shows that both laminate eversion and mixed eversion produce Nu_m very close to the twisted-tape data with twist ratio of 5. Ideal eversion, again, is seen to perform poorly at higher Reynolds numbers. From these two figures, it is evident that, in theory, properly designed evertors could perform better than twisted-tapes, depending upon the application.

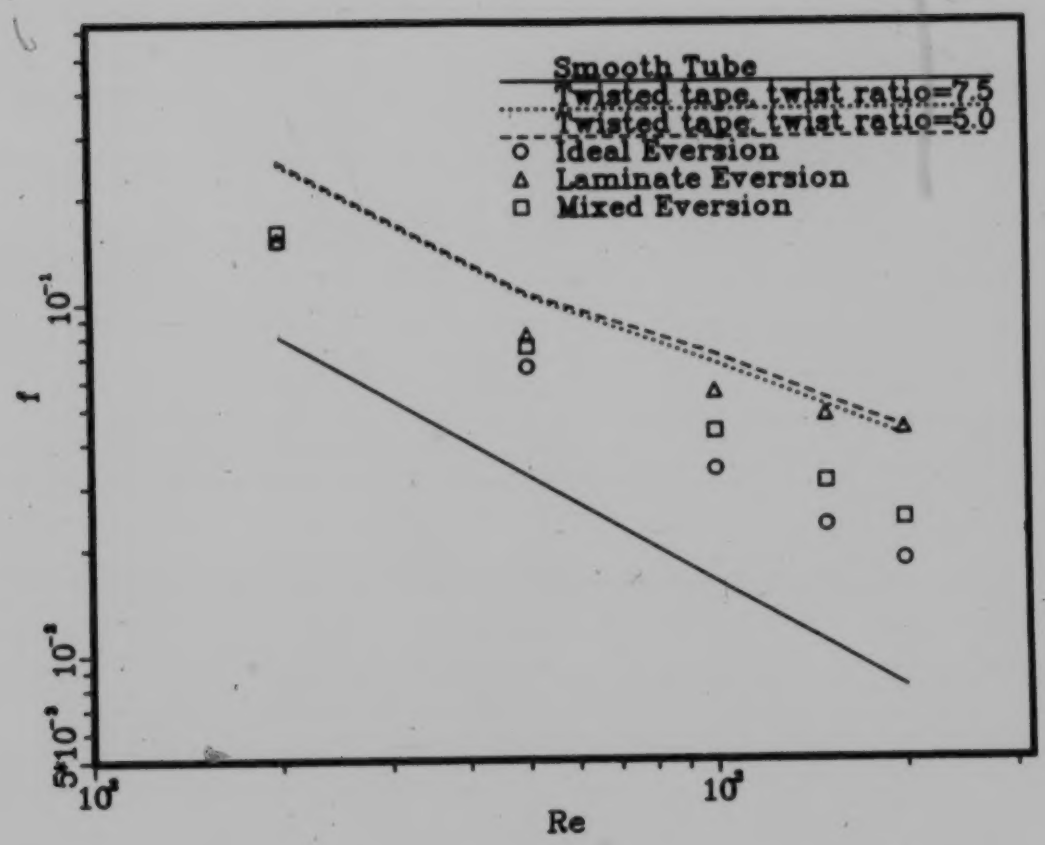

Figure 5.11: Comparison of friction factor with twisted-tape data for $Pr = 10$, $s = 8$, and $r_* = 0.707$.

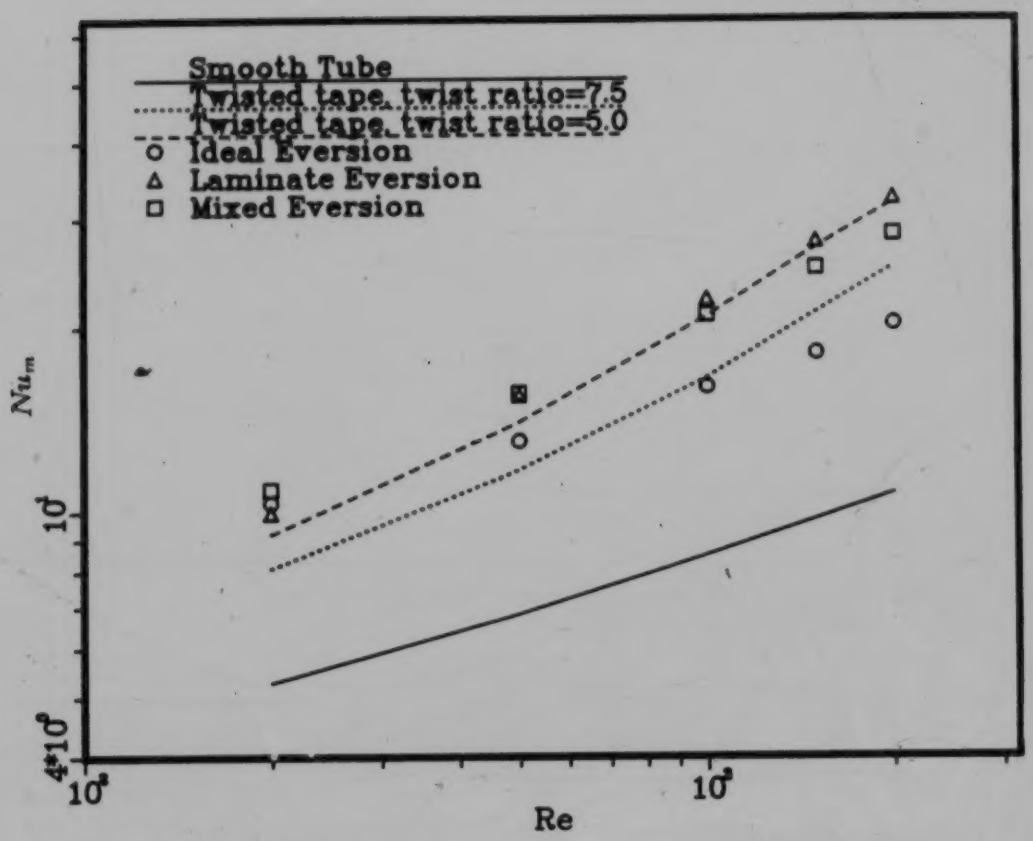

Figure 5.12: Comparison of mean Nusselt number with twisted-tape data for $Pr = 10$, $s = 8$, and $r_* = 0.707$.

Chapter 6

Conclusions and Recommendations

The objective of this study was to analyze eversion as a means of augmenting the surface heat transfer coefficient within tubes of tubular heat exchangers under laminar flow conditions. Numerical analysis has been performed in a straight horizontal circular tube containing a hypothetical evertor, or a series of five regularly spaced evertors, with a thermal boundary condition of uniform wall temperature. These evertors were assumed to divide the fluid flow into two parts, a core and an annulus, which were then interchanged. Thus, the relatively cooler fluid in the core is directed into an annulus adjacent to the wall while the relatively hotter fluid in the annulus is directed into a central core. This eversion process is the basis of the heat transfer augmentation.

No particular eversion device has been considered in this study. Instead, the eversion process has been idealized by three separate models: ideal eversion model, in which the innermost regions of the core are exchanged with the outermost regions

of the annulus; laminate eversion, in which the core and annulus are exchanged in bulk with both streams maintaining the laminate structure; and mixed eversion, in which the bulk exchange is accompanied by complete mixing. The models have been formulated by imposing the requirements of conservation of mass and (sensible heat) energy. Conservation of momentum during eversion has been satisfied by incorporating a pressure change corresponding to the change in momentum flux produced.

The analysis of eversion has been performed by comparing the heat transfer and pressure drop characteristics with those of a smooth tube. First, an air-filled tube containing a single evertor of each type was studied as a thermal entry length problem with a tube Reynolds number of 1000. A finite difference method using SIMPLE-C algorithm was used to solve the problem numerically. Solutions have been used to show the development of velocity and temperature profiles. With $r_* = 0.707$, the velocity profiles of all eversion models reveal a significant surge near the wall immediately downstream of the evertor and begin to develop towards the fully developed form further downstream. This, together with the everted temperature profile and its subsequent development, results in increases in friction factor and local Nusselt number. These increases are most noticeable in the first 7 diameters downstream of the evertor and only minor increases occur further downstream.

Next, a tube containing five regularly spaced evertors was studied. The results show marked repetitions of single eversion effects, producing a very high increase in mean Nusselt number and friction factor. The heat transfer results indicate that the Nusselt number is a function of Re, Pr, s, and r_*, while the pressure drop results indicate that friction factor is function of Re, s, and r_*. Correlations of the data have not been attempted because the present study is not an analysis of a specific eversion device. Good heat transfer augmentation with a relatively mild increase in

friction factor was found to occur with $r_o = 0.707$ and $s = 6$. With these conditions and $Pr = 5$, the mean Nusselt number at $Re = 1000$ is 1.9, 2.6 and 2.5 times that for a plain tube for ideal, laminate, and mixed eversion, respectively, while the ratios for friction factor are 2.1, 3.5, and 2.7, respectively. These numbers indicate a better overall performance than full length twisted-tape inserts, which have a Nusselt number ratio of 2.4 and friction factor ratio of 4.4 for the given conditions and a twist ratio of 5.

The numerical results, of course, must be validated by experimental data. To this end, an experimental eversion rig has been built in the department. A series of carefully controlled experiments should be conducted using various real evertors. The designer of evertors should be particularly aware of the fact that both heat transfer and pressure drop results are very sensitive to the ratio of core to tube radius of evertors.

References

[1] Shah, R. K., and London, A. L., "Laminar Flow Forced Convection in Heat Transfer", Supplement 1 to Advances in Heat Transfer, Academic Press, New York, 1978

[2] Kays, W. M., and Crawford, M. E., "Convective Heat and Mass Transfer", 2nd ed., McGraw-Hill, New York, 1980

[3] Kakac, S., and Yener, Y., in "Advanced Study Institute on Low Reynolds Number Forced Convection in Channels and Bundles: Applied in Heat Exchangers", ASI Proceedings of NATO Advanced Study Institute, July 13-24, Ankara, Turkey, 1981

[4] Bergles, A. E., "Survey and Evaluation of Techniques to Augment Convective Heat Transfer", Progress in Heat and Mass Transfer, Vol. 1, Pergamon Press, New York, pp. 331-334, 1969

[5] Bergles, A. E., "Recent Development in Convective Heat Transfer Augmentation", Applied Mechanics Reviews, Vol. 21, pp. 675-682, 1973

[6] Bergles, A. E., "Enhancement of Heat Transfer", Sixth international Heat Transfer Conference, Vol. 6, pp. 89-108, 1978

[7] Bergles, A. E., "Principles of Heat Transfer Augmentation", Proceedings of the NATO Advanced Study Institute on Heat Exchangers: Thermal- hydraulic fundamentals and design, Aug. 4-15, Istanbul, Turkey, 1980, Eds., Kakac, S., Bergles, A. E., and Mayinger, F., Hemisphere Publishing Co., New York, New York, pp. 819-881, 1981

[8] Bergles, A. E., and Joshi, S. D., "Augmentation Techniques for Low Reynolds Number In-Tube Flow", in Low Reynolds Number Flow Heat Exchangers, Eds., Kakac, S., Shah, R. K., and Bergles, A. E., Hemisphere Publishing Co., Washington, D. C., pp. 695-720, 1983

[9] Sununu, J. H., "Heat Transfer with Static Mixers System", Kenics corporation Technical Report 1002, 1970

[10] Genetti, W. E., and Priebe, S. J., "Heat Transfer with a Static Mixer", American Society of Chemical Engineers Paper presented at the Forth Joint Chemical Engineering Conference, Vancouver, Canada, 1973

[11] Van Der Meer, T. H., and Hoogendoorn, C. J., "Heat Transfer Coefficients for Viscous Fluids in a Static Mixer", Chemical Engineering Conference, Vol. 33, pp. 1277-1282, 1978

[12] Marner, W. J., and Bergles, A. E., "Augmentation of Tubeside Laminar Flow Heat Transfer by Means of Twisted-Tape Inserts, Static-Mixer Inserts, and Internally Finned Tubes", Proceedings of Sixth International Heat Transfer Conference, Vol. 2, Hemisphere Publishing Co., Washington, D. C., pp. 583-588, 1978

[13] Marner, W. J., and Bergles, A. E., "Augmentation of Highly Viscous Laminar Tubeside Heat Transfer by Means of a Twisted-Tape Insert and an Internally

Finned Tube", Advances in Enhanced Heat Transfer, presented at the 23rd AIChE-ASME National Heat Transfer Conference, Aug. 4-7, Denver, Colorado, pp. 19-28, 1985

[14] Lopina, R. F., and Bergles, A. E., "Heat Transfer and Pressure Drop in Tape-Generated Swirl Flow of Single-Phase Water", Journal of Heat Transfer, Vol. 91, pp. 434-442, 1969

[15] Date, A. W., "Prediction of Fully-Developed Flow in a Tube Containing a Twisted Tape", International Journal of Heat and mass Transfer, Vol. 17, pp. 845-859, 1974

[16] Hong, S. W., and Bergles, A. E., "Augmentation of Laminar Flow Heat Transfer in Tubes by Means of Twisted-Tape Inserts", Journal of Heat Transfer, Vol. 98, pp. 251-256, 1976

[17] Manglik, R. M., and Bergles, A. E., "A Correlation of laminar Flow Enhanced Heat Transfer in Uniform Wall Temperature Circular Tubes with Twisted-Tape Inserts", Advances in Enhanced Heat Transfer, presented at the 24th AIChE-ASME National Heat Transfer Conference and Exhibition, Aug. 9-12, Pittsburgh, Pennsylvania, pp. 19-25, 1987

[18] Saha, S. K., Gaitonde, U. N., and Date, A. W., " Heat Transfer and Pressure Drop Characteristics of Laminar Flow in a Circular Tube Fitted with Regularly Spaced Twisted-Tape Elements", presented at the 1st World Conference in Experimental Fluid Mechanics, Thermodynamics and Heat Transfer, Yugoslavia, Sept. 1988

[19] Masliyah, J. H., and Nandakumar, K., "Steady Laminar Flow Through Twisted Pipes", Journal of Heat Transfer, Vol. 103, pp. 785-790, 1981

[20] Masliyah, J. H., and Nandakumar, K., "Steady Laminar Flow Through Twisted Pipes", Journal of Heat Transfer, Vol. 103, pp. 791-796, 1981

[21] Bayley, F. J., and Lock, G. S. H., " Heat Transfer Characteristics of the Closed Thermosyphon", Journal of Heat Transfer, Vol. 87, pp. 30-39, 1965

[22] Maezawa, S. and Lock, G. S. H., "Heat Transfer Inside a Tube with a Novel Promoter", Proceedings of the Sixth International Heat Transfer Conference, Vol. 2, Hemisphere Publishing Co., Washington, D. C., pp. 595-600, 1978

[23] Megerlin, F. E., Murphy, R. W., and Bergles, A. E., "Augmentation of Heat Transfer in Tubes by Use of Mesh and Brush Inserts", Journal of Heat Transfer, Vol. 96, pp. 145-151, 1974

[24] Patankar, S. V., and Spalding, D. B., "A Calculation Procedure for Heat, Mass, and Momentum Transfer in Three-dimensional Parabolic Flow", International Journal of Heat and Mass Transfer, Vol. 15, pp. 1787-1806, 1972

[25] Chilukuri, R., and Pletcher, R. H., "Numerical Solutions to the Partially Parabolized Navier-Stokes Equations for Developing Flow in a Channel", Numerical Heat Transfer, Vol. 3, pp. 169-188, 1980

[26] Pratap, V. S., and Spalding, D. B., "Fluid Flow and Heat Transfer in Three-Dimensional Duct Flows", Journal of Heat and Mass Transfer, Vol. 19, pp.1183-1188, 1976

[27] Patankar, S. V., "Numerical Heat Transfer and Fluid Flow", Hemisphere Publishing Co., Washington, D. C., 1980

[28] Patankar, S. V., "A Calculation Procedure for Two-Dimensional Elliptic Situations", Numerical Heat Transfer, Vol. 4, pp. 409-425, 1981

[29] Van Doormaal, J. P., and Raithby, G. D., "Enhancements of The SIMPLE Method for Predicting Incompressible Fluid flows", Numerical Heat Transfer, Vol.7, pp. 147-163, 1984

[30] Humphrey, J. A. C., "Numerical Calculation of Developing Laminar Flow in Pipe of Arbitrary Curvature Radius", The Canadian Journal of Chemical Engineering, Vol. 56, pp. 151-164, 1978.

[31] Harlow, F. H., and Welch, J. E., "Numerical Calculation of Time-dependent Viscous Incompressible Flow of Fluid with Free Surface", The Physics of Fluids, Vol. 8, pp. 2182-2189, 1965

[32] Barakat, H. Z., and Clack, J. A., " Analytical and Experimental Study of Transient Laminar Natural Convection Flows in Partially Filled Containers", Proceedings of 3rd International Heat Transfer Conference, Vol. 2, pp. 152-162, 1966

[33] Runchal, A. K., "Convergence and Accuracy of Three Finite Difference Schemes for a Two-Dimensional Conduction and Convection Problem", International Journal for Numerical Methods in Engineering, Vol. 4, pp. 541-550, 1972

[34] Spalding, D. B., "A Novel Finite-Difference Formulation for Differential Expressions Involving Both First and Second Derivatives", International Journal for Numerical Methods in Engineering, Vol. 4, pp. 551-559, 1972

[35] Patel, M. K., and Markatos, N. C., "An Evaluation of Eight Discretization Schemes For Two-Dimensional Convection-Diffusion Equations", International Journal for Numerical Methods in Fluid, Vol. 6, pp. 129-154, 1986

[36] Pollard, A., and Siu, L. W. A., "The Calculation of Some Laminar Flows Using

Various Discretization Schemes", Computer Methods in Applied Mechanics and Engineering, Vol. 35, pp. 293-313, 1982

[37] Raithby, G. D., and Torrance, K. E., "Upstream-Weighted Differencing Schemes and Their Application to Elliptic Problems Involving Fluid Flows", Computers and Fluids, Vol. 2, pp. 191-206, 1974

[38] McDonald, J. W., Denny, V. E., and Mills, A. F., "Numerical Solutions of the Navier-Stokes Equations in Inlet Regions", Journal of Applied Mechanics, Vol. 39, Ser. E, pp. 873-878, 1972

[39] Morihara, H., and Cheng, R. T., " Numerical Solution of the Viscous Flow in the Entrance Region of Parallel Plates", Journal of Computational Physics, Vol. 11, pp. 550-572, 1973

[40] Schmidt, F. W., and Zeldin, B., "Laminar Flow in Inlet Sections of Tubes and Ducts", AIChE Journal, Vol. 15, pp. 612-614, 1969

[41] Zeldin, B., and Schmidt F. W., "Developing Flow with Combined Forced-Free Convection in an Isothermal Vertical Tube", Journal of Heat Transfer, Vol. 94, pp. 211-223, 1972

[42] Manohar, R., "Analysis of Laminar-Flow Heat Transfer in the Entrance Region of Circular Tubes", International Journal of Heat and Mass Transfer, Vol. 12, pp. 15-22, 1969

[43] Hwang, G. J., and Shew, J. P., "Effect of Radial Velocity Component on Laminar Forced Convection in Entrance Region of a Circular Tubes", International Journal of Heat and Mass Transfer, Vol. 17, pp. 372-375, 1974

[44] DuPlessis, J. P., "Laminar Flow and Heat Transfer in a Smooth Tube with a Twisted-Tube Inserts", Ph.D Thesis, University of Stellenbosch, South Africa, 1982.

[45] Webb,R.L., "Performance Evaluation Criteria for Use of Enhanced heat transfer surfaces in Heat Exchanger Design", International Journal of Heat and Mass Transfer, Vol. 24, pp. 715-726, 1981

[46] Bergles, A. E., Blumenkrantz, A. R., and Taborek, K., "Performance Evaluation Criteria for Enhanced Heat Transfer Surface", Proceedings of International Heat and Mass Transfer Conference, Vol. 2, pp. 239- 243, 1974.

Appendix A

Listing of Computer Program

```
C This program solves a fluid flow and heat transfer
C problem in a circular duct containing five equally
C spaced evertors.

      PROGRAM EVERT
      IMPLICIT REAL(A-H,O-Z)
      PARAMETER(ID=24,JD=24)
      COMMON /VEL/ U(ID,JD),V(ID,JD),P(ID,JD),T(ID,JD)
      COMMON /XINDEX/ X(ID),XU(ID),XDIF(ID),XCV(ID)
      COMMON /RINDEX/ R(JD),RV(JD),RDIF(JD),RCV(JD)
      COMMON /BL/ ULB(JD),TLB(JD)
      DIMENSION AP(ID,JD),AE(ID,JD),AW(ID,JD),AN(ID,JD)
      DIMENSION AS(ID,JD),S(ID,JD),DU(ID,JD),DV(ID,JD)
      DIMENSION PC(ID,JD),USTAR(ID,JD),VSTAR(ID,JD)
      DIMENSION R1(JD),U1(JD),Q(ID),OLDX(ID)
      DIMENSION UU(99),RR(99),TT(99),SUMN(99),QX(99)
      DIMENSION XX(99),YY(99),B(99),C(99),D(99),HH(99)
      DIMENSION F(ID),PM(ID),RNU(ID),RNUX(99),RNUM(99)
      DIMENSION RNU12(6),XXX(99),FFF(99),PPP(99)
      LOGICAL FLAG

C Read in and write out the input data.

      READ(5,*) M,N,RENOL,PR,EK,H
      READ(5,*) MODEL,RSTAR,PF,CON,NDIV,NDCON
      READ(5,*) UTOL,VTOL,PTOL,TTOL,TOL
      READ(5,*) NPAS,NPPAS,NITER,RELAX
      READ(5,*) (X(I),I=1,M)
      WRITE(6,*) '
      WRITE(6,*) 'DATA USED IN THIS RUN ARE : '
      WRITE(6,*) 'M=',M,' N= ',N,' REYNOLDS NUM=',RENOL,
     &           ' PRANDTL NUM=',PR,' ECKERT NUM=',EK
      WRITE(6,*) 'H=',H,' EVERSION MODEL=',MODEL,' R*=',
     &           RSTAR,' INLET VELOCITY PROFILE=',PF
      WRITE(6,*) 'PRESSURE CONSTANT=',CON,' NDIV=',NDIV,
     &           ' END CONDITION IN SPLINE=',NDCON
      WRITE(6,*) 'UTOL=',UTOL,' VTOL=',VTOL,' PTOL=',PTOL
     &           ,' TTOL=',TTOL,' TOL=',TOL
      WRITE(6,*) 'NPAS=',NPAS,' NPPAS=',NPPAS,
     &           ' NITER=',NITER,' RELAX=',RELAX
      WRITE(6,*) '

C Initialize variables.

      OLDH=H
      DO 10 I=1,M
        DO 10 J=1,N
          U(I,J)=1.0
```

```
            V(I,J)=-0.001
            USTAR(I,J)=0.0
            VSTAR(I,J)=0.0
            P(I,J)=0.0
            T(I,J)=0.0
            PC(I,J)=0.0
 10   CONTINUE

      DO 12 J=1,N
C        ULB(J)=1.0 (for block velocity entry)
         ULB(J)=((PF+1.0)/PF)*(1.0-R(J)**(PF+1.0))
         TLB(J)=0.0
 12   CONTINUE

C Calculate staggered grid point locations.
C Axially, uneven grid points are read in from
C data file. Radially, ten even nodal points
C are calculated from r=0 to r=r* and another
C ten points from r=r* to r=1. In this program,
C the case of r*=0.707 is written.

      RV(2)=0.0
      DR=0.689/8.0
      DO 15 J=3,10
         RV(J)=RV(J-1)+DR
 15   CONTINUE
      RV(11)=0.725
      DR=(1.0-0.725)/8.0
      DO 17 J=12,N
         RV(J)=RV(J-1)+DR
 17   CONTINUE

      R(1)=0.0
      DO 19 J=2,N-1
         R(J)=0.5*(RV(J)+RV(J+1))
 19   CONTINUE
      R(N)=RV(N)

      DO 21 J=2,N
         RDIF(J)=R(J)-R(J-1)
 21   CONTINUE

      DO 25 J=2,N-1
         RCV(J)=RV(J+1)-RV(J)
 25   CONTINUE

      ISWTCH=1
      NEVT=1
```

```
888  CONTINUE

     XU(2)=0.0
     DO 27 I=3,M
        XU(I)=X(I-1)+X(I-1)-XU(I-1)
27   CONTINUE

     DO 28 I=2,M
        XDIF(I)=X(I)-X(I-1)
28   CONTINUE

     DO 30 I=2,M-1
        XCV(I)=XU(I+1)-XU(I)
30   CONTINUE

     DO 32 I=1,M
        DO 32 J=1,N
           P(I,J)=0.0
32   CONTINUE

     WRITE(6,*) 'H=',H,'   M=',M,'   N=',N
     WRITE(6,*) 'AXIAL GRID POINT LOCATIONS:'
     WRITE(6,*) 'X(I)'
     WRITE(6,1) (X(I),I=1,M)
     WRITE(6,*) 'X(I)*H/RENOL'
     WRITE(6,1) (X(I)*H/RENOL,I=1,M)
     WRITE(6,*) 'X(I)*H/PE'
     WRITE(6,1) (X(I)*H/(RENOL*PR),I=1,M)
     WRITE(6,*) 'RADIAL GRID POINT LOCATIONS:'
     WRITE(6,1) (R(J),J=1,N)

C Iteration begins here.
C Using the guessed pressure field P*, soive the
C momentum equations to get U* and V*. Since they are
C are non-linear equations, solution requires iterative
C procedure. Begin with guessed fields and keep updating
C u and v ultil the changes in u velocity or in mass
C source (continuity unbalance) for two successive
C iterations is sufficiently small.

     HH4=4.0*H*H
     ITER=0
555  CONTINUE

     ITER=ITER+1
     WRITE(7,*) '
     WRITE(7,*) '       ITERATION NUMBER = ',ITER
```

```
C Specify boundary conditiions for u equation.
C Boundary indices are (2, M, 1, N).

      DO 50 J = 2, N-1

C Left boundary condition(value specified).

        AP(2,J) = 1.0
        AE(2,J) = 0.0
        S(2,J)=ULB(J)

C Right boundary condition(Du/Dx = 0.0).

        AP(M,J) = 1.0
        AW(M,J) = 1.0
        S(M,J) = 0.0

 50   CONTINUE

      DO 52 I = 3, M-1

C Bottom boundary condition (Du/Dr = 0.0).

        AP(I,1) = 1.0
        AN(I,1) = 1.0
        S(I,1) = 0.0

C Top boundary cconcition (value known, no slip).

        AP(I,N) = 1.0
        AS(I,N) = 0.0
        S(I,N) = 0.0

 52   CONTINUE

      CALL COEFFU(M,N,RENOL,H,RELAX,DU,AP,AE,AW,AN,AS,S)
      CALL TDMA(AP,AE,AW,AN,AS,S,2,M,1,N,
     &          N,.FALSE.,NPAS,UTOL,USTAR,RESIDU)

C Specify boundary conditions for v equation.
C Boundary indices are (1, M, 2, N).

      DO 54 J = 3, N-1

C Left boundary condition (value=0, or Dv/Dx=0).

        AP(1,J) = 1.0
        AE(1,J) = 1.0
```

```
C       AE(1,J) = 0.0 (for V=0 condition)
        S(1,J) = 0.0

C Right ccundary condition (value=0).

        AP(M,J) = 1.0
        AW(M,J) = 0.0
        S(M,J) = 0.0

 54   CONTINUE

      DO 56 I = 2, M-1

C Bottom boundary condition (value=0).

        AP(I,2) = 1.0
        AN(I,2) = 0.0
        S(I,2) = 0.0

C Top boundary condition (value=0).

        AP(I,N) = 1.0
        AS(I,N) = 0.0
        S(I,N) = 0.0

 56   CONTINUE

      CALL COEFFV(M,N,RENOL,H,RELAX,DV,AP,AE,AW,AN,AS,S)
      CALL TDMA(AP,AE,AW,AN,AS,S,1,M,2,N,
     &          N,.FALSE.,NPAS,VTOL,VSTAR,RESIDU)

C Using this new velocity field, solve the pressure
C correction equation.

      DO 60 I=2,M-1
         DO 60 J=2,N-1
            PC(I,J)=0.0
 60   CONTINUE

      SOURCE=0.0
      DO 62 I=2,M-1
      DO 62 J=2,N-1
         RE=R(J)
         RW=R(J)
         RN=RV(J+1)
         RS=RV(J)
         DELX=XCV(I)
         DELR=RCV(J)
```

```
      IF(J.EQ.2) RS=0.5*R(2)
      IF(J.EQ.2) DELR=RCV(2)-0.5*R(2)
      IF(I.NE.M-1) AE(I,J)=DU(I+1,J)*RE*DELR
      IF(I.EQ.M-1) AE(I,J)=0.0
      IF(I.NE.2) AW(I,J)=DU(I,J)*RW*DELR
      IF(I.EQ.2) AW(I,J)=0.0
      IF(J.NE.N-1) AN(I,J)=HH4*DV(I,J+1)*RN*DELX
      IF(J.EQ.N-1) AN(I,J)=0.0
      IF(J.NE.2) AS(I,J)=HH4*DV(I,J)*RS*DELX
      IF(J.EQ.2) AS(I,J)=0.0
      IF(I.EQ.M-1) AW(I,J)=0.0
      AP(I,J)=AE(I,J)+AW(I,J)+AN(I,J)+AS(I,J)
      S(I,J)=(USTAR(I,J)-USTAR(I+1,J))*RE*DELR
     &      +(VSTAR(I,J)*RS-VSTAR(I,J+1)*RN)*DELX
      SOURCE=SOURCE+S(I,J)
62    CONTINUE

C specify pressure at points across exit boundary.

      DO 64 J=2,N-1
         AP(M-1,J)=AP(M-J,J)
         AE(M-1,J)=0.0
         AW(M-1,J)=0.0
         AN(M-1,J)=0.0
         AS(M-1,J)=0.0
         S(M-1,J)=0.0
64    CONTINUE
      SOURCE=SOURCE/FLOAT(M-2)/FLOAT(N-2)
      CALL TDMA(AP,AE,AW,AN,AS,S,1,M,1,N,
     &          N,.TRUE.,NPPAS,PTOL,PC,RESIDU)

C     WRITE(7,*) 'PRESSURE CORRECTION IN CURRENT ITER'
C     WRITE(7,4) ((PC(I,J),I=2,M-1),J=N-1,2,-1)

C Correct the pressure fields and velocity fields.

      DO 66 I=2,M-1
         DO 66 J=2,N-1
         P(I,J)=P(I,J) + PC(I,J)
         IF(I.NE.2) USTAR(I,J)=USTAR(I,J)+DU(I,J)*
     &                 (PC(I-1,J)-PC(I,J))
         IF(J.NE.2) VSTAR(I,J)=VSTAR(I,J)+HH4*DV(I,J)*
     &                 (PC(I,J-1)-PC(I,J))
66    CONTINUE
      DO 70 I=3,M-1
      DO 70 J=2,N-1
      USTAR(I,1)=9.0/8.0*USTAR(I,2)-1.0/8.0*USTAR(I,3)
      USTAR(M,J)=9.0/8.0*USTAR(M-1,J)-1.0/8.0*USTAR(M-2,J)
```

```
 70   CONTINUE
      CALL CRIT(U,USTAR,3,M-1,2,N-1,ERRU)
      CALL CRIT(V,VSTAR,2,M-1,3,N-1,ERRV)
      WRITE(7,*) 'ERRU= ',ERRU,'    ERRV=',ERRV

      DO 72 I=1,M
         DO 72 J=1,N
            IF(I.NE.1) U(I,J)=USTAR(I,J)
            IF(J.NE.1) V(I,J)=VSTAR(I,J)
 72   CONTINUE

C     WRITE(7,*) 'CORRECTED PRESSURE'
C     WRITE(7,4) ((P(I,J),I=2,M-1),J=N-1,2,-1)
C     WRITE(7,*) 'CORRECTED U-FIELD'
C     WRITE(7,3) ((U(I,J),I=2,M),J=N,1,-1)
C     WRITE(7,*) 'CORRECTED V-FIELD'
C     WRITE(7,1) ((V(I,J),I=1,M),J=N,2,-1)

  1   FORMAT(11E11.3)
  2   FORMAT(12E11.3)
  3   FORMAT(10E11.3)
  4   FORMAT(9E11.3)
  5   FORMAT(F11.4)
  6   FORMAT(E15.5,2F15.4)
  7   FORMAT(E15.5,3F15.4)

C One iteration is now completed. Using updated values,
C go to the beginning of the iteration.

      WRITE(7,*) 'MASS SOURCE= ',SOURCE
      SOURCE=ABS(SOURCE)
      IF(ITER.GT.NITER) THEN
         WRITE(7,*) 'NOT CONVERGED AFTER 100 ITERATIONS'
         WRITE(6,*) 'NOT CONVERGED AFTER 100 ITERATIONS'
         GOTO 777
      ENDIF
      IF(ERRU.GT.0.00005.OR.SOURCE.GT.TOL) GOTO 555
 777  CONTINUE
      U(2,1)=U(2,2)

      WRITE(6,*) 'NUMBER OF ITERATIONS=',ITER
C     WRITE(6,*) 'MASS SOURCE AFTER FINAL ITER=',SOURCE
C     WRITE(6,*) 'PRESSURE CORRECTION FIELD'
C     WRITE(6,1) ((PC(I,J),I=2,M-1),J=N-1,2,-1)
C     WRITE(6,*) 'CORRECTED PRESSURE FIELD'
C     WRITE(6,1) ((P(I,J),I=2,M-1),J=N-1,2,-1)
C     WRITE(6,*) 'CORRECTED U-FIELD'
C     WRITE(6,1) ((U(I,J),I=2,M-1),J=N,1,-1)
```

```
C     WRITE(6,*) 'CORRECTED V-FIELD'
C     WRITE(6,1) ((V(I,J),I=1,M),J=N,2,-1)

C Evaluate friction factor.
C First calculate area integral mean pressure at each
C axial location.

      WRITE(6,*) 'MEAN PRESSURE DISTRIBUTION'
      DO 75 I=2,M-1
         DO 77 J=2,N-1
            XX(J-1)=R(J)
            YY(J-1)=P(I,J)*R(J)
77       CONTINUE
      CALL SPLINE(N-2,NDCON,XX,YY,SUMN,VAL,1,B,C,D,HH)
      PM(I)=2.0*VAL/(R(N-1)**2-R(2)**2)
75    CONTINUE

      IF(NEVT.EQ.1) THEN
         X2=X(2)
         P2=PM(2)
         PIN=PM(2)/OLDH*CON
         DO 79 I=3,M-1
         F(I)=RENOL*(PM(2)-PM(I))/(2.0*OLDH*(X(I)-X(2)))
79       CONTINUE
         WRITE(8,*) 'FILE 8'
         WRITE(8,*) 'Smooth Pipe$-Mean Pressure PM(x)'
         WRITE(8,1) (X(I)*H,I=2,M-1)
         WRITE(8,1) (PM(I),I=2,M-1)
         WRITE(10,*) 'FILE 10'
         WRITE(10,*) 'Smooth Pipe$ - f*Re'
         WRITE(10,1) (X(I)*H/RENOL,I=3,M-1)
         WRITE(10,1) (F(I),I=3,M-1)
      ENDIF

      IF(NEVT.EQ.2) THEN
         PDIFF=PM(2)-P2
         DO 80 I=3,M-1
         PM(I)=PM(I)-PFLUX-PIN-PDIFF
         F(I)=RENOL*(P2-PM(I))/(2.0*OLDH*(X(I)-X(2)))
80       CONTINUE
         DO 81 I=3,12
         XXX(I)=X(I)
         FFF(I)=F(I)
         PPP(I)=PM(I)
81       CONTINUE
         P12=PM(12)
         XXX(2)=X(2)
         PPP(2)=P2
```

```
      ENDIF

      IF(NEVT.EQ.3) THEN
         PDIFF=PM(2)-P12
         DO 84 I=2,M-1
         PM(I)=PM(I)-PFLUX-PIN-PDIFF
         XX(I)=0.2+0.8*X(I)
         OLDX(I)=XX(I)
         F(I)=RENOL*(P2-PM(I))/(2.0*OLDH*(XX(I)-X2))
84       CONTINUE
         DO 85 I=13,23
         XXX(I)=XX(I-11)
         FFF(I)=F(I-11)
         PPP(I)=PM(I-11)
85       CONTINUE
         P12=PM(12)
      ENDIF

      IF(NEVT.EQ.4) THEN
         PDIFF=PM(2)-P12
         DO 88 I=2,M-1
         PM(I)=PM(I)-PFLUX-PIN-PDIFF
         XX(I)=0.4+0.6*X(I)
         OLDX(I)=XX(I)
         F(I)=RENOL*(P2-PM(I))/(2.0*OLDH*(XX(I)-X2))
88       CONTINUE
         DO 89 I=24,34
         XXX(I)=XX(I-22)
         FFF(I)=F(I-22)
         PPP(I)=PM(I-22)
89       CONTINUE
         P12=PM(12)
      ENDIF

      IF(NEVT.EQ.5) THEN
         PDIFF=PM(2)-P12
         DO 90 I=2,M-1
         PM(I)=PM(I)-PFLUX-PIN-PDIFF
         XX(I)=0.6+0.4*X(I)
         OLDX(I)=XX(I)
         F(I)=RENOL*(P2-PM(I))/(2.0*OLDH*(XX(I)-X2))
90       CONTINUE
         DO 91 I=35,45
         XXX(I)=XX(I-33)
         FFF(I)=F(I-33)
         PPP(I)=PM(I-33)
91       CONTINUE
         P12=PM(12)
```

```
      ENDIF

      IF(NEVT.EQ.6) THEN
         PDIFF=PM(2)-P12
         DO 94 I=2,M-1
         PM(I)=PM(I)-PFLUX-PIN-PDIFF
         XX(I)=0.8+0.2*X(I)
         OLDX(I)=XX(I)
         F(I)=RENOL*(P2-PM(I))/(2.0*OLDH*(XX(I)-X2))
94       CONTINUE
         DO 95 I=46,55
         XXX(I)=XX(I-44)
         FFF(I)=F(I-44)
         PPP(I)=PM(I-44)
95       CONTINUE
         P12=PM(12)
      ENDIF

      IF(NEVT.EQ.6) THEN
         WRITE(10,*) 'Repeated Eversion$-f*Re'
         WRITE(10,1) (XXX(I)*OLDH/RENOL,I=3,55)
         WRITE(10,1) (FFF(I),I=3,55)
         WRITE(8,*) 'Repeated Eversion$-p'
         WRITE(8,1) (XXX(I)*OLDH,I=2,55)
         WRITE(8,1) (PPP(I),I=2,55)
      ENDIF

      WRITE(6,*) 'THE FRICTION FACTOR DISTRIBUTION'
      WRITE(6,*) 'OLDH*X(I)/RENOL,      F(I))'
      DO 170 I=3,M-1
      IF(NEVT.LE.2) WRITE(6,6) OLDH*X(I)/RENOL,F(I)
      IF(NEVT.GE.3) WRITE(6,6) OLDH*OLDX(I)/RENOL,F(I)
170   CONTINUE

C Interpolate u values at the T nodal points to
C calculate Nusselt number later on.

      DO 174 J=1,N
        DO 176 I=1,M-2
          XX(I)=XU(I+1)
          YY(I)=U(I+1,J)
176     CONTINUE
        CALL SPLINE(M-2,NDCON,XX,YY,SUMN,VAL,0,B,C,D,HH)
        DO 178 I=1,M-3
          USTAR(I+1,J)=U(I+1,J)+B(I)*0.5*HH(I)
     &    +C(I)*0.5*HH(I)**2+D(I)*0.5*HH(I)**3
178     CONTINUE
174   CONTINUE
```

```
      DO 182 J=1,N
        USTAR(1,J)=U(2,J)
        USTAR(M-1,J)=U(M,J)
        USTAR(M,J)=U(M,J)
182   CONTINUE
      USTAR(1,1)=U(2,2)
      USTAR(M-1,1)=USTAR(M-1,2)
      USTAR(M,1)=USTAR(M,2)

C Now, solve the energy equation for temperature field.

      WRITE(7,*) 'Now solve energy equation'
      WRITE(6,*) 'Now solve energy equation'

C Specify boundary conditions for energy equation.
C Boundary indices are ( 1, M, 1, N ).

      DO 186 J = 2, N

C Left boundary condition (T=T(R)=const)

        AP(1,J) =  1.0
        AE(1,J) = 0.0
        S(1,J) = TLB(J)

C Right boundary condition (DT/DX = 0)

        AP(M,J) = 1.0
        AW(M,J) = 1.0
        S(M,J) = 0.0

186   CONTINUE

      DO 188 I = 2, M-1

C Bottom boundary condition (DT/DR = 0)

        AP(I,1) = 1.0
        AN(I,1) = 1.0
        S(I,1) = 0.0

C Top boundary condition (T = const)

        AP(I,N) = 1.0
        AS(I,N)=0.0
        S(I,N)=1.0

188   CONTINUE
```

```
      CALL COEFFT(M,N,RENOL,PR,EK,H,AP,AE,AW,AN,AS,S)
      CALL TDMA(AP,AE,AW,AN,AS,S,1,M,1,N,
     &          N,.FALSE.,NPPAS,TTOL,T,RESIDU)

      WRITE(6,*) 'WHEN SOLVING FOR T, RESIDU = ',RESIDU

      T(1,1)=T(1,2)
      T(M,1)=T(M-1,1)
      T(1,N)=T(2,N)
      T(M,N)=T(M-1,N)

      IF(NEVT.EQ.1) THEN
      WRITE(6,*) 'THE CONVERGED TEMPERATURE FIELD'
      WRITE(6,1) ((T(I,J),I=1,M),J=N,1,-1)
      ENDIF

C Calculate Nusselt Number by first calculating
C the mixing cup temperature.

      DO 190 I=2,M
         DO 192 J=1,N
            XX(J)=R(J)
            YY(J)=R(J)*USTAR(I,J)*T(I,J)
192      CONTINUE
         CALL SPLINE(N,NDCON,XX,YY,SUMN,VAL,1,B,C,D,HH)
         TMEAN=2.0*VAL
         RNU(I)=(T(I,N)-T(I,N-1))/RDIF(N)
         Q(I)=RNU(I)
         RNU(I)=2.0*RNU(I)/(1.0-TMEAN)
         PM(I)=TMEAN
190   CONTINUE

      IF(NEVT.EQ.1) THEN
         WRITE(9,*) 'FILE 9'
         WRITE(9,*) 'Smooth pipe$-Heat Transfer dT/dr'
         WRITE(9,1) (X(I)*OLDH,I=2,M)
         WRITE(9,1) (Q(I),I=2,M)
         WRITE(11,*) 'FILE 11'
         WRITE(11,*) 'Smooth pipe$ - Local Nu'
         WRITE(11,1) (X(I)*OLDH,I=2,M)
         WRITE(11,1) (RNU(I),I=2,M)
      ENDIF
      IF(NEVT.EQ.2) THEN
         DO 230 I=2,12
            RNUX(I)=RNU(I)
            QX(I)=Q(I)
230      CONTINUE
```

```
      ELSEIF(NEVT.EQ.3) THEN
         DO 232 I=13,23
            RNUX(I)=RNU(I-11)
            QX(I)=Q(I-11)
232      CONTINUE
      ELSEIF(NEVT.EQ.4) THEN
         DO 234 I=24,34
            RNUX(I)=RNU(I-22)
            QX(I)=Q(I-22)
234      CONTINUE
      ELSEIF(NEVT.EQ.5) THEN
         DO 236 I=35,45
            RNUX(I)=RNU(I-33)
            QX(I)=Q(I-33)
236      CONTINUE
      ELSEIF(NEVT.EQ.6) THEN
         DO 238 I=46,56
            RNUX(I)=RNU(I-44)
            QX(I)=Q(I-44)
238      CONTINUE
         WRITE(11,*) 'Repeated Eversion$-Local Nu'
         WRITE(11,1) (XXX(I)*OLDH,I=2,55)
         WRITE(11,1) (RNUX(I),I=2,55)
         WRITE(9,*) 'Repeated Eversion$-Dt/Dr'
         WRITE(9,1) (XXX(I)*OLDH,I=2,55)
         WRITE(9,1) (QX(I),I=2,55)

C Calculate overall mean Nusselt Number.

         DO 240 I=2,55,3
            J=(I+1)/3
            RR(J)=XXX(I)
            UU(J)=RNUX(I)
240      CONTINUE
         CALL SPLINE(18,NDCON,RR,UU,SUMN,VAL,1,B,C,D,HH)
         DO 242 I=2,18
            J=3*I-1
            RNUM(I)=SUMN(I-1)/(XXX(J)-XXX(2))
            XX(I)=XXX(J)
242      CONTINUE
         WRITE(11,*) 'Repeated Eversion$-Mean Nu'
         WRITE(11,1) (XX(I)*OLDH,I=2,18)
         WRITE(11,1) (RNUM(I),I=2,18)
      ENDIF

      DO 195 I=2,M
         XX(I-1)=X(I)
         YY(I-1)=RNU(I)
```

```
195   CONTINUE
      CALL SPLINE(M-1,NDCON,XX,YY,SUMN,VAL,1,B,C,D,HH)
      DO 196 I=1,M-2
         RNUM(I+2)=SUMN(I)/(X(I+2)-X(2))
196   CONTINUE
      RNUM(2)=0.0
      RNU12(NEVT)=RNUM(12)
      RNUH=RNUM(M-1)
      IF(NEVT.EQ.1) RNUONE=RNUH

      WRITE(6,*) 'NUSSELT NUMBER(CONST WALL TEMPERATURE)'
      WRITE(6,*) ' HX/PE,    TMEAN,    RNU(I),    RNUM(I)'
      DO 200 I=2,M
      IF(NEVT.LE.2) WRITE(6,7) H*X(I)/RENOL/PR,PM(I),RNU(I)
     &                ,RNUM(I)
      IF(NEVT.GE.3) WRITE(6,7) OLDH*OLDX(I)/RENOL/PR,PM(I)
     &                ,RNU(I),RNUM(I)
200   CONTINUE
      WRITE(6,*) 'NU12(NEVT)=',RNU12(NEVT),' MEAN NU=',RNUH
      IF(NEVT.EQ.6) THEN
      RNU12M=(RNU12(2)+RNU12(3)+RNU12(4)+RNU12(5)1
     &       +RNU12(6))/5.0
      WRITE(6,*) 'Overall Mean Nu=', RNU12M
      WRITE(6,*) 'Mean Nu for Smooth Tube=',RNUONE,
     &           'Ratio of Increase=',RNU12M/RNUONE
      ENDIF

C Store U and T values at the locations of eversion.

      IF(NEVT.EQ.1) THEN
         WRITE(6,*) ' EVERSION @ L/D=0.0'
         DO 300 J=1,N
            XX(J)=R(J)
            YY(J)=USTAR(1,J)
300      CONTINUE
         CALL INCRSE(N,XX,YY,NDCON,NDIV,KK,RR,UU)
         DO 310 J=1,KK-1
            TT(J)=0.0
310      CONTINUE
         UU(KK)=0.0
         TT(KK)=1.0
         DO 314 J=1,N
            XX(J)=R(J)
            YY(J)=R(J)*USTAR(1,J)*USTAR(1,J)
314      CONTINUE
         CALL SPLINE(N,NDCON,XX,YY,SUMN,VAL,1,B,C,D,HH)
         FLUX=2.0*VAL
         WRITE(6,*) 'MOMENTUM FLUX=',FLUX
```

```
      IF(MODEL.EQ.1) CALL EVERT1(N,KK,RR,UU,TT,NDIV)
      IF(MODEL.EQ.2) CALL EVERT2(N,KK,RR,UU,TT,NDIV)
      IF(MODEL.EQ.3) CALL EVERT3(N,KK,RR,UU,TT,NDIV)
      DO 316 J=1,N
         XX(J)=R(J)
         YY(J)=R(J)*ULB(J)*ULB(J)
316   CONTINUE
      CALL SPLINE(N,NDCON,XX,YY,SUMN,VAL,1,B,C,D,HH)
      PFLUX=2.0*VAL-FLUX
      WRITE(6,*)'MOMENTUM FLUX=',2.0*VAL,'PFLUX=',PFLUX
      DO 317 J=1,N
         XX(J)=R(J)
         YY(J)=R(J)*ULB(J)
317   CONTINUE
      CALL SPLINE(N,NDCON,XX,YY,SUMN,VAL,1,B,C,D,HH)
      WRITE(6,*) 'MASS FLOW AFTER EVERSION = ',2.0*VAL
      DO 318 J=1,N
         XX(J)=R(J)
         YY(J)=R(J)*TLB(J)*ULB(J)
318   CONTINUE
      CALL SPLINE(N,NDCON,XX,YY,SUMN,VAL,1,B,C,D,HH)
      WRITE(6,*) 'MEAN TEMP AFTER EVERSION=',2.0*VAL
      NEVT=NEVT+1
      GOTO 888
   ENDIF

   IF(NEVT.EQ.2) THEN
      WRITE(6,*) ' EVERSION @ L/D=0.2H'
      DO 320 J=1,N
         XX(J)=R(J)
         YY(J)=USTAR(12,J)
320   CONTINUE
      CALL INCRSE(N,XX,YY,NDCON,NDIV,KK,RR,UU)
      DO 330 J=1,N
         XX(J)=R(J)
         YY(J)=T(12,J)
330   CONTINUE
      CALL INCRSE(N,XX,YY,NDCON,NDIV,KK,RR,TT)
      DO 331 J=1,N
         XX(J)=R(J)
         YY(J)=R(J)*USTAR(12,J)*USTAR(12,J)
331   CONTINUE
      CALL SPLINE(N,NDCON,XX,YY,SUMN,VAL,1,B,C,D,HH)
      FLUX=2.0*VAL
      WRITE(6,*) 'MOMENTUM FLUX BEFORE=',FLUX
      IF(MODEL.EQ.1) CALL EVERT1(N,KK,RR,UU,TT,NDIV)
      IF(MODEL.EQ.2) CALL EVERT2(N,KK,RR,UU,TT,NDIV)
      IF(MODEL.EQ.3) CALL EVERT3(N,KK,RR,UU,TT,NDIV)
```

```
      DO 332 J=1,N
         XX(J)=R(J)
         YY(J)=R(J)*ULB(J)
332   CONTINUE
      CALL SPLINE(N,NDCON,XX,YY,SUMN,VAL,1,B,C,D,HH)
      WRITE(6,*) 'MASS FLOW AFTER EVERSION = ',2.0*VAL
      DO 334 J=1,N
         XX(J)=R(J)
         YY(J)=R(J)*ULB(J)*ULB(J)
334   CONTINUE
      CALL SPLINE(N,NDCON,XX,YY,SUMN,VAL,1,B,C,D,HH)
      PFLUX=2.0*VAL-FLUX
      WRITE(6,*)'MOMENTUM FLUX=',2.0*VAL,'PFLUX=',PFLUX
      DO 337 J=1,N
         XX(J)=R(J)
         YY(J)=R(J)*TLB(J)*ULB(J)
337   CONTINUE
      CALL SPLINE(N,NDCON,XX,YY,SUMN,VAL,1,B,C,D,HH)
      WRITE(6,*) 'MEAN TEMP AFTER EVERSION=',2.0*VAL
      NEVT=NEVT+1
      M=21
      DO 338 I=1,M
         X(I)=X(I)/X(M)
338   CONTINUE
      H=0.8*H
      GOTO 888
   ENDIF

   IF(NEVT.EQ.3) THEN
      WRITE(6,*) ' EVERSION @ L/D=0.4H'
      DO 340 J=1,N
         XX(J)=R(J)
         YY(J)=USTAR(12,J)
340   CONTINUE
      CALL INCRSE(N,XX,YY,NDCON,NDIV,KK,RR,UU)
      DO 342 J=1,N
         YY(J)=T(12,J)
342   CONTINUE
      CALL INCRSE(N,XX,YY,NDCON,NDIV,KK,RR,TT)
      DO 343 J=1,N
         XX(J)=R(J)
         YY(J)=R(J)*USTAR(12,J)*USTAR(12,J)
343   CONTINUE
      CALL SPLINE(N,NDCON,XX,YY,SUMN,VAL,1,B,C,D,HH)
      FLUX=2.0*VAL
      WRITE(6,*) 'MOMENTUM FLUX=',FLUX
      IF(MODEL.EQ.1) CALL EVERT1(N,KK,RR,UU,TT,NDIV)
      IF(MODEL.EQ.2) CALL EVERT2(N,KK,RR,UU,TT,NDIV)
```

```
      IF(MODEL.EQ.3) CALL EVERT3(N,KK,RR,UU,TT,NDIV)
      DO 344 J=1,N
         XX(J)=R(J)
         YY(J)=R(J)*ULB(J)*ULB(J)
344   CONTINUE
      CALL SPLINE(N,NDCON,XX,YY,SUMN,VAL,1,B,C,D,HH)
      PFLUX=2.0*VAL-FLUX
      WRITE(6,*)'MOMENTUM FLUX=',2.0*VAL,'PFLUX=',PFLUX
      DO 346 J=1,N
         XX(J)=R(J)
         YY(J)=R(J)*ULB(J)
346   CONTINUE
      CALL SPLINE(N,NDCON,XX,YY,SUMN,VAL,1,B,C,D,HH)
      WRITE(6,*) 'MASS FLOW AFTER EVERSION = ',2.0*VAL
      DO 348 J=1,N
         XX(J)=R(J)
         YY(J)=R(J)*TLB(J)*ULB(J)
348   CONTINUE
      CALL SPLINE(N,NDCON,XX,YY,SUMN,VAL,1,B,C,D,HH)
      WRITE(6,*) 'MEAN TEMP AFTER EVERSION=',2.0*VAL
      NEVT=NEVT+1
      M=19
      DO 349 I=1,M
         X(I)=X(I)/X(M)
349   CONTINUE
      H=0.6/0.8*H
      GOTO 888
   ENDIF

   IF(NEVT.EQ.4) THEN
      WRITE(6,*) ' EVERSION @ L/D=0.6H'
      DO 350 J=1,N
         XX(J)=R(J)
         YY(J)=USTAR(12,J)
350   CONTINUE
      CALL INCRSE(N,XX,YY,NDCON,NDIV,KK,RR,UU)
      DO 352 J=1,N
         YY(J)=T(12,J)
352   CONTINUE
      CALL INCRSE(N,XX,YY,NDCON,NDIV,KK,RR,TT)
      DO 354 J=1,N
         XX(J)=R(J)
         YY(J)=R(J)*USTAR(12,J)*USTAR(12,J)
354   CONTINUE
      CALL SPLINE(N,NDCON,XX,YY,SUMN,VAL,1,B,C,D,HH)
      FLUX=2.0*VAL
      WRITE(6,*) 'MOMENTUM FLUX=',FLUX
      IF(MODEL.EQ.1) CALL EVERT1(N,KK,RR,UU,TT,NDIV)
```

```
      IF(MODEL.EQ.2) CALL EVERT2(N,KK,RR,UU,TT,NDIV)
      IF(MODEL.EQ.3) CALL EVERT3(N,KK,RR,UU,TT,NDIV)
      DO 355 J=1,N
         XX(J)=R(J)
         YY(J)=R(J)*ULB(J)*ULB(J)
355   CONTINUE
      CALL SPLINE(N,NDCON,XX,YY,SUMN,VAL,1,B,C,D,HH)
      PFLUX=2.0*VAL-FLUX
      WRITE(6,*)'MOMENTUM FLUX=',2.0*VAL,'PFLUX=',PFLUX
      DO 356 J=1,N
         XX(J)=R(J)
         YY(J)=R(J)*ULB(J)
356   CONTINUE
      CALL SPLINE(N,NDCON,XX,YY,SUMN,VAL,1,B,C,D,HH)
      WRITE(6,*) 'MASS FLOW AFTER EVERSION = ',2.0*VAL
      DO 358 J=1,N
         XX(J)=R(J)
         YY(J)=R(J)*TLB(J)*ULB(J)
358   CONTINUE
      CALL SPLINE(N,NDCON,XX,YY,SUMN,VAL,1,B,C,D,HH)
      WRITE(6,*) 'MEAN TEMP AFTER EVERSION=',2.0*VAL
      NEVT=NEVT+1
      M=16
      DO 359 I=1,M
         X(I)=X(I)/X(M)
359   CONTINUE
      H=0.4/0.6*H
      GOTO 888
   ENDIF

   IF(NEVT.EQ.5) THEN
      WRITE(6,*) ' EVERSION @ L/D=0.8H'
      DO 360 J=1,N
         XX(J)=R(J)
         YY(J)=USTAR(12,J)
360   CONTINUE
      CALL INCRSE(N,XX,YY,NDCON,NDIV,KK,RR,UU)
      DO 362 J=1,N
         YY(J)=T(12,J)
362   CONTINUE
      CALL INCRSE(N,XX,YY,NDCON,NDIV,KK,RR,TT)
      DO 364 J=1,N
         XX(J)=R(J)
         YY(J)=R(J)*USTAR(12,J)*USTAR(12,J)
364   CONTINUE
      CALL SPLINE(N,NDCON,XX,YY,SUMN,VAL,1,B,C,D,HH)
      FLUX=2.0*VAL
      WRITE(6,*) 'MOMENTUM FLUX=',FLUX
```

```
      IF(MODEL.EQ.1) CALL EVERT1(N,KK,RR,UU,TT,NDIV)
      IF(MODEL.EQ.2) CALL EVERT2(N,KK,RR,UU,TT,NDIV)
      IF(MODEL.EQ.3) CALL EVERT3(N,KK,RR,UU,TT,NDIV)
      DO 365 J=1,N
         XX(J)=R(J)
         YY(J)=R(J)*ULB(J)*ULB(J)
365   CONTINUE
      CALL SPLINE(N,NDCON,XX,YY,SUMN,VAL,1,B,C,D,HH)
      PFLUX=2.0*VAL-FLUX
      WRITE(6,*)'MOMENTUM FLUX=',2.*VAL,' PFLUX=',PFLUX
      DO 366 J=1,N
         XX(J)=R(J)
         YY(J)=R(J)*ULB(J)
366   CONTINUE
      CALL SPLINE(N,NDCON,XX,YY,SUMN,VAL,1,B,C,D,HH)
      WRITE(6,*) 'MASS FLOW AFTER EVERSION = ',2.0*VAL
      DO 368 J=1,N
         XX(J)=R(J)
         YY(J)=R(J)*TLB(J)*ULB(J)
368   CONTINUE
      CALL SPLINE(N,NDCON,XX,YY,SUMN,VAL,1,B,C,D,HH)
      WRITE(6,*) 'MEAN TEMP AFTER EVERSION=',2.0*VAL
      NEVT=NEVT+1
      M=12
      DO 369 I=1,M
         X(I)=X(I)/X(M)
369   CONTINUE
      H=0.2/0.4*H
      GOTO 888
   ENDIF

   STOP
   END

C This subroutine solves the following type of
C descretized equation using TDMA algorithm.
C
C  AP(I,J)*X(I,J) = AE(I,J)*X(I+1,J) + AW(I,J)*X(I-1,J)
C        + AN(I,J)*X(I,J+1) + AS(I,J)*X(I,J-1) + S(I,J)

C Inputs:
C   IL    - index of the left boundary
C   IR    - index of the right boundary
C   JB    - index of the bottom boundary
C   JT    - index of the top boundary
C   NPASS - number of sweeps to be made

C   AP - coefficient vector of X(I,J) in the equation.
```

```
C   AN - coefficient vector of X(I,J+1) in the equation.
C   AS - coefficient vector of X(I,J-1) in the equation.
C   AE - coefficient vector of X(I+1,J) in the equation.
C   AW - coefficient vector of X(I-1,J) in the equation.

C It requires values of the above vectors for I=IL+1 to
C I=IR-1 and J=JB+1 to J=JT-1.
C It also requires the following vectors which specifiey
C boundary conditions.

C   AP(IL,J)   AE(IL,J)   S(IL,J)    J = JB+1 TO JT-1
C   AP(IR,J)   AW(IR,J)   S(IR,J)    J = JB+1 TO JT-1
C   AP(I,JB)   AN(I,JB)   S(I,JB)    I = IL+1 TO IR-1
C   AP(I,JT)   AS(I,JT)   S(I,JT)    I = IL+1 TO IR-1

C Output:
C   X(I,J) :  solution vector

      SUBROUTINE TDMA(AP,AE,AW,AN,AS,S,IL,IR,JB,JT,
     &                NF,FLAG,NPASS,TOLER,X,RELERR)
      IMPLICIT REAL(A-H,O-Z)
      PARAMETER(ID=24,JD=24)

      DIMENSION AP(ID,JD),AE(ID,JD),AW(ID,JD),AN(ID,JD)
     &         ,AS(ID,JD),S(ID,JD),X(ID,JD)
      DIMENSION A(JD),B(JD),C(JD),D(JD),Q(JD),P(JD)
      LOGICAL FLAG

      NPOINT = ( IR-IL-1)*(NF-JB-1)
      IF(FLAG.EQV..TRUE.) NPOINT=(IR-IL-3)*(NF-JB-3)

C Make double sweep NPASS times, or until RELERR
C becomes small.

      ISWICH = 0
      DO 333  ITER = 1, NPASS
      DO 444  ILOOP = 1,2

C Set the sweep direction.

       IF (ISWICH .EQ. 0) THEN
          I1 = IL+1
          IINC = 1
          I2 = IR-1
          J1 = JB+1
          JINC = 1
          J2 = JT-1
          ISWICH = 1
```

```
      ELSE
         I1 = IR-1
         IINC = -1
         I2 = IL+1
         J1 = JT-1
         JINC = -1
         J2 = JB+1
         ISWICH = 0
      ENDIF

C Sweep from left to right boundaries beginning from
C J=bottom or from J=top.

      DO  100  J = J1, J2, JINC

C Set up the tri-diagonal matrix as required by TDMA.

      DO 10 I=IL+1,IR-1
         A(I) = AP(I,J)
         B(I) = AE(I,J)
         C(I) = AW(I,J)
         D(I)=S(I,J)+AN(I,J)*X(I,J+1)+AS(I,J)*X(I,J-1)
 10   CONTINUE

      IF(FLAG.EQV..TRUE.) THEN
         IL=IL+1
         IR=IR-1
         GOTO 15
      ENDIF
      C(IL) = 0
      B(IR) = 0

C Left boundary conditions.

      A(IL) = AP(IL,J)
      B(IL) = AE(IL,J)
      D(IL) = S(IL,J)

C Right boundary conditions.

      A(IR) = AP(IR,J)
      C(IR) = AW(IR,J)
      D(IR) = S(IR,J)

C Now calculate P(I) and Q(I).

 15   P(IL) = B(IL) / A(IL)
      Q(IL) = D(IL) / A(IL)
```

```
      DO 20 I = IL+1,IR
         DENOM = A(I) - C(I) * P(I-1)
         P(I) = B(I) / DENOM
         Q(I) = ( D(I) + C(I) * Q(I-1) ) / DENOM
 20   CONTINUE

C Obtain solution by back substitution.

      X(IR,J)=Q(IR)
      DO 30 I=IR-1,IL,-1
         X(I,J) = P(I) * X(I+1,J) + Q(I)
 30   CONTINUE
      IF(FLAG.EQV..TRUE.) THEN
         IL=IL-1
         IR=IR+1
      ENDIF
 100  CONTINUE

C Now sweep from bottom to top boundaries beginning from
C I=left or from I=right.

      DO 200 I = I1, I2, IINC

C Set up the tri-diagonal matrix as required by TDMA.

      DO 40 J = JB+1, NF-1
         A(J) = AP(I,J)
         B(J) = AN(I,J)
         C(J) = AS(I,J)
         D(J)=S(I,J)+AE(I,J)*X(I+1,J)+AW(I,J)*X(I-1,J)
 40   CONTINUE
      IF(FLAG.EQV..TRUE.) THEN
         JB=JB+1
         JT=JT-1
         GOTO 45
      ENDIF

      C(JB) = 0
      B(JT) = 0

C Bottom boundary conditions.

      A(JB) = AP(I,JB)
      B(JB) = AN(I,JB)
      D(JB) = S(I,JB)

C Top boundary conditions.
```

```
      A(NF) = AP(I,NF)
      C(NF) = AS(I,NF)
      D(NF) = S(I,NF)

C Now calculate P(J) and Q(J).

 45   P(JB) = B(JB) / A(JB)
      Q(JB) = D(JB) / A(JB)
      DO 50 J = JB+1, JT
         DENOM = A(J) - C(J) * P(J-1)
         P(J) = B(J) / DENOM
         Q(J) = ( D(J) + C(J) * Q(J-1) ) / DENOM
 50   CONTINUE

C Obtain solution by back substitution.

      X(I,JT) = Q(JT)
      DO 60 J = JT-1, JB, -1
         X(I,J) = P(J) * X(I,J+1) + Q(J)
 60   CONTINUE
      IF(FLAG.EQV..TRUE.) THEN
         JB=JB-1
         JT=JT+1
      ENDIF

 200  CONTINUE

 444  CONTINUE

C The double sweep has been completed.
C Now test for convergence.

      RELERR=0.0
      DO 123 I = IL+1, IR-1
      DO 123 J = JB+1, NF-1
      T=AP(I,J)*X(I,J)-AE(I,J)*X(I+1,J)-AW(I,J)*X(I-1,J)
     & -AN(I,J)*X(I,J+1)-AS(I,J)*X(I,J-1)-S(I,J)
        RELERR=RELERR+ABS(T)
 123  CONTINUE
      RELERR=RELERR/NPOINT
      IF (RELERR.LT.TOLER) GOTO 999
 333  CONTINUE
C     WRITE(6,*) 'NOT CONVERGED IN SUB TDMA'
 999  CONTINUE
      WRITE(7,*) 'NO OF DOUBLE SWEEP IN SUB TDMA= ',ITER
      WRITE(7,*) 'RESIDU IN SUB TDMA = ',RELERR
      RETURN
      END
```

```
      SUBROUTINE COEFFU(M,N,RENOL,H,RELAX,DU,AP,
     &                  AE,AW,AN,AS,S)
      IMPLICIT REAL(A-H,O-Z)
      PARAMETER(ID=24,JD=24)
      COMMON /VEL/ U(ID,JD),V(ID,JD),P(ID,JD),T(ID,JD)
      DIMENSION AP(ID,JD),AE(ID,JD),AW(ID,JD),AN(ID,JD),
     &          AS(ID,JD),S(ID,JD),DU(ID,JD)
      COMMON /XINDEX/ X(ID),XU(ID),XDIF(ID),XCV(ID)
      COMMON /RINDEX/ R(JD),RV(JD),RDIF(JD),RCV(JD)

      DO 10 I=3,M-1
         DO 10 J=2,N-1
            RE=R(J)
            RW=R(J)
            RN=RV(J+1)
            RS=RV(J)

            DELX=XDIF(I)
            DELR=RCV(J)
            DELXE=XCV(I)
            DELXW=XCV(I-1)
            DELRN=RDIF(J+1)
            DELRS=RDIF(J)

            UE=(U(I,J)+U(I+1,J))*0.5
            UW=(U(I,J)+U(I-1,J))*0.5
            CALL AINTP(XCV(I-1),XCV(I),V(I-1,J+1),
     &                 V(I,J+1),VN)
            CALL AINTP(XCV(I-1),XCV(I),V(I-1,J),V(I,J),VS)

            FN=VN*RN*DELX
            FS=VS*RS*DELX
            FE=UE*RE*DELR
            FW=UW*RW*DELR

            DN=4.0*H*RN*DELX/(RENOL*DELRN)
            DS=4.0*H*RS*DELX/(RENOL*DELRS)
            DE=RE*DELR/(RENOL*H*DELXE)
            DW=RW*DELR/(RENOL*H*DELXW)

            CALL POWER(FN,DN,ACOF)
            AN(I,J)=ACOF+AMAX1(0.0,-FN)
            CALL POWER(FS,DS,ACOF)
            AS(I,J)=ACOF+AMAX1(0.0,FS)
            CALL POWER(FE,DE,ACOF)
            AE(I,J)=ACOF+AMAX1(0.0,-FE)
            CALL POWER(FW,DW,ACOF)
```

```
            AW(I,J)=ACOF+AMAX1(0.0,FW)

            USUM=AE(I,J)+AW(I,J)+AN(I,J)+AS(I,J)
            AP(I,J)=(1.0/RELAX)*USUM

            S(I,J)=AP(I,J)*(1.0-RELAX)*U(I,J)
            S(I,J)=S(I,J)+(P(I-1,J)-P(I,J))*RE*DELR
            DU(I,J)=(RW*DELR)/(AP(I,J)-USUM)
C           DU(I,J)=(RW*DELR)/AP(I,J)  ,for SIMPLE Algorithm.

 10   CONTINUE
      RETURN
      END

      SUBROUTINE COEFFV(M,N,RENOL,H,RELAX,DV,AP,
     &                  AE,AW,AN,AS,S)
      IMPLICIT REAL(A-H,O-Z)
      PARAMETER(ID=24,JD=24)
      COMMON /VEL/ U(ID,JD),V(ID,JD),P(ID,JD),T(ID,JD)
      DIMENSION AP(ID,JD),AE(ID,JD),AW(ID,JD),AN(ID,JD),
     &          AS(ID,JD),S(ID,JD),DV(ID,JD)
      COMMON /XINDEX/ X(ID),XU(ID),XDIF(ID),XCV(ID)
      COMMON /RINDEX/ R(JD),RV(JD),RDIF(JD),RCV(JD)

      DO 10 I=2,M-1
         DO 10 J=3,N-1
            RE=RV(J)
            RW=RE
            RN=R(J)
            RS=R(J-1)

            DELX=XCV(I)
            DELR=RDIF(J)
            VOL=DELX*DELR
            DELXE=XDIF(I+1)
            DELXW=XDIF(I)
            DELRN=RCV(J)
            DELRS=RCV(J-1)

            CALL AINTP(RCV(J-1),RCV(J),U(I+1,J-1),
     &                 U(I+1,J),UE)
            CALL AINTP(RCV(J-1),RCV(J),U(I,J-1),U(I,J),UW)
            VN=(V(I,J)+V(I,J+1))*0.5
            VS=(V(I,J)+V(I,J-1))*0.5

            FN=VN*RN*DELX
            FS=VS*RS*DELX
            FE=UE*RE*DELR
```

```
            FW=UW*RW*DELR

            DN=(4.0*H*RN*DELX)/(RENOL*DELRN)
            DS=(4.0*H*RS*DELX)/(RENOL*DELRS)
            DE=(RE*DELR)/(RENOL*H*DELXE)
            DW=(RW*DELR)/(RENOL*H*DELXW)

            CALL POWER(FN,DN,ACOF)
            AN(I,J)=ACOF+AMAX1(0.0,-FN)
            CALL POWER(FS,DS,ACOF)
            AS(I,J)=ACOF+AMAX1(0.0,FS)
            CALL POWER(FE,DE,ACOF)
            AE(I,J)=ACOF+AMAX1(0.0,-FE)
            CALL POWER(FW,DW,ACOF)
            AW(I,J)=ACOF+AMAX1(0.0,FW)

            VSUM=AE(I,J)+AW(I,J)+AN(I,J)+AS(I,J)
            AP(I,J)=(1.0/RELAX)*(VSUM+4.0*H*VOL/(RENOL*RE))
            S(I,J)=(1.0-RELAX)*AP(I,J)*V(I,J)
            S(I,J)=S(I,J)+4.0*H*H*(P(I,J-1)-P(I,J))*RE*DELX
            DV(I,J)=(RE*DELX)/(AP(I,J)-VSUM)
C           DV(I,J)=(RE*DELX)/AP(I,J), for SIMPLE Algorithm.

 10     CONTINUE
        RETURN
        END

        SUBROUTINE COEFFT(M,N,RENOL,PR,EK,H,AP,AE,AW,AN,AS,S)
        IMPLICIT REAL(A-H,O-Z)
        PARAMETER(ID=24,JD=24)
        COMMON /VEL/ U(ID,JD),V(ID,JD),P(ID,JD),T(ID,JD)
        DIMENSION AP(ID,JD),AE(ID,JD),AW(ID,JD),AN(ID,JD),
       &                AS(ID,JD),S(ID,JD)
        COMMON /XINDEX/ X(ID),XU(ID),XDIF(ID),XCV(ID)
        COMMON /RINDEX/ R(JD),RV(JD),RDIF(JD),RCV(JD)

        DO 10 I=2,M-1
           DO 10 J=2,N-1
              RE=R(J)
              RW=RE
              RN=RV(J+1)
              RS=RV(J)

              DELX=XCV(I)
              DELR=RCV(J)
              DELXE=XDIF(I+1)
              DELXW=XDIF(I)
              DELRN=RDIF(J+1)
```

```
      DELRS=RDIF(J)
      VOL=R(J)*DELX/DELR

      UE=U(I+1,J)
      UW=U(I,J)
      VN=V(I,J+1)
      VS=V(I,J)
      IF(J.EQ.2) THEN
         UD=0.5*(U(I,J-1)+U(I+1,J-1))
      ELSE
         UD1=0.5*(U(I,J-1)+U(I+1,J-1))
         UD2=0.5*(U(I,J)+U(I+1,J))
         CALL AINTP(RCV(J-1),RCV(J),UD1,UD2,UD)
      ENDIF
      IF(J.EQ.N-1) THEN
         UP=0.5*(U(I,J+1)+U(I+1,J+1))
      ELSE
         UP1=0.5*(U(I,J)+U(I+1,J))
         UP2=0.5*(U(I,J+1)+U(I+1,J+1))
         CALL AINTP(RCV(J),RCV(J+1),UP1,UP2,UP)
      ENDIF

      FN=VN*RN*DELX
      FS=VS*RS*DELX
      FE=UE*RE*DELR
      FW=UW*RW*DELR

      DN=(4.0*H*RN*DELX)/(RENOL*PR*DELRN)
      DS=(4.0*H*RS*DELX)/(RENOL*PR*DELRS)
      DE=(RE*DELR)/(RENOL*PR*H*DELXE)
      DW=(RW*DELR)/(RENOL*PR*H*DELXW)

      CALL POWER(FN,DN,ACOF)
      AN(I,J)=ACOF+AMAX1(0.0,-FN)
      CALL POWER(FS,DS,ACOF)
      AS(I,J)=ACOF+AMAX1(0.0,FS)
      CALL POWER(FE,DE,ACOF)
      AE(I,J)=ACOF+AMAX1(0.0,-FE)
      CALL POWER(FW,DW,ACOF)
      AW(I,J)=ACOF+AMAX1(0.0,FW)

      AP(I,J)=AE(I,J)+AW(I,J)+AN(I,J)+AS(I,J)
      S(I,J)=(4.0*H*EK/RENOL)*VOL*(UP-UD)**2

10    CONTINUE
      RETURN
      END
```

```
      SUBROUTINE POWER(F,D,ACOF)
      IMPLICIT REAL(A-H,O-Z)
      ACOF=D
      IF(F.EQ.0.0) RETURN
      TEMPO=D-ABS(F)*0.1
      ACOF=0.0
      IF(TEMPO.LE.0.0) RETURN
      TEMPO=TEMPO/D
      ACOF=D*TEMPO*TEMPO*TEMPO*TEMPO*TEMPO
      RETURN
      END

      SUBROUTINE AINTP(DB,DF,VB,VF,VALUE)
      VALUE=(DB*VF+DF*VB)/(DB+DF)
      RETURN
      END

      SUBROUTINE CRIT(G,GSTAR,IL,IR,JB,JT,RELERR)
      PARAMETER(ID=24,JD=24)
      DIMENSION G(ID,JD),GSTAR(ID,JD)
      NPOINT=(IR-IL+1)*(JT-JB+1)
      RELERR=0.0
      DO 10 I=IL,IR
         DO 10 J=JB,JT
            DIFF=GSTAR(I,J)-G(I,J)
            DIFF=(DIFF*DIFF)/(GSTAR(I,J)*GSTAR(I,J))
            RELERR=RELERR+DIFF
10    CONTINUE
      RELERR=SQRT(RELERR)
      RELERR=RELERR/NPOINT
      RETURN
      END

C This subroutine calculates post-eversion velocity and
C temperature profiles based on ideal eversion model.

      SUBROUTINE EVERT1(N,KK,RR,UU,TT,NDIV)
      PARAMETER(ID=24,JD=24)
      REAL RR(99),UU(99),TT(99),UUM(99)
      COMMON /BL/ ULB(JD),TLB(JD)

C First calculate the everted mean element velocities.

      DO 10 J=1,KK-1
         ARATIO=(RR(J+1)**2-RR(J)**2)/(RR(KK-J+1)**2
     &          -RR(KK-J)**2)
         UUM(KK-J)=0.5*(UU(J+1)+UU(J))*ARATIO
10    CONTINUE
```

```
C Now translate the mean element velocities into
C nodal velocities (for B.C. of const wall temp only).

      JJ=KK/2+1
      TT(KK)=1.0
      UU(KK)=0.0
      DO 12 J=1,KK-2
         L=KK-J
         UU(L)=0.5*(UUM(L)+UUM(L-1))
12    CONTINUE
      UU(1)=2.0*UUM(1)-UU(2)
      DO 14 J=1,JJ-1
         L=KK-J
         SAVE=TT(L)
         TT(L)=TT(J+1)
         TT(J+1)=SAVE
14    CONTINUE
      TT(1)=TT(KK)
      DO 15 I=KK,1,-1
15    CONTINUE
      ULB(1)=UU(1)
      TLB(1)=TT(1)
      DO 20 J=2,N
         I=NDIV*J-NDIV+1
         ULB(J)=UU(I)
         TLB(J)=TT(I)
20    CONTINUE
      WRITE(6,*) 'EVERTED U AND T PRIFILE (IDEAL)'
      DO 25 J=N,1,-1
         WRITE(6,1) ULB(J),TLB(J)
25    CONTINUE
1     FORMAT(2F15.5)
      RETURN
      END

C This subroutine calculates post-eversion velocity and
C temperature profiles based on laminate eversion model.

      SUBROUTINE EVERT2(N,KK,RR,UU,TT,NDIV)
      PARAMETER(ID=24,JD=24)
      REAL RR(99),UU(99),TT(99),UUM(99)
      COMMON /BL/ ULB(JD),TLB(JD)

C Evert using RR radial index system.
C First calculate everted mean element velocities.

      JJ=KK/2+1
```

```
      DO 10 J=1,JJ-1
      K=JJ-J
      L=KK-J
      ARATIO=(RR(K+1)**2-RR(K)**2)/(RR(L+1)**2-RR(L)**2)
      UUM(L)=0.5*(UU(K+1)+UU(K))*ARATIO
10    CONTINUE
      DO 20 J=1,JJ-1
      K=JJ-J
      L=KK-J
      ARATIO=(RR(L+1)**2-RR(L)**2)/(RR(K+1)**2-RR(K)**2)
      UUM(K)=0.5*(UU(L+1)+UU(L))*ARATIO
20    CONTINUE

C Then translate the mean element velocities into
C nodal velocities.

      UU(KK)=0.0
      DO 22 J=1,KK-2
         L=KK-J
         UU(L)=0.5*(UUM(L)+UUM(L-1))
22    CONTINUE
      UU(1)=2.0*UUM(1)-UU(2)
      TT(KK)=1.0
      DO 25 J=1,JJ-1
         L=KK-J
         SAVE=TT(L)
         TT(L)=TT(JJ-J)
         TT(JJ-J)=SAVE
25    CONTINUE

C Now go back to the original index system.
C ie. from RR system to R system.

      ULB(1)=UU(1)
      TLB(1)=TT(1)
      DO 30 J=2,N
         I=NDIV*J-NDIV+1
         ULB(J)=UU(I)
         TLB(J)=TT(I)
30    CONTINUE

      WRITE(6,*) 'EVERTED U AND T PROFILE (LAMINATE)'
      DO 32 I=N,1,-1
         WRITE(6,1) ULB(I),TLB(I)
32    CONTINUE
1     FORMAT(2F15.5)
      RETURN
      END
```

```
C This subroutine calculates post-eversion velocity and
C temperature profiles based on mixed eversion model.

      SUBROUTINE EVERT3(N,KK,RR,UU,TT,NDIV)
      PARAMETER(ID=24,JD=24)
      REAL RR(99),UU(99),TT(99),SUMN(99),B(99),C(99),
     &     D(99),HH(99),XX(99),YY(99)
      COMMON /BL/ ULB(JD),TLB(JD)

C Mean core and annulus velocities are calculated
C and everted.

      JJ=KK/2+1
      DO 10 J=1,KK
         XX(J)=RR(J)
         YY(J)=RR(J)*UU(J)
 10   CONTINUE
      CALL SPLINE(KK,NDCON,XX,YY,SUMN,VAL,1,B,C,D,HH)
      UAMEAN=2.0*SUMN(JJ-1)/(RR(KK)**2-RR(JJ)**2)
      UCMEAN=2.0*(VAL-SUMN(JJ-1))/RR(JJ)**2
      DO 20 J=1,KK
         XX(J)=RR(J)
         YY(J)=RR(J)*UU(J)*TT(J)
 20   CONTINUE
      CALL SPLINE(KK,NDCON,XX,YY,SUMN,VAL,1,B,C,D,HH)
      TAMEAN=2.0*SUMN(JJ-1)/(RR(KK)**2-RR(JJ)**2)/UAMEAN
      TCMEAN=2.0*(VAL-SUMN(JJ-1))/RR(JJ)**2/UCMEAN

      L=(JJ+NDIV-1)/NDIV
      DO 25 J=1,L-1
         ULB(J)=UCMEAN
         TLB(J)=TCMEAN
 25   CONTINUE
      DO 30 J=L+1,N-1
         ULB(J)=UAMEAN
         TLB(J)=TAMEAN
 30   CONTINUE
      ULB(L)=0.5*(UAMEAN+UCMEAN)
      TLB(L)=0.5*(TAMEAN+TCMEAN)
      ULB(N)=0.0
      TLB(N)=1.0
      WRITE(6,*) 'EVERTED U AND T PROFILE (MIXED)'
      DO 35 I=N,1,-1
         WRITE(6,1) ULB(I),TLB(I)
 35   CONTINUE
 1    FORMAT(2F15.5)
      RETURN
```

```
      END

      SUBROUTINE SPLINE(N,ENDCON,XX,YY,SUMN,VAL,IER,
     &                  B,C,D,H)
      INTEGER ENDCON
      REAL XX(99),YY(99),B(99),C(99),D(99),H(99)
      REAL SUMN(99),SAVEXX(99)

      DO 5 I=1,N
         SAVEXX(I)=XX(I)
5     CONTINUE
      DO 10 I=1,N-1
         H(I)=XX(I+1)-XX(I)
10    CONTINUE
      IF(ENDCON.EQ.1) GOTO 20
      IF(ENDCON.EQ.2) GOTO 30
      IF(ENDCON.EQ.3) GOTO 40

20    C1=2.0*(H(1)+H(2))
      C2=H(2)
      C3=H(N-2)
      C4=2.0*(H(N-2)+H(N-1))
      GOTO 50

30    C1=3.0*H(1)+2.0*H(2)
      C2=H(2)
      C3=H(N-2)
      C4=2.0*H(N-2)+3.0*H(N-1)
      GOTO 50

40    C1=( (H(1)+H(2))*(H(1)+2.0*H(2)) )/H(2)
      C2=( H(2)**2-H(1)**2 )/H(2)
      C3=( H(N-2)**2-H(N-1)**2 )/H(N-2)
      C4=( (H(N-1)+H(N-2)) * (H(N-1)+2.0*H(N-2)) )/H(N-2)

50    DO 60 I=2,N-1
      B(I-1)=6.0*((YY(I+1)-YY(I))/H(I)-(YY(I)-YY(I-1))
     &       /H(I-1))
60    CONTINUE

      II=N-2
      LL=N-3
      C(1)=C1
      D(1)=C2/C(1)
      DO 70 J=2,LL
         C(J)=2.0*(H(J)+H(J+1))-H(J)*D(J-1)
         D(J)=H(J+1)/C(J)
70    CONTINUE
```

```
      C(N-2)=C4-C3*D(N-3)
      XX(1)=B(1)/C(1)
      DO 80 I=2,LL
         XX(I)=( B(I)-H(I)*XX(I-1) )/C(I)
 80   CONTINUE
      XX(II)=( B(II)-C3*XX(II-1) )/C(II)
      C(II)=XX(II)

C Solve for the second derivatives using
C Thomas Algorithm.

      DO 90 I=1,LL
         K=LL+1-I
         C(K)=XX(K)-C(K+1)*D(K)
 90   CONTINUE
      DO 100 I=1,II
         XX(I+1)=C(I)
 100  CONTINUE

      IF(ENDCON.EQ.1) GOTO 110
      IF(ENDCON.EQ.2) GOTO 120
      IF(ENDCON.EQ.3) GOTO 130

 110  XX(1)=0.0
      XX(N)=0.0
      GOTO 140

 120  XX(1)=XX(2)
      XX(N)=XX(N-1)
      GOTO 140

 130  XX(1)=((H(1)+H(2))*XX(2)-H(1)*H(3))/H(2)
      XX(N)=((H(N-2)+H(N-1))*XX(N-1)-H(N-1)*XX(N-2))
     &      /H(N-2)

 140  DO 150 I=1,N-1
         B(I)=(YY(I+1)-YY(I))/H(I)-(2.0*H(I)*XX(I)+H(I)
     &        *XX(I+1))/6.0
         C(I)=XX(I)/2.0
         D(I)=(XX(I+1)-XX(I)) / (6.0*H(I))
 150  CONTINUE

      IF(IER.EQ.1) THEN
         VAL=0.0
         DO 160 J=1,N-1
            AA=YY(J)*H(J)
            BB=0.5*B(J)*H(J)**2
            CC=(1.0/3.0)*C(J)*H(J)**3
```

```
            DD=0.25*D(J)*H(J)**4
            EACH=AA+BB+CC+DD
            SUMN(J)=VAL+EACH
            VAL=VAL+EACH
160      CONTINUE
      ENDIF

      DO 170 I=1,N
         XX(I)=SAVEXX(I)
170   CONTINUE
      RETURN
      END

C This subroutine increases the number of radial
C nodal points and interpolate U-velocities for
C the new nodal points using cubic spline. Call
C this radial indexing system RR(J).

      SUBROUTINE INCRSE(N,R1,U1,NDCON,NDIV,KK,RR,UU)
      PARAMETER(ID=24,JD=24)
      REAL R1(99),U1(99),RR(99),UU(99),B(99),C(99),
     &     D(99),H(99),SAVER1(99)

      DO 5 J=1,N
         SAVER1(J)=R1(J)
5     CONTINUE
      CALL SPLINE(N,NDCON,R1,U1,SUMN,VAL,0,B,C,D,H)
      RR(1)=SAVER1(1)
      UU(1)=U1(1)

      K=0
      DO 10 J=1,N-1
         DEL=(SAVER1(J+1)-SAVER1(J))/NDIV
         I=0
11       IF(I.LT.NDIV) THEN
            I=I+1
            K=K+1
            RR(K+1)=RR(K)+DEL
            DELL=FLOAT(I)*DEL
            UU(K+1)=U1(J)+B(J)*DELL+C(J)*DELL**2+D(J)
     &              *DELL**3
            GOTO 11
         ENDIF
10    CONTINUE
      KK=K+1
      DO 12 I=1,KK
13       FORMAT(2F11.5)
12    CONTINUE
```

```
      DO 20 J=1,N
         R1(J)=SAVER1(J)
20    CONTINUE
      RETURN
      END
```